Heavy Quark-Pair Production in Electron Positron Collisions at Next-to-Next-to-Leading Order QCD

Von der Fakultät für Mathematik, Informatik und Naturwissenschaften der RWTH Aachen University zur Erlangung des akademischen Grades eines Doktors der Naturwissenschaften genehmigte Dissertation

vorgelegt von

Master of Science
Long Chen

aus Lin yi, China

Berichter: Prof. Dr.rer.nat. Werner Bernreuther
Universitätsprofessor Dr. Michal Czakon

Tag der mündlichen Prüfung: 12.07.2017

Diese Dissertation ist auf den Internetseiten der Universitätsbibliothek online verfügbar.

Contents

Abstract

Standard Model high-precision computations of observables related to heavy quark physics are very important, both for testing the consistency of Standard Model and for providing a precision tool for data analysis in the context of searches for new physics. The calculation of differential cross sections and (exclusive) observables at higher order perturbation theory in Quantum Chromodynamics (QCD) requires a method for handling the soft and collinear singular configurations that arise from the radiation of massless partons and appear in individual contributions. In this thesis, we present a set-up, within the antenna subtraction framework, for computing the production of a massive quark-antiquark pair in electron positron collisions at next-to-next-to-leading order in the coupling α_s of QCD at the differential level. Our set-up applies to the calculation of any infrared-safe observable. We apply this formalism to the production of top-quark pair ($t\bar{t}$) production in the continuum and also to bottom-pair ($b\bar{b}$) production at the Z resonance. We compute the respective production cross sections and several distributions. We determine, in particular, the forward-backward asymmetries A_{FB}^{Q} of these heavy quarks at order α_s^2, which are important observables for electroweak precision tests and for determining the neutral-current couplings of these quarks. The order α_s^2 corrections turn out to be significant. In the top quark case we compute A_{FB}^{t} for several center-of-mass energies above the $t\bar{t}$ production threshold. For $b\bar{b}$ production at the Z peak, we compute A_{FB}^{b} both for the b-quark axis and the oriented thrust axis definition of the asymmetry. We find that if one takes into account the complete massive order α_s^2 corrections to the leading-order asymmetry, which is a new result, then the magnitude of the QCD corrections increases slightly compared to previously known results. This reduces the well-known tension between the experimentally determined bare b-quark asymmetry and the value obtained by a global fit from 2.5σ to 2.2σ.

Zusammenfassung

Die präzise Berechnung von Observablen mit Bezug zur Physik schwerer Quarks ist von großer Bedeutung sowohl für Konsistenztests des Standardmodells als auch für Präzisions-Datenanalysen zur Suche nach neuer Physik. Die Berechnung differentieller Wirkungsquerschnitte und (exklusiver) Observablen in höheren Ordnungen der Störungstheorie in der Quantenchromodynamik (QCD) erfordert insbesondere eine Methode zur Behandlung der sogenannten weichen und kollinearen Infrarot-Singularitäten, die durch die Abstrahlung masseloser Partonen verursacht werden. In dieser Dissertation wird im Rahmen der sog. Antennen-Subtraktionsmethode ein Formalismus entwickelt, der die Berechnung der Produktion eines massiven Quark-Antiquark Paares in Elektron-Positron Kollisionen in der nächst-nächstführenden Ordnung der QCD Störungstheorie erlaubt. Der Formalismus ermöglicht die Berechnung beliebiger infrarot-sicherer Observablen. Wir wenden unsere Formeln auf die Topquark Paarerzeugung ($t\bar{t}$) im Kontinuum und auf die b-Quark Paarerzeugung ($b\bar{b}$) auf der Z Resonanz an. Wir berechnen die jeweiligen Wirkungsquerschnitte und eine Reihe differentieller Verteilungen. Insbesondere berechnen wir die jeweiligen Vorwärts-Rückwärts-Asymmetrien $A_{\rm FB}^{Q}$ zur Ordnung α_s^2. Dies sind wichtige Observablen für Präzisionstests der elektroschwachen Wechselwirkungen und für die Bestimmung der neutralen Strom-Kopplungen der t und b Quarks. Die Korrekturen der Ordung α_s^2 erweisen sich als signifikant. Im Falle des Top-Quarks berechnen wir $A_{\rm FB}^{t}$ für verschiedene Schwerpunktsenergien oberhalb der $t\bar{t}$ Schwelle. Für die $b\bar{b}$ Erzeugung auf der Z Resonanz berechnen wir $A_{\rm FB}^{b}$ sowohl bezüglich der b-Quarkachse als auch der orientierten thrust Achse. Unser neues Resultat, die vollständigen massiven b-Quark QCD Korrekturen bis zur Ordnung α_s^2, vergrössern etwas den Betrag des bisher bekannten Wertes der Korrekturen. Als Folge wird die seit langem bekannte 2.5σ Diskrepanz zwischen der aus den Daten bestimmten nackten b-Quark Asymmetrie und dem Wert resultierend aus einem globalen Fit auf 2.2σ reduziert.

List of publications

This thesis is based othe author's research conducted at the Institut für Theoretische Teilchenphysik und Kosmologie of the RWTH Aachen University. Parts of this work have already been published in the following two articles:

L. Chen, O. Dekkers, D. Heisler, W. Bernreuther and Z. G. Si, *Top-quark pair production at next-to-next-to-leading order QCD in electron positron collisions,* JHEP **1612** (2016) 098 doi:10.1007/JHEP12(2016)098 [arXiv:1610.07897 [hep-ph]].

W. Bernreuther, L. Chen, O. Dekkers, T. Gehrmann and D. Heisler, *The forward-backward asymmetry for massive bottom quarks at the Z peak at next-to-next-to-leading order QCD,* JHEP **1701** (2017) 053 doi:10.1007/JHEP01(2017)053 [arXiv:1611.07942 [hep-ph]].

Chapter 1

Introduction

The exploration of the physics of heavy quarks, that is, bottom and top quarks, is among the core issues of elementary particle physics. Precision measurements of observables related to these quarks allow for stringent tests of the Standard Model (SM) and for searches of new interactions. On the other hand they constitute also an important background to a number of new physics searches. The topic of this thesis is devoted to the precision physics of top and bottom quarks at (future) e^+e^- colliders. We analyze heavy quark-antiquark ($Q\bar{Q}$) pair production in e^+e^- collisions,

$$e^+e^- \to \gamma^*, Z^* \to Q\ \bar{Q} + X\,, \tag{1.1}$$

at the differential level at next-to-next-to-leading order (NNLO) perturbation theory in Quantum Chromodynamics (QCD) and apply it to $t\bar{t}$ production above the pair-production threshold and to $b\bar{b}$ production at the Z resonance.

Before outlining the contents of this thesis, let us briefly review some major results on the physics of top and bottom quarks. As to the top quark, much insight into the properties and interactions of this quark has been gained in recent years by the experiments ATLAS and CMS at the Large Hadron Collider (LHC), improving significantly the explorations at the Tevatron, where the top quark was discovered [1, 2]. The LHC is a top-quark factory. Millions of top-antitop ($t\bar{t}$) pairs have been produced at this machine, predominantly by QCD interactions.

In addition, (anti)top quarks have also been produced in abundance singly at the LHC. In single top production, which mainly proceeds via the t-channel, tW-, and s-channel modes, electroweak interactions are involved. The $t\bar{t}$ production cross section has been measured at 7, 8, and 13 TeV center-of-mass energy and the experimental results agree well with the respective QCD predictions at NNLO [3] in the perturbative expansion in the QCD coupling α_s. At present both the experimental and the theoretical precision on $\sigma_{t\bar{t}}$ is $\lesssim 5\%$. The experimental results on single (anti)top production at the Tevatron and the LHC are also in agreement with QCD predictions [4–6].

The top quark is special compared to other quarks because it decays before it can form hadrons. Thus it provides a 'laboratory' for studying the interactions of a bare quark. The top quark decays by almost hundred percent via $t \to bW$ with the subsequent decay of the W boson into leptons $W \to \ell\nu_\ell$ or to quarks $W \to q\bar{q}'$ which fragment to hadrons that form hadronic jets. The Cabibbo-Kobayashi-Maskawa suppressed decay modes $t \to qW$, $q = s, d$, which have branching ratios $Br \lesssim 10^{-3}$, have not yet been observed – nor have any non-standard top-decay modes been found. If one wants to explore the properties and interactions of top quarks in $t\bar{t}$ production at hadron colliders, the two important signal channels are the dileptonic and lepton + jets channels, that is, $t\bar{t} \to \ell^+\nu_\ell\ell'^-\bar{\nu}_\ell b\bar{b}$ and $t\bar{t} \to \ell^+\nu_\ell b\bar{b}q\bar{q}' + \text{c.c.}$. By using templates for fits to the top-quark invariant mass distribution that were measured in these channels, experiments at the Tevatron and the LHC measured the top quark mass with high precision. The average (taken in the year 2014) of values determined with this method and with other variables yields $m_t^{\text{exp}} = 173.34 \pm 0.76$ GeV [7]. This means at first sight that the mass of the top quark is more precisely known than that of any other quark, but the question is what is the precise definition of this mass parameter? Strictly speaking it is the mass parameter that is contained in the Monte Carlo programs that are used to compute the templates for the fits to data. Yet, it is quite common to identify this mass with the top-quark mass defined in the on-shell scheme, because this mass definition is the natural choice for the predominantly on-shell production and decay of a 'bare' quark. Approaches which are conceptually more satisfactory use an observable that is computed beyond leading-order QCD, for example the $t\bar{t}$ cross section, and express this observable in terms of the on-shell mass m_t or the short-distance top-mass parameter in the $\overline{\text{MS}}$

scheme, $\overline{m}_t(\mu)$. Fits to data yield m_t or $\overline{m}_t(\overline{m}_t)$, but at present the error on these parameters is larger by a factor $\gtrsim 3$ (see, for example [8]) than the error on $m_t^{\rm exp}$ given above. For a discussion concering the interpretation of top-mass measurements, see for example [9].

Top-quark production and decay has been investigated at the level of differential distributions, including top-spin effects, at the Tevatron and in much more detail at the LHC. So far the experimental results agree with the SM predictions. (For recent reviews, see [10–12].) One observable has received considerable attention in recent years, namely the top-quark forward-backward asymmetry measured in $t\bar{t}$ production at the Tevatron. At the Tevatron, which is a proton antiproton collider, top quarks are produced predominantly in the hemisphere defined by the direction of the proton beam. The asymmetry observable, which turned out to be the most useful one, is defined by $A_{\rm FB}^t = (N_F - N_B)/(N_F + N_B)$, where N_F and N_B are the number of $t\bar{t}$ events where the rapidity difference $\Delta y \equiv y_t - y_{\bar{t}}$ is larger and smaller than zero, respectively. While the latest $A_{\rm FB}^t$ measurement of the D$\emptyset$ collaboration [13] is in reasonable agreement agreement with SM predictions at next-to-leading order (NLO) QCD including electroweak corrections [14–16], the $A_{\rm FB}^t$ measurements of the CDF collaboration persistently showed deviations from these predictions. The CDF measurement [17] of $A_{\rm FB}^t$ as a function of the $t\bar{t}$ invariant mass, $M_{t\bar{t}}$, is at high $M_{t\bar{t}}$ about $2\sigma - 3\sigma$ above the NLO SM results. This triggered the publication of a large number of articles that aimed at explaining this seeming discrepancy with new physics effects. (For a review, see [18].) However, it was shown in ref. [19] that the NNLO QCD corrections to $A_{\rm FB}^t$ are substantial and that after inclusion of these corrections the SM prediction is only about 1.5σ below the CDF result.

At the LHC the top-quark forward-backward asymmetry $A_{\rm FB}^t = 0$ because the initial pp state is symmetric under rotations that put the beam axis into the opposite direction. Inspecting the $t\bar{t}$ events produced at the LHC, more t than $\bar{t}$ are produced in the forward and backward regions, while there are more $\bar{t}$ than t in the central region. Thus one can define a charge asymmetry $A_C = (N_> - N_<)/(N_> + N_<)$, where where $N_>$ and $N_<$ are the number of $t\bar{t}$ events where the difference of the moduli of the rapidities, $\Delta|y| \equiv |y_t| - |y_{\bar{t}}|$ is larger and smaller than zero, respectively. The asymmetry A_C is quite small in the SM. It was measured by the ATLAS and CMS experiment [20, 21] and the experimental results agree with the NLO SM

predictions [15, 16]. The lesson to be learned from the experimental and theoretical investigations of $A_{\rm FB}^t$ and A_C is that (differential) observables such as these asymmetries are important for getting insight into the $t\bar{t}$ production dynamics, provided that respective precision SM predictions are available.

For quite some time, there have been plans for a high-energy linear e^+e^- collider [22]. Such plans have been pursued further in recent years in the context of the ILC design [23] and CLIC design [24]. Also a high-energy circular e^+e^- collider is under discussion [25]. The core physics issues of these e^+e^- colliders include the exploration of the production of $t\bar{t}$ pairs and their decays [22, 23, 25–27]. In view of the detailed information about the properties and interactions of the top quark that the LHC has provided and will provide in the future, what can be done better at a high-luminosity e^+e^- collider? Simulation studies indicate that measurements of the reaction $e^+e^- \to t\bar{t}$ in the threshold region and in the continuum allow to precisely determine a number of key observables associated with the top quark, including its mass, its width, its Yukawa coupling to the 125 GeV Higgs resonance, and its electroweak neutral current couplings (see, for example, the recent reviews [26, 27] and references therein). An energy scan of the $t\bar{t}$ cross section in the threshold region and a fit to the SM prediction of $\sigma_{t\bar{t}}(s)$ allows to determine the top mass (defined in a so-called threshold mass scheme and then converted to the $\overline{\rm MS}$ scheme) with an unprecedented precision of about $\delta\overline{m}_t \lesssim 100$ MeV. Moreover, also the total top-quark width Γ_t can be obtained from such a fit (for instance, using the lepton + jets decay channels) with an expected uncertainty of $\delta\Gamma_t/\Gamma_t \simeq 15\%$. At the LHC a direct measurement of Γ_t is not possible with reasonable precision because the width of the top quark is much smaller than the experimental resolution that can be achieved at a hadron collider. (In the SM the top width is predicted to be $\Gamma_t \simeq 1.3$ GeV at NNLO QCD including electroweak and finite W-width corrections [28–30]. The value of Γ_t depends on the value of the top mass.) Also for $t\bar{t}$ production in the continuum the top-quark mass and the top width can be determined precisely if the measurements of the top-quark invariant mass distribution in the fully hadronic and lepton + jets decay channels of $t\bar{t}$ are combined. Ref. [31] found by Monte Carlo simulation that a precision of $\delta m_t \simeq 100$ MeV and $\delta\Gamma_t/\Gamma_t \simeq 16\%$ can be achieved in this way. Such a measurement in the continuum would allow to extract the top-quark mass in the on-shell scheme,

provided one would use templates computed beyond leading-order QCD. It would certainly be valuable, from the point of view of assessing systematic errors, to get precise values of the top mass from measurements at threshold and in the continuum, where different methods will be used. As is well known, measuring the top mass as precisely as possible is not an idle effort, because it is an important parameter, together with the W-boson and Higgs-boson mass, for testing the consistency of the Standard Model at the loop level. The exchange of the 125 GeV Higgs boson H between t and $\bar{t}$ leads to a dependence of $\sigma_{t\bar{t}}$ on the top Yukawa coupling h_t. From a high-precision scan of $\sigma_{t\bar{t}}(s)$ and measurements of other top-quark observables in the threshold region one expects that h_t can be extracted with a precision of about 5% [26, 27]. The associated production $e^+e^- \to t\bar{t}H$ (which has a threshold of approximately 500 GeV) allows to measure h_t with a precision of about 10%, depending on the luminosity of the collider. A further asset of high-energy e^+e^- colliders concerning top physics is that the neutral current couplings of the top-quark can be determined much more precisely than at the LHC. At the LHC these couplings can be measured in the associated production of $t\bar{t}Z$ and $t\bar{t}\gamma$. These are rare processes compared to the production of $t\bar{t}$ (+ jets). Therefore, the precision with which these production modes can be analyzed is limited due to the large background. On the contrary, in $e^+e^- \to Z^*, \gamma^* \to t\bar{t}$, the cross section, the top-quark forward backward asymmetry, and differential distributions can be measured precisely both near and (far) above the $t\bar{t}$ threshold. This allows for very precise measurements of the neutral current couplings of the top quark and searches for new physics effects in the $Z^*t\bar{t}$ and $\gamma^*t\bar{t}$ vertices at several center-of-mass energies [32–36].

Obviously, precise predictions are required on the theoretical side in order to achieve this precision in the analysis of future data from the planned e^+e^- colliders. A large effort has been made to investigate $t\bar{t}$ production at threshold. At present the threshold cross section is known at next-to-next-to-next-to-leading order QCD [37]. The higher-order SM results that were obtained so far for $t\bar{t}$ production in the continuum do not match these efforts. This has served as a motivation to analyze in this thesis the production of $t\bar{t}$ pairs, or more general the production of massive quark- antiquark pairs, above the pair-production threshold at the differential level at NNLO QCD.

Next, let us briefly address some aspects of the physics of b quarks. Contrary to top quarks bottom quarks hadronize to $b\bar{b}$ mesons, B mesons, and b-baryons before they decay. Especially the weak decays of B mesons and b-baryons have been for years a vast field of experimental and theoretical research. At present the experimental research is pursued at the B factories SuperKEKB in Japan and LHC (CERN). The multitude of weak B decays, including rare decays, that have been experimentally analyzed with high precision, provide deep insights into the flavor structure of the weak interactions. In particular these weak decays offer a window to new physics at high energy scales through possible virtual new heavy particle exchanges in the respective decay amplitudes. Most of the experimental data agree well with SM predictions; see, for example, the reviews [38–42]. Yet, several tensions and discrepancies between experimental results and SM predictions exist [42], especially in B decays induced by $b \to s\ell^+\ell^-$ [43–50]. It remains to be seen whether these tensions will persist in the future or disappear by improved experimental and theoretical results.

Bottom quarks and $b\bar{b}$ pairs that are produced in high-energetic hard reactions fragment and form hadronic jets. The physics of b-jets can be described, usually in a large kinematic region, by (higher-order) perturbative QCD, supplemented by Monte Carlo programs that describe parton showering and hadronization. At the LHC, hard reactions that involve b quarks, for instance b-flavored dijets [51] or the associated production of a b jet and an electroweak gauge boson [52] allow for tests of the SM in the high-energy regime. These processes constitute also a background to new physics searches. At the e^+e^- colliders LEP1 and SLC, which are no longer in operation, the experimental and theoretical results on $Z \to b\bar{b}$ received a considerable amount of attention, especially in the context of high-precision analysis of the electroweak sector of the Standard Model. The b-quark forward-backward asymmetry at the Z resonance, which is the most precisely measured quark asymmetry at $\sqrt{s} = m_Z$, was determined with an accuracy of 1.7% [53–55]. This allowed a very precise extraction of $\sin^2\theta_{eff}$. However, among the measured set of precision observables at the Z pole, this observable shows the largest deviation, about 2.5σ, from the respective Standard Model global fit [56]. So far, it has not been clarified whether this deviation is due to underestimated experimental and/or theoretical uncertainties or whether it is a hint of new physics. At a future linear or circular e^+e^- collider [22, 23, 25],

precision determinations of electroweak parameters will again involve forward-backward asymmetries $A_{\rm FB}^f$, where f = quark or lepton. If such a collider will be operated at the Z peak, an accuracy of about 0.1 percent may be reached for these observables [57, 58]. The persistent discrepancy between experiment and theory on $A_{\rm FB}^b$ at the Z pole and the prospects for its improved measurement at a future e^+e^- collider are the motivation to consider in this thesis, besides $t\bar{t}$ production for $\sqrt{s} > 2m_t$, also $b\bar{b}$ production at the Z resonance and make improved predictions at NNLO QCD at the differential level, especially for $A_{\rm FB}^b$.

Before coming to the contents of this thesis, we recapitulate existing theoretical results for $e^+e^- \to Q\bar{Q}$ ($Q = t, b$) in the continuum within the SM. Differential predictions at next-to-leading order (NLO) QCD have been known for a long time for $Q\bar{Q}$ [59] and $Q\bar{Q}$ + jet [60–65] final states. Also the NLO electroweak corrections are known [66–69]. The production of $Q\bar{Q}$ in an arbitrary spin configuration was computed at NLO QCD in [70, 71]. Off-shell $t\bar{t}$ production and decay including non-resonant and interference contributions at NLO QCD was investigated in [72]. The total $Q\bar{Q}$ cross section $\sigma_{Q\bar{Q}}$ was computed to order α_s^2 and order α_s^3 in [73–76] and [77], respectively, using approximations as far as the dependence of $\sigma_{Q\bar{Q}}$ on the mass of Q is concerned. A calculation of the total cross section of $e^-e^+ \to \gamma^* \to Q\bar{Q}$ with full quark-mass dependence was made in [78]. A computation of the cross section and of differential distributions for $t\bar{t}$ production at order α_s^2 with full top-mass dependence was reported in [79, 80]. This calculation is are based on a NNLO generalization of a phase-space slicing method [81, 82]. As to the b-quark forward-backward asymmetry at the Z resonance, the fully massive next-to-leading order electroweak and QCD corrections were determined in [83–85] and in [59, 86, 87], respectively. The order α_s^2 corrections were calculated so far only in the limit of vanishing b-quark mass [88–91].

In this thesis we set up a formalism within the antenna subtraction framework for calculating the electroweak production of a massive quark-antiquark pair in e^+e^- collisions (1.1) at order α_s^2 and to lowest order in the electroweak couplings. We apply our general results to the production of top-quark pairs above the $t\bar{t}$ production threshold and to the production of $b\bar{b}$ pairs at the Z resonance. Our approach is fully differential and applies to any infrared-finite observable. We calculate the respective production cross sections at NNLO QCD and a number of differ-

ential distributions, some of which were not determined before. In particular we compute, at order α_s^2, the top-quark forward-backward asymmetry as a function of the e^+e^- center-of-mass energy and, for the first time, the NNLO QCD corrections to the b-quark forward-backward asymmetry at the Z pole for a *massive* b quark both with respect to the quark and the thrust direction. Also the phenomenological implications of this result are briefly discussed.

The contents of this thesis is organized as follows. In the next section we briefly review existing methods for handling soft and collinear divergences that appear in the individual contributions to differential cross sections beyond leading-order QCD, or more general, in quantum fields theories that contain massless particles. In particular we discuss some salient features of the antenna subtraction method. Section 3 contains a detailed exposition of our antenna-subtraction formalism that allows to compute the differential cross section and distributions of IR-safe observables at order α_s^2 for the reactions (1.1). In section 4 we apply this formalism first to top-quark pair production above the $t\bar{t}$ threshold. We compute the total $t\bar{t}$ cross section and a number of differential distributions. Then we apply it to $b\bar{b}$ production at the Z pole and compute the cross section, the distribution of the transverse momentum of the b quark, and the $\cos\theta$ distribution associated with the b-quark direction and the oriented thrust direction. In section 5 we compute the t-quark forward-backward asymmetry at NNLO QCD for several center-of-mass energies above the $t\bar{t}$ threshold. Moreover we calculate b-quark forward-backward asymmetry at NNLO QCD for a massive b quark, both for the quark axis and the thrust axis definition of $A_{\rm FB}^b$. Then we compute $A_{\rm FB}^b$ for $m_b \to 0$ and show that our results agree in this limit with existing results on $A_{\rm FB}^b(m_b = 0)$. Finally we briefly discuss phenomenological implications of our new result on $A_{\rm FB}^b(m_b \neq 0)$ at NNLO QCD. We conclude in section 6. In appendix A some formulas used in thesis are collected, including our conventions for electroweak coupling factors, relevant renormalization constants, and the matching relation for the $\overline{\rm MS}$ coupling α_s defined for n_f and $(n_f + 1)$ quark flavors. Appendix B contains details about our momentum mappings in the 3- and 4-particle phase spaces with massive quarks required for the antenna subtraction terms at NLO and NNLO QCD. Appendix C contains our procedure of computing rotated momenta of the massless partons that are used in the construction of the antenna-subtracted squared matrix elements for the $Q\bar{Q}q\bar{q}$ and $Q\bar{Q}gg$ final states.

Chapter 2

Methods for handling IR divergences

Models of elementary particles and their interactions are in general (but not exclusively) formulated in terms of local quantum field theories (QFT). The main method to evaluate QFTs, in particular for computing particle reactions, is perturbation theory in powers of coupling constant(s), provided these couplings are sufficiently small. This method is applicable to QCD at sufficiently high energies and to the Standard Model electroweak interactions.

Amplitudes in local QFTs are in general divergent beyond the tree-level approximation, These divergences in loop amplitudes are caused by short-distance singularities, i.e., ultraviolet (UV) singularities, and they can be removed by local counterterms. In a renormalizable QTF there is, to arbitrary order of perturbation theory, a finite number of counterterms of different structure, and these counterterms can be absorbed by redefining the couplings, masses, and fields of the theory. In particular, this is the case in the SM based on the gauge group $\mathrm{SU}(3)_c \times \mathrm{SU}(2)_L \times \mathrm{U}(1)_Y$. Moreover, the equal number of $\mathrm{SU}(2)_L$ quark and lepton doublets and singlets ensures that the electroweak chiral gauge currents and thus the SM are anomaly-free (see, for example the textbook [92]). In the following we are not concerned with UV singularities. SM amplitudes, in particular QCD amplitudes considered below are assumed to be renormalized.

2.1 Infrared divergences and factorization

In QFTs that contain massless particles, such as QED and QCD, scattering amplitudes can suffer from other types of divergences that occur when the energy of a massless particle becomes arbitrarily small (soft mode) or when two (or more) massless particles become collinear. These soft and collinear divergences, which are collectively called infrared (IR) divergences, appear both in real emission and in virtual-correction amplitudes.

Let us briefly recapitulate the structure of soft divergences in a real emission amplitude in QED and QCD. Consider first in QCD a n-particle real emission amplitude M_n where a gluon that is radiated from an outgoing external quark becomes soft, as depicted in figure 2.1a. Then, by neglecting the soft gluon momentum in the numerator of the quark propagator, the matrix element M_n shows the well-known eikonal factorization:

$$M_n \quad \stackrel{k^\mu \to 0}{\longrightarrow} \quad g_s \frac{p^\mu \varepsilon^*_\mu(k)}{p \cdot k + i\epsilon} T^a \bar{u}(p) M_{n-1} \,, \tag{2.1}$$

where g_s is the QCD coupling and T^a is a generator of $\mathrm{SU}(3)_c$ in the fundamental representation. Eikonal factors analogous to the one in (2.1) apply when a soft gluon is radiated from a final-state antiquark or a (anti)quark from the initial state. When a soft gluon with four-momentum k_1 color label a_1 is radiated from an external gluon with four-momentum k_2 color label a_2 as illustrated in figure 2.1b, an associated n-particle matrix element M_n behaves as

$$M_n \quad \stackrel{k_1^\mu \to 0}{\longrightarrow} \quad g_s [T^{a_2}, T^{a_1}] \frac{k_2^\mu \varepsilon^*_\mu(k_1)}{k_1 \cdot k_2 + i\epsilon} \varepsilon^*_\nu(k_2) M^\nu_{n-1} \,. \tag{2.2}$$

In QED (or, more general, in an abelian gauge theory), when a soft photon is emitted from an external charged outgoing fermion with charge Qe, the eikonal factorization formula (2.1) applies with $g_s \to Qe$ and $T^a \to 1$. Obviously there is no analogue of Eq. (2.2) in QED. The eikonal factors in Eq. (2.1) and in Eq. (2.2) show that the emission of a soft gluon does not affect the spin and the momentum of the radiating parton. But it changes its color, because also a soft gluon carries color charge. As the color factors (2.1) and (2.2) signify, soft gluon emission from different external parton lines leads to color correlations in the squared S matrix

element.

In the case of QED, the eikonal factors are uncorrelated. The amplitude of a hard process involving charged particles is corrected, for each emission of a soft photon from an external charged particle line, by an eikonal factor that is independent of the eikonal factors associated with soft photon emission from other external charged particle legs. The eikonal identity (see, for example, [92]) guarantees that this factorized product of independent eikonal factors amounts to taking into account all possible permutations among the soft photons in the soft limit[1]. The eikonal factors can be summed up and exponentiate [94–96]. The exponential correction factor is known as the Sudakov form factor.

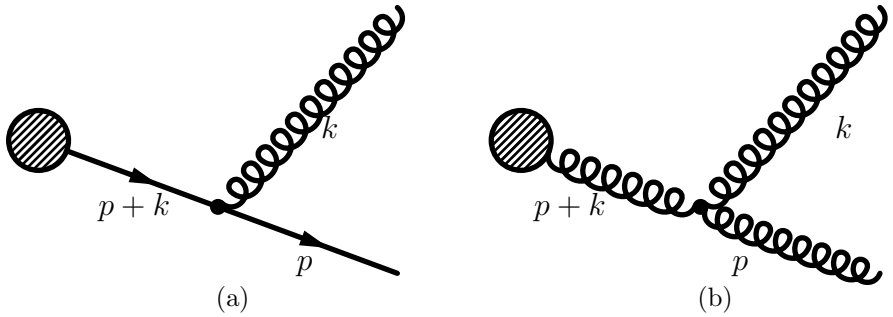

Figure 2.1: Soft gluon (photon) radiation from an outgoing quark (charged fermion) (a) and soft gluon radiation from an external gluon (b).

The QCD amplitudes have also a factorized structure when a soft gluon is emitted, although their structure is not as simple as in QED, as can already be seen from Eq. (2.2). The pattern of this soft-gluon factorization is embodied in the following generic formula:

$$M_n^a|_{q\to 0} \;\cong\; \varepsilon_\mu^*(q)\; \mathrm{J}^{a,\mu}(q)\; M_{n-1}\,, \tag{2.3}$$

where with M_n^a denotes a n-particle amplitude and q^μ is the momentum of the radiated soft gluon with polarization-vector $\varepsilon_\mu(q)$ carrying color index a. (Other color indices are suppressed.) The symbol $\cong$ means that on the right-hand side contributions that are less singular than $1/q$ in the limit $q \to 0$ are neglected. The current J_a^μ which is implicitly defined through this factorization formula is called the eikonal current. Its tree-level form can be read off from

[1]In QED the eikonal-factorized amplitudes can be reproduced by a semi-classical Wilson-line factor (also called gauge-link operator) attached onto the amplitude of the hard process [93].

Eq. (2.1) and Eq. (2.2). Factorization formulas analogous to (2.3) hold for multiple soft gluon emissions from tree-level QCD amplitudes [97]. For the emission of a soft masslees $q\bar{q}$ pair, a factorization formula can be derived for squared amplitudes [97]. The eikonal current for the emission of a soft gluon at 1-loop in massless QCD and QCD with massive quarks was studied and derived in [98–101] and in [102], respectively. The factorization of two-loop QCD amplitudes when a soft gluon is radiated was analyzed in [103, 104].

Likewise, when two (or more) massless partons become collinear, for instance, in the splitting of a gluon into two gluons or into a massless quark-antiquark pair, QCD amplitudes also factorize. The ensuing infrared singularities in squared tree-level amplitudes are accounted for by collinear splitting functions [105] (see, for instance, [106] for a review). Factorization of one-loop amplitudes in collinear limits were studied extensively in the literature, including refs. [98, 107–109]. Collinear factorization may also be formulated at the level of amplitudes, rather than squared amplitudes. At tree-level this was analyzed in [106, 110, 111] and at one loop in [100, 112]. (These papers used the decomposition of a QCD amplitude into a sum of independent color ordered partial amplitudes times color factors.) For an n-point QCD amplitude M_n collinear factorization can be schematically written as (cf. for example [113])

$$M_n|_{p_1||\cdots||p_m} \;\cong\; \mathrm{Sp}\,(p_1,\cdots,p_m)\;\; M_{n-m}\,, \tag{2.4}$$

where Sp is the splitting amplitude and $p_1,\cdots,p_m$ are the external momenta of massless partons which become collinear. Color and polarization indices are suppressed. Beyond leading order both M_{n-m} and Sp have a perturbative expansion in α_s such that the right-hand side matches the perturbative order of M_n. The factorization property refers to the feature that the factor $\mathrm{Sp}\,(p_1,\cdots,p_m)$, has no dependence on any of the non-collinear momenta involved in the above amplitude. The meaning of the symbol $\cong$ is as in Eq. (2.3). At tree-level, squaring Sp and summing over polarizations recovers the Altarelli-Parisi splitting functions. Note that, unlike the soft current defined in the soft factorization formula Eq. (2.3), the splitting amplitudes introduced in (2.4) do depend on the spin of the splitting parent particle. This spin dependence translates, after squaring the amplitude, into azimuthal spin correlations in the un-averaged splitting functions. We will come back to this issue in section 3.3 when we discuss such angular

terms in the context of antenna subtraction method.

Soft and collinear factorization is the basis for the methods of handling the IR singularities that appear in individual contributions to (differential) cross sections beyond the leading order. Before we discuss such methods, we briefly recapitulate the general theorems that state the prerequisites for the IR-finiteness of cross sections or expectation values of observables at arbitrary orders of QCD perturbation theory.

2.2 Bloch-Nordsieck, KLN, and factorization theorem

Infrared singularities that appear in QFTs with massless quanta beyond the leading perturbative order cancel, in general, only in the computation of sufficiently inclusive physical quantities when the real and virtual contributions are combined. Let's consider here for definiteness a physical cross section.

In QED with massive charged particles, the idea of solving the IR divergence problem goes back to Bloch and Nordsieck [114], which is now called the Bloch-Nordsieck theorem. It states that in the computation of a physical quantity the IR singularities cancel if one sums the contributions from energy-degenerate final states. For instance, if one considers the production cross section of a muon pair $\mu^+\mu^-$ beyond the leading order in the QED coupling α one has to sum up the incoherent contributions from the final states $\mu^+\mu^-$ and $\mu^+\mu^- + n$ soft photons, where n depends on the order of perturbation theory. On the experimental side this corresponds to the fact that a cross section can be measured only wih a finite (i.e., non-zero) energy resolution. The all-order proof [94–96] of the Bloch-Nordsieck theorem rests on the exponentiation of the soft photon eikonal factors discussed above.

In QCD, where besides soft also collinear singularities due to gluons or massless quarks appear, the Bloch-Nordsieck theorem does not hold in general. However, if the initial state is colorless (that is, if there is no QCD radiation from the initial state), for instance $e^+e^- \to$ hadrons, then summing over kinematically degenerate final states that include soft and collinear massless parton radiation leads to IR finite cross sections [115], for example multi-jet cross sections provided an IR-safe jet algorithm is used.

The Kinoshita-Lee-Nauenberg (KLN) theorem [116,117] extends the Bloch-Nordsieck theorem and applies to unitary QFTs with massless particles that lead to soft and collinear divergences. The KLN theorem states states that an IR-finite physical quantity is obtained in such a QFT if one sums over all kinematically degenerate final *and* initial states. For a proof, see [118].

The KLN theorem applies in particular to QCD but is only of formal interest, because in practice one does not sum over degenerate initial states when computing an observable. Let's consider a cross section in QCD associated with hadronic collisions. Using the parton model such a cross section is related to cross sections $\hat{\sigma}$ of hard partonic reactions $a_1+a_2 \to b_1+\ldots+b_n$, where a_1 and a_2 denotes a gluon or a massless (anti)quark, and $b_1,\ldots b_n$ denote hard (i.e. energetic and non-collinear) gluons and/or hard massless or massive (anti)quarks. If one wants to obtain an IR-finite partonic cross section $\hat{\sigma}$ beyond LO QCD, then according to the KLN theorem, one has to sum not only the contributions from kinematically degenerate final states in the appropriate order of perturbation theory, but also from degenerate initial states. That is, in addition to contributions from the initial state $|a_1,a_2\rangle$ also contributions $|a_1,a_2\rangle$ plus soft incoming gluons/massless $q\bar{q}$ pairs and from $|a_1,a_2\rangle$ plus incoming massless partons that are collinear to a_1 and/or a_2 must be taken into account. This is impractical and not in the spirit of the parton model.

If one sums all kinematically degenerate final-state contributions to the hard parton reaction $a_1+a_2 \to b_1+\ldots+b_n$ (where a_1,a_2 are massless partons) then all IR singularities cancel in $\hat{\sigma}$, except those associated with collinear initial-state singularities. Fortunately, these surviving collinear singularities do obey a nice factorization property (to arbitrary order in α_s). They are universal in the sense that these singularities do not depend on the final state of the process, but only on the massless partons a_1 and a_2 in the initial state [119–122]. Therefore, these singularities can be absorbed into the parton distribution functions associated with a_1 and a_2 by a redefinition of these functions. This is the essence of the so-called factorization theorem [119–123] that is expected to hold to all orders in α_s for sufficiently inclusive quantities in hadron hadron scattering. (It can be proven elegantly for deep-inelastic lepton nucleon scattering using the operator product expansion, see for example [123].) The factorization theorem is the basis for the QCD-improved parton model and the QCD phenomenology at hadron

colliders and of lepton-nucleon scattering.

We close this section with a side remark that refers to processes $a_1 a_2 \to n$ beyond LO QCD with two massive quarks in the initial state. Summing over all degenerate final states and color-averaging of the initial state leaves, starting at two loops [124, 125], uncanceled initial-state soft singularities which are process-dependent. Thus a factorization theorem would not apply in this case. Unlike collinear radiation which pertains to a "locally" well-identified single parent object, soft (long-wavelength) gluon exchange can spread the color flow over (infinite) large distances, thus leading to (non-local) color correlations among colored particles in the squared S-matrix elements. This indicates that the concept of universal process-independent parton distribution functions inside one isolated hadron cannot be consistently introduced for massive quarks in hadron collisions at and beyond two-loop order. However, these uncanceled soft singularities are proportional to some power of the quark mass and thus disappear when the quark mass is put to zero.

2.3 IR subtraction and slicing methods

In this section we give a short overview of methods that have been developed for handling the IR divergences that appear in individual contributions to a physical quantity, for instance a differential cross section, at higher-order QCD. Cancellation of soft and collinear divergences are only guaranteed when contributions from real emission and virtual-correction amplitudes, that is, from contributions involving different final states are properly combined. It is standard to use dimensional regularization for regularizing the IR divergences of the various contributions, that is, to compute them in $D = 4 - 2\epsilon$ space-time dimensions. The methods to be discussed below have the purpose of modifying the individual contributions to a physical quantity such that they are separately finite in $D = 4$ dimensions, but of course the sum of the contributions must remain unchanged. The IR factorization properties of QCD amplitudes discussed above have been essential for the development of such 'IR-methods' that allow to compute arbitrary processes involving quarks, gluons, and uncolored particles at NLO and NNLO QCD at the differential level.

Methods at NLO QCD:

Let us first outline the essential features of the class of subtraction methods at NLO QCD. For definiteness we consider a hard reaction

$$a_1 + a_2 \longrightarrow b_1 + \ldots + b_n \,, \tag{2.5}$$

where the two particles in the initial state are either uncolored or a_1 and/or a_2 is a massless (anti)quark or gluon, and $b_1, \ldots, b_n$ denote massless or massive (anti)quarks and/or gluons. The n partons in the final state are assumed to be well identifiable, that is, resolved. Moreover, let's consider for definiteness an n-jet cross section. To LO QCD the partonic cross section is

$$\sigma_{\rm LO} \;\; = \;\; \int_n d\sigma_{\rm LO} \; \mathcal{F}_n^{(n)} \,, \tag{2.6}$$

where $d\sigma_{\rm LO} = \overline{|M_{0,n}|^2} d\Phi_n/(2s)$ and $M_{0,n}$ is the LO matrix element of the above process. Averaging and summing over the colors and spins of the particles in the initial and final state is understood. The symbol $\int_n$ denotes integration over the n-particle phase space. The jet-defining algorithm is encoded in the phase-space function $\mathcal{F}_J^{(n)}$. It specifies the procedure of how to build J jets via clustering out of n partons. (At LO $J = n$.) For simplicity we suppress in (2.6) and below the dependence of the matrix elements and $\mathcal{F}_J^{(n)}$ on the particle momenta. The essential property required for the jet-defining function is that it must be infrared safe. This means that this function should return the same result when applied to kinematically degenerate configurations. When in an $(n+1)$-parton final state one parton b_i becomes soft ($E_i \to 0$) or two partons b_i and b_j become collinear, then $\mathcal{F}_J^{(n+1)}$ must obey

$$\mathcal{F}_J^{(n+1)}(k_1, .., k_i = \lambda q, .., k_{n+1}) \;\; \longrightarrow \;\; \mathcal{F}_J^{(n)}(k_1, .., k_n) \quad \text{if} \quad \lambda \to 0 \,, \tag{2.7}$$

$$\mathcal{F}_J^{(n+1)}(k_1, .., k_i, .., k_j, .., k_n) \;\; \longrightarrow \;\; \mathcal{F}_J^{(n)}(k_1, .., k, .., k_n) \quad \text{if } k_i \to zk, \; k_j \to (1-z)k \,. \tag{2.8}$$

The phase-space function need not necessarily describe a jet cross section. If $\mathcal{F}_J^{(n)}$ is chosen to be 1 then Eq. (2.6) provides the cross section for the reaction (2.5). If $\mathcal{F}_J^{(n)}$ is chosen to be

a delta function in some kinematical variable, then Eq. (2.6) yields the respective differential distribution. In the determination of a forward-backward asymmetry one has to compute forward and backward cross sections with respect to a certain IR-safe direction. For such computations $\mathcal{F}_J^{(n)}$ is given by a respective step (theta) function. Phase-space cuts on the cross section can be implemented by choosing $\mathcal{F}_J^{(n)}$ to be a product of theta functions. If one wants to compute the expectation value of an observable one constructs $\mathcal{F}_J^{(n)}$ in terms of respective kinematical factors. As to jet cross sections, a number of IR-safe jet-defining algorithms were proposed and are available on the market. For an extensive reference see [126].

At next-to-leading order in α_s the LO cross section receives two types of corrections: real radiation corrections that involve $(n+1)$ partons in the final state, where the additional parton is massless, and virtual one-loop corrections to the Born amplitude. The n-jet cross section at NLO QCD is given by

$$\sigma_{\mathrm{NLO}} = \sigma_{\mathrm{LO}} + \sigma_1 \,, \tag{2.9}$$

where

$$\sigma_1 = \sigma_{n+1}^R + \sigma_n^V = \int_{n+1} d\sigma^R \; \mathcal{F}_n^{(n+1)} + \int_n d\sigma^V \; \mathcal{F}_n^{(n)} \,. \tag{2.10}$$

It is understood that all UV divergences have been renormalized in (2.10).

Both the real radiation and the virtual contributions to σ_1 are infrared divergent due to soft and/or collinear singularities. If the initial state i is uncolored, the IR divergences cancel in the sum (2.10) according to Kinoshita-Lee-Nauenberg theorem as discussed above. If the initial state consists of one or two massless quarks or gluons, uncanceled collinear singularities remain in (2.10). They result from the collinear emission of a massless parton from a parton in the initial state. As outlined above, the factorization theorem of QCD tells us that these collinear singularities are *universal*, that means they are independent of the specific process (2.5) (as long as one considers massless partons in the initial state) and can therefore be absorbed into the bare parton distribution function associated with the parton from which the collinear emission takes place.

The cancellation of soft and collinear divergences is obscured by the fact that the real and virtual corrections are associated with phase-spaces of different particle multiplicity. While infrared singularities in the virtual-corrections σ_n^V are obtained immediately in terms of poles in the dimensional regularization parameter ϵ after integration over the loop-momentum, it is less straightforward to identify and extract the IR singularities of the real emission contributions σ_{n+1}^R. Here the infrared singularities become explicit as poles in ϵ only after integrating the real radiation matrix elements over the phase-space regions related to unresolved radiations (appropriate to the jet-observable under consideration). Often this can be done only numerically, especially when additional phase-space cuts are applied.

The general idea that underlies the so-called subtraction methods to get around this (numerical) evaluation problem is to insert the identify $0 = \int d\sigma^{\mathcal{S}} - \int d\sigma^{\mathcal{S}}$ into Eq. (2.10). Let's first consider the case where the initial state is uncolored. Adding this zero on the right-hand side of Eq. (2.10) it can be reorganized in the following way:

$$\begin{aligned}\sigma_1 &= \int_{n+1} d\sigma^R \, \mathcal{F}_n^{(n+1)} + \int_n d\sigma^V \, \mathcal{F}_n^{(n)} + \left[\int_{n+1} d\sigma^{\mathcal{S}} - \int_{n+1} d\sigma^{\mathcal{S}}\right] \\ &= \int_{n+1} \left[\left(d\sigma^R \, \mathcal{F}_n^{(n+1)}\right)_{\epsilon=0} - \left(d\sigma^{\mathcal{S}}\right)_{\epsilon=0}\right] + \int_n \left[d\sigma^V \, \mathcal{F}_n^{(n)} + \int_1 d\sigma^{\mathcal{S}}\right]_{\epsilon=0} . \end{aligned} \tag{2.11}$$

The unintegrated subtraction term $d\sigma^S$, living in the $(n+1)$-particle phase space as $d\sigma^R$, must be constructed such that it has the same singular behavior in all single unresolved regions of the $(n+1)$-particle phase space. The single unresolved regions are those where a gluon becomes soft or two massless partons become collinear. Hence by construction, $d\sigma^S$ cancels point-wise the IR singularities of $d\sigma^R$, i.e., it acts as a local counterterm. Therefore, as indicated in the first term of the last line of Eq. (2.11) both the evaluation of the two integrands in the square bracket and the $(n+1)$-particle phase-space integration can be done in $D = 4$ dimensions. The last term in the second square bracket in the last line of Eq. (2.11), $\int_1 d\sigma^{\mathcal{S}}$, denotes the integration of the subtraction term over the unresolved phase-space regions. This must de done in $D \neq 4$ dimensions. This integration produces $1/\epsilon$ and possibly also $1/\epsilon^2$ poles that cancel the IR poles contained in $d\sigma^V \, \mathcal{F}_n^{(n)}$. The remaining integration over the n-particle phase-space can then be done in $D = 4$ dimensions. Thus the two terms in the last line of Eq. (2.11) and

hence the NLO QCD correction σ_1 are IR finite in $D = 4$ dimensions.

The integration $\int_1 d\sigma^{\mathcal{S}}$, which must be done in $d \neq 4$ dimensions and should be done preferably in analytic fashion, is the main technical complication of the subtraction method. The integration is possible by exploiting the factorization of the soft and collinear singularities in the construction of $d\sigma^R$. Moreover, the jet function that is contained in $d\sigma^{\mathcal{S}}$ is constructed to be a function of the momenta of n resolved partons. These four-momenta are obtained by a momentum mapping from the $(n+1)$-parton to the phase-space of n resolved partons. This mapping should be constructed such that, in terms of the remapped momenta, the $(n+1)$-parton phase-space measure factorizes into a product of an n-particle phase space element associated with the resolved partons and a measure for the unresolved one-parton phase-space. This allows the analytic integration of $\int_1 d\sigma^{\mathcal{S}}$. We shall outline this in somewhat more detail below.

If the initial state in the reaction (2.5) contains one or two partons, then $d\sigma^{\mathcal{S}}$ is again constructed such that all soft and collinear singularities in $d\sigma^R$ associated with massless parton radiation in the final and initial state are cancelled point-wise. In this case uncanceled initial-state collinear singularities remain in $[d\sigma^V \; \mathcal{F}_n^{(n)} + \int_1 d\sigma^{\mathcal{S}}]$ which can be absorbed into the bare parton distribution functions associated with the partons in the initial state. Technically this can be implemented by adding a so-called collinear counterterm $d\sigma^C$ to $\sigma_{\rm NLO}$. In this case the NLO correction σ_1 to the LO parton cross section is replaced by a 'subtracted' correction $\tilde{\sigma}_1$ given by

$$\sigma_1 \longrightarrow \tilde{\sigma}_1 = \int_{n+1} \Big[\left(d\sigma^R \; \mathcal{F}_n^{(n+1)}\right)_{\epsilon=0} - \left(d\sigma^S\right)_{\epsilon=0} \Big] + \int_n \left[d\sigma^V \; \mathcal{F}_n^{(n)} + d\sigma^C + \int_1 d\sigma^S \right]_{\epsilon=0} . \quad (2.12)$$

The criteria stated above that the subtraction term $d\sigma^S$ must fulfill does not fix it uniquely. Consequently, a number of subtraction methods have been developed. An early version can be found in [127] where the NLO corrections to the three-jet cross section in e^+e^- collisions in massless QCD were computed. The most widely used subtraction method that applies to any process at NLO QCD is the dipole subtraction method. It was developed for massless QCD in [128] and extended in [129,130] to the case where the final state contains also massive colored particles. The strategy of the dipole subtraction method is to keep the subtraction term rather

simple. In general $d\sigma^S$ consists of a sum of terms. Each term is the product of a function which contains the soft and/or collinear singularities of the squared tree-level matrix element M_{n+1} and a squared tree-level matrix element M_n that depends on the redefined momenta of the n resolved partons. All integrals $\int_1 d\sigma^{\mathcal{S}}$ can be done analytically in $D \neq 4$ dimensions [128, 130] and thus all IR ϵ poles can be canceled in analytic fashion. Slight modifications of this method which allow for a more efficient numerical implementation were developed in [131–135]. For the decay of a massive colored particle, for instance, the top quark, the method was worked out at NLO in [136, 137]. Other NLO subtraction methods include those of [138–142] and the antenna subtraction method [143–145] that will be discussed in more detail in the next section.

Within the so-called phase-space slicing method the NLO QCD corrections to a process like (2.5) are computed as follows. Let's consider for simplicity the case where the initial state is uncolored. The $(n+1)$-parton phase-space of the real radiation contribution is decomposed as follows. When the additional parton is a gluon and becomes soft, the soft region is defined by the requirement that the scaled gluon energy in the c.m. frame of the initial state, $x_g = 2E_g/\sqrt{\hat{s}}$, is smaller than some cut parameter $x_{\min}$, where $x_{\min} \ll 1$. In the soft gluon region one uses the eikonal approximation for the real radiation matrix element M_{n+1} and the soft limit of the D-dimensional phase-space measure $d\Phi_{n+1}$ and integrates the squared matrix element approximated in this way over the soft gluon region $x_g \leq x_{\min}$. The result contains poles in ϵ and depends on $x_{\min}$. Likewise, one can use the parameter $x_{\min}$ to define the collinear region(s) of the $(n+1)$-parton phase-space – if there are such regions depending on the final state – and one uses the collinear approximation of the squared matrix element M_{n+1} and of the phase-space measure in D dimensions and integrates over the collinear region(s). Also this result contains poles in ϵ and depends on $x_{\min}$. If one combines the virtual corrections and the real-radiation contributions from the soft and collinear regions, the ϵ poles cancel, but the sum depends on the arbitrary slicing parameter $x_{\min}$. The remaining task is to integrate the real radiation matrix element M_{n+1} over the hard radiation region, that is, the non-soft and non-collinear region. This integration is finite and can be done in $D = 4$ dimensions, but the result also depends on $x_{\min}$. Now the parameter $x_{\min}$ has to be chosen such that the sum of the virtual, soft, collinear, and hard contributions to the NLO QCD correction is to

very good approximation independent of this parameter. Usually this requires a sequence of calculations for several values of $x_{\min}$. Ideally $x_{\min} \to 0$, but if $x_{\min}$ is chosen to be too small one runs into numerical instabilities. A nice feature of the phase-space slicing method is that no momentum mappings are necessary. On the other hand, beyond NLO the decomposition of the real-radiation phase-spaces becomes in general very complicated, which has prohibited so far an extension of this method to NNLO QCD. Early versions of the method at NLO QCD include [115, 146]. A systematic outline of the method for massless QCD and uncolored initial states at NLO was given in [147]. The method was used in [148] to compute the NLO QCD corrections to hadronic $t\bar{t}$ production. In this case also a collinear counterterm as in (2.12) is required.

Methods at NNLO QCD:

The NNLO QCD contribution $d\sigma_2$ to the differential LO cross section $d\sigma_{\rm LO}$ of a parton reaction is schematically,

$$d\sigma_2 = d\sigma^{VV} + d\sigma^{RV} + d\sigma^{RR}\,, \tag{2.13}$$

where the first, second, and third term on the right-hand side of this equation denotes the double virtual (two-loop times Born and one-loop squared), the real-virtual (one-loop times Born, with one additional parton), and double real radiation (squared Born with two additional partons) corrections, respectively. (If the initial state is colored, a collinear counterterm is required.) There have been quite a few proposals to attack the problem of handling the IR divergences of the terms on the right-hand side of (2.13). Assuming that $d\sigma^{VV}$ can be computed in D dimensions, i.e., its IR poles in the dimensional regulator ϵ are then known, these methods boil down to handling the IR divergences of $d\sigma^{RR}$ and those of $d\sigma^{RV}$ which are simpler in structure. Most of these methods are subtraction methods, and the main technical problem is the integration of the real radiation subtraction terms such that the IR divergences become explicit after integration as poles in ϵ. Methods range from integration of the subtraction terms over the unresolved regions in phase-space in completely analytic fashion to numerical integration where the residues of the ϵ poles are determined numerically. Here we give give only a very short overview over some of the NNLO 'infrared methods'.

To date the most successful NNLO IR method is STRIPPER (SecToR Improved Phase sPacE for real Radiation) [149, 150], which is a subtraction scheme for double real radiation. It uses aspects of the so-called FKS subtraction [138] and sector decomposition [151, 152] methods. In the STRIPPER method the double real radiation phase space is suitably parametrized and decomposed into various sectors according to the singularity structure of the respective matrix elements, with the aim of disentangling overlapping IR divergences such that they factorize. The IR singularities can the be regularized in terms of plus distributions. Integration of the subtraction terms is done with numerical Monte Carlo methods and subsequent IR pole cancellation as also done numerically. The method is completely general, it can be applied to arbitrary reactions with uncolored and colored initial states and massless and massive partons in the final state. It has found a number of applications, most notably in the computation of hadronic $t\bar{t}$ production at NNLO QCD, both in the calculation of the $t\bar{t}$ cross section [3,153–155] as well as differential distributions [19, 156, 157].

The antenna subtraction scheme which is at NLO QCD, as mentioned above, an alternative to the dipole subtraction method, was generalized in [145] for massless partons to NNLO QCD. The method can, in principle, be applied to general partonic reactions. In the subsequent chapters of this thesis we formulate this method and apply it to massive quark-pair production in e^+e^- collisions at NNLO QCD. The basics of this method will be reviewed in the next section. Subtraction methods that aim at a more restricted class of reactions include those of [158–162]. The method of [158] uses sector decomposition [151, 152] and is applicable to the hadronic production of uncolored final states, especially hadronic Higgs production [163], and to reactions with uncolored initial states [158]. The scheme of [160–162], which uses completely local subtraction terms, was developed for reactions with uncolored initial states.

There are also NNLO infrared methods that bear a resemblance to the NLO phase-space slicing method sketched above. The method proposed in [159] applies to the hadronic production of colorless final states, for instance Higgs, ZZ, WW production. It uses the transverse momentum of the uncolored final-state system for separating the double-virtual from the single and double real radiation corrections. The two latter corrections can be handled in this approach with an NLO subtraction method. Other approaches, which share the same spirit, have been pushed

forward more recently in [80–82, 164] for specific reactions. Let us briefly describe it for reactions with an uncolored initial state, e.g. $e^+e^- \to t\bar{t} + X$ [80, 82] at order α_s^2, where X denotes additional partons. One uses the unit decomposition $1 = \Theta(\lambda - E_X) + \theta(E_X - \lambda) = \Theta_I + \Theta_{II}$, where E_X is the energy of X and λ is an arbitrary parameter. Using this decomposition on can write the order α_s^2 contribution $d\sigma_2/dO$, where O is some observable associated with t and/or $\bar{t}$:

$$\frac{d\sigma_2}{dO} = \frac{d\sigma_{2,I}}{dO} + \frac{d\sigma_{2,II}}{dO}\,. \tag{2.14}$$

Because of the above unit decomposition, $d\sigma_{2,II}/dO$ receive contributions form final states which contain, besides $t\bar{t}$, at least one additional parton with non-zero energy. Thus, $d\sigma_{2,II}/dO$ can be computed using a NLO infrared method, for instance, the dipole subtraction method discussed above. The term $d\sigma_{2,I}/dO$ receives the two-loop and squared one-loop contributions from the $t\bar{t}$ final state and, assuming $\lambda \ll m_t$, soft parton contributions that may be computed using the eikonal approximation. In this approximation, terms suppressed by powers of λ/m_T are neglected. Finally, in the numerical evaluation of (2.14) one has to choose the parameter λ such that the dependence on λ of the sum (2.14) is minimized, which means that neglecting the power-suppressed terms is justified. The scheme of [164] that addresses the hadronic production of colored final states uses the global event-shape variable N-jettiness [165] for separating unresolved and resolved parton kinematics at NNLO QCD.

2.4 The antenna subtraction method

The antenna subtraction method is a systematic (process-independent) procedure for the construction of infrared subtraction terms that was developed for NLO QCD calculations in [143, 144] and has been generalized to NNLO QCD in [145]. In this reference, NNLO antenna subtractions terms for massless QCD were derived.

The antenna method is based on the use of color-ordered amplitudes into which an n-point parton amplitude at l loops, $M_n^{(l)}$, can be decomposed [110, 166, 167]:

$$M_n^{(l)} = \sum_i C_{i,n}^{(l)} \mathcal{M}_i^{(l)}\,, \tag{2.15}$$

where i runs over the $(n-1)!$ non-cyclic permutations of the external parton spin and momentum labels. This means that the ordering of the external partons is fixed in the color-stripped partial amplitudes $\mathcal{M}_i^{(l)}$. The coefficients $C_{i,n}^{(l)}$ contain the color information. Thus, kinematics and gauge-group information is separated in (2.15). The development of the antenna formalism relies on two important features. First, the construction of subtraction terms for the color-ordered partial amplitudes is considerably simpler than for the full amplitudes. It relies on the IR factorization properties of the color-ordered partial amplitudes. This factorization was explicitly worked out both at tree-level [106, 110, 111, 143, 166, 168] and at one-loop level (cf. for instance, [100, 112]). The determination of the integrated subtraction terms in analytic fashion in $D \neq 4$ dimensions takes advantage of multi-loop integration techniques. It has been accomplished at NNLO QCD for the massless case [145, 169], but also for a number of cases involving massive quarks (see the references given below).

Let us consider a reaction of the form (2.5) with n resolved partons in the final state. For simplicity we confine ourselves to the case where the initial state is uncolored. At NLO QCD the construction of the subtraction term $d\sigma_{NLO}^S$ for the tree level real-radiation term $d\sigma^R$ with $(n+1)$ partons in the final state is based on the so-called tree-level three-parton antenna functions that are proportional to a ratio of tree-level color-ordered amplitudes

$$X_{ijk}^0(k_i, k_j, k_k) \propto \frac{|\mathcal{M}_{ijk}^{(0)}|^2}{|\mathcal{M}_{IK}^{(0)}|^2}\,, \tag{2.16}$$

where the labels i, j, k, I, K denote a massless or massive (anti)quark or a gluon. Summing/averaging over the spins in the numerator and denominator of (2.16) is understood. The proportionality factor in (2.16) contains powers of coupling constants and other normalization factors. We will provide an example for (2.16), which is relevant for this thesis, in section 3.2. The subtraction term $d\sigma_{NLO}^S$ that enters the formula (2.11) is obtained as a sum of so-called antennas[2]

$$\begin{aligned} \mathrm{d}\sigma_{NLO}^S = &\sum \mathcal{N}\, \mathrm{d}\Phi_{n+1}(k_1, \ldots, k_{n+1}; q) \frac{1}{S_{n+1}} \\ &\times \sum_j X_{ijk}^0\, |\mathcal{M}_n(k_1, \ldots, \tilde{k}_I, \tilde{k}_K, \ldots, k_{n+1})|^2\, \mathcal{F}_J^{(n)}(k_1, \ldots, \tilde{k}_I, \tilde{k}_K, \ldots, k_{n+1})\,, \end{aligned} \tag{2.17}$$

[2]The choice of this terminology is explained below Eq. (2.19).

such that the subtracted quantity[3]

$$\begin{aligned} \mathrm{d}\sigma^R_{NLO} - \mathrm{d}\sigma^S_{NLO} = \sum \mathcal{N}\, \mathrm{d}\Phi_{n+1}(k_1,\ldots,k_{n+1};q)\frac{1}{S_{n+1}} \\ \times \quad \Big[|\mathcal{M}_{n+1}(k_1,\ldots,k_{n+1})|^2\, \mathcal{F}^{(n+1)}_J(k_1,\ldots,k_{n+1}) \\ - \sum_j X^0_{ijk}\, |\mathcal{M}_n(k_1,\ldots,\tilde{k}_I,\tilde{k}_K,\ldots,k_{n+1})|^2\, \mathcal{F}^{(n)}_J(k_1,\ldots,\tilde{k}_I,\tilde{k}_K,\ldots,k_{n+1}) \Big] \end{aligned} \tag{2.18}$$

is free of soft and collinear singularities locally in the $(n+1)$-parton phase space in $D = 4$ dimensions. The first sum in Eqs. (2.17) and (2.18) refers to the case where the real radiation consists of more than one process. For example, for the LO process $e^+e^- \to Q\bar{Q}g$ there are the two NLO real radiation reactions with $Q\bar{Q}gg$ and $Q\bar{Q}q\bar{q}$ in the final state which must be summed. The factor $\mathcal{N}$ is a normalization factor that includes the incident flux factor, a spin-averaging factor for the initial state and a color factor, and S_{n+1} is a symmetry factor if there are identical partons in the final state. Moreover, $|\mathcal{M}_n|^2$ and $|\mathcal{M}_{n+1}|^2$ denotes the squared tree-level color-ordered S-matrix element involving n-partons and $(n+1)$-partons, respectively (the superscript '0' has been dropped and spin summation/averaging is understood), and, as above, $\mathcal{F}^{(n)}_J$ represents a measurement function constructed out of n parton momenta. The sum over j denotes that all single unresolved configurations have to be taken into account.

The subtraction term $\mathrm{d}\sigma^S_{NLO}$ in Eq. (2.17) involves the n-parton partial amplitude $\mathcal{M}_n$ which depends by construction on n redefined on-shell momenta, $k_1,\ldots,\tilde{k}_I,\tilde{k}_K,\ldots,k_{m+1}$ where $\tilde{k}_I,\tilde{k}_K$ are linear combinations of k_i,k_j,k_k, while the tree-level antenna function X^0_{ijk} depends only on k_i,k_j,k_k. For massless QCD such momentum mappings are given in [170]. For processes that involve massive quarks these mappings are more complicated. In appendix B we give a numerical method to construct mapped on-shell momenta for this case, which applies to the observables considered in this thesis.

The choice of $\mathrm{d}\sigma^S_{NLO}$ in Eq. (2.17) is justified because of the particular factorization properties of color-ordered amplitudes referred to above. For example, when particle j is a gluon between

[3] From now on the symbols $d\sigma^R$, etc., contain the measurement function.

the hard partons i and k, and j and becomes soft, the color-ordered S-matrix element undergoes a "QED-like" factorization: an eikonal factor multiplied by the color-ordered S-matrix element with this gluon removed, but the ordering of all the remaining particles is preserved:

$$|\mathcal{M}_{n+1}(k_1,\ldots,k_i,k_j,k_k,\ldots,k_{n+1})|^2 \overset{k_j\to 0}{\longrightarrow} S(i,j,k)|\mathcal{M}_n(k_1,\ldots,\tilde{k}_I,\tilde{k}_K,\ldots,k_{n+1})|^2\,,$$

where

$$S(i,j,k) = \frac{2s_{ik}}{s_{ij}s_{jk}} - \frac{2m_i^2}{s_{ij}^2} - \frac{2m_k^2}{s_{jk}^2}\,, \tag{2.19}$$

where $s_{ij} = 2k_i \cdot k_j$ and m_i, m_k are the masses of partons i and k. We have replaced in the matrix element $\mathcal{M}_n$ the momenta k_i, k_k by $\tilde{k}_I$ and $\tilde{k}_K$, because the mapping used must satisify $\tilde{k}_I = k_i$ and $\tilde{k}_K = k_k$ in the soft limit.

In this example, the partons I and K form a color-connected hard antenna that radiates particle j. In doing so, the momenta of the radiators change to form particles i and k. The use of the momentum mapping decouples the momentum of this unresolved parton from those of the hard radiators I and K.

Notice that the measurement function $\mathcal{F}_J^{(n)}$ in (2.18) depends, by construction, on the mapped momenta $\tilde{k}_I, \tilde{k}_K$, but not on k_i, k_j, k_k. One can therefore carry out the integration over the antenna phase space associated with k_i, k_j and k_k analytically in $D \neq 4$ by using the following factorization of the phase-space measure,

$$\mathrm{d}\Phi_{n+1}(k_1,\ldots,k_{n+1};q) = \mathrm{d}\Phi_n(k_1,\ldots,\tilde{k}_I,\tilde{k}_K,\ldots,k_{n+1};q) \times \mathrm{d}\Phi_{X_{ijk}}(k_i,k_j,k_k;\tilde{k}_I+\tilde{k}_K)\,. \tag{2.20}$$

In order to appreciate this factorization formula of the $(n+1)$-particle phase-space measure in $D \neq 4$, we may consider a much simpler case: the three-particle phase-space measure in four dimensions, $\mathrm{d}\Phi_3(k_1,k_2,k_3;q)$. It can be written as the product of a two-particle measure $\mathrm{d}\Phi_2(\tilde{k}_1,\tilde{k}_2;q)$ and an antenna phase-space measure $\mathrm{d}\Phi_{X_{ijk}}(k_1,k_2,k_3;\tilde{k}_1+\tilde{k}_2)$. Recall that out of the five independent variables used to parametrize the three-particle phase-space $\mathrm{d}\Phi_3(k_1,k_2,k_3;q)$, two of them can be chosen to be angles related to the orientation of the coordinate frame on which the physical spin-summed/averaged S-matrix element does not depend. These two angular variables are separated from the rest and used in the two-particle

phase-space measure $\mathrm{d}\Phi_2(\tilde{k}_1, \tilde{k}_2; q)$. The remaining three-dimensional integration constitutes the antenna phase-space measure $\mathrm{d}\Phi_{X_{ijk}}(k_1, k_2, k_3; \tilde{k}_1 + \tilde{k}_2)$ which retains no reference to the absolute orientation of the underlying coordinate frame. This thee-dimensional measure $\mathrm{d}\Phi_{X_{ijk}}$ can be parametrized using the only two independent Lorentz-invariants that can be constructed out of k_1, k_2, k_3 plus an angle on which the the spin-averaged tree-level antenna function does not not depend.

For the analytic integration of the subtraction term $\mathrm{d}\sigma^S_{NLO}$ in Eq. (2.17), which is required in order to produce the IR poles in ϵ that cancel the IR poles of the virtual correction (cf. Eq. (2.11)), we can use (2.20) and rewrite each of the subtraction terms in (2.17) into the form

$$|\mathcal{M}_n|^2 \, \mathcal{F}_J^{(n)} \, \mathrm{d}\Phi_n \int \mathrm{d}\Phi_{X_{ijk}} \, X^0_{ijk},$$

where $|\mathcal{M}_n|^2$, $\mathcal{F}_J^{(n)}$ and $\mathrm{d}\Phi_n$ depend on $k_1, , \ldots, \tilde{k}_I, \tilde{k}_K, \ldots, k_{n+1}$, while $\mathrm{d}\Phi_{X_{ijk}}$ and X^0_{ijk} depend on k_i, k_j, k_k. The integral $\int_1 \mathrm{d}\sigma^S_{NLO}$ in the generic NLO formula Eq. (2.11) is therefore reduced here to the D-dimensional analytic integration of the antenna function over the antenna phase space.

At NNLO QCD one needs in addition to the antenna functions (2.16) also tree-level four-parton antenna functions for the subtraction of singularities caused by double unresolved parton configurations in the double real-radiation tree-level matrix elements. In analogy to (2.16) they are proportional to a ratio of tree-level color-ordered amplitudes,

$$X^0_{ijkl}(k_i, k_j, k_k, k_l) \propto \frac{|\mathcal{M}^{(0)}_{ijkl}|^2}{|\mathcal{M}^{(0)}_{IK}|^2} \,, \tag{2.21}$$

where the labels i, j, k, l, I, K denote a massless or massive (anti)quark or a gluon. Summing/averaging over the spins in the numerator and denominator of (2.21) is understood. We shall give examples in section 3.3 that are required for the analysis of this thesis.

For the sake of brevity we will not discuss here the general set-up of the antenna subtraction method at NNLO QCD, but refer to the next chapter, where the formalism will be presented in detail for the reaction $e^+e^- \to Q\bar{Q} + X$ which is the subject of this thesis. We close this section with two remarks. i) At NNLO QCD the antenna subtraction terms do not, in general, cancel

all IR singularities of the double real emission amplitudes in a point-wise manner. These unsubtracted matrix elements contain, as a subamplitude, the splitting of a virtual gluon into two gluons or a pair of massless quarks, $g^* \to gg, q\bar{q}$, which leads to spin correlations in the squared matrix element. However, these spin-correlations are absent in the subtraction terms because the antenna functions are constructed with spin-summed/averaged squared matrix elements. Nevertheless, one can remedy this deficiency by 'azimuthal angle averaging' [171, 172] which will be described in section 3.3.1. This provides an efficient cancellation of the IR singularities of the double real emission contributions. ii) A more serious issue is, generally speaking, the construction of antenna subtraction terms for the subleading-color terms of the real emission squared matrix elements. In general these subleading-color terms are given in terms of incoherent interferences of color-ordered partial amplitudes. That is to say, amplitudes with different orderings of the external legs interfere. Therefore, antenna functions constructed from squared color-ordered amplitudes according to (2.16) and (2.21) will in general not be able to cancel the singularities of subleading-color terms. The construction of appropriate subleading-color antenna subtraction terms is, in the case of hadronic reactions, quite complicated in general. For hadronic dijet production due to gluon scattering it was described in [173]. For the reactions considered in this thesis, the construction of the subleading-color antenna functions is, however, straightforward (cf. [78, 174] and section 3.3.1).

Chapter 3

Ingredients for computing $e^+e^- \to Q\bar{Q} \ + \ X$ at $\mathcal{O}(\alpha_s^2)$

In this chapter we recapitulate all the ingredients needed and the formalism employed for calculating the production of a massive quark-antiquark pair in e^+e^- collisions,

$$e^-(p_1)e^+(p_2) \to \gamma^*, Z^*(q) \to Q(k_1)\ \bar{Q}(k_2) + X\,, \tag{3.1}$$

at order α_s^2 in QCD and to lowest order in the electroweak couplings within the antenna subtraction framework.

3.1 Classification of contributions to order α_s^2

Before we introduce the IR subtraction formulas employed for calculating the process (3.1) to order α_s^2, let us briefly list the various terms that contribute to (3.1) contributing terms to this process to this order in perturbation theory. To order α_s^2, the (differential) cross section of the reaction (3.1) receives contributions from

i) the two-parton $Q\bar{Q}$ state (at Born level, to order α_s, and to order α_s^2),

ii) the three-parton state $Q\bar{Q}g$ (to order α_s and to order α_s^2),

iii) and the four-parton states $Q\bar{Q}gg$, $Q\bar{Q}q\bar{q}$, and above the $4Q$-threshold from $Q\bar{Q}Q\bar{Q}$ (to order

α_s^2).

The $Q\bar{Q}Q\bar{Q}$ final state deserves a separate discussion, in view of the fact that for these states the particle-multiplicity $n_Q \neq 1$ if one considers so-called inclusive heavy-quark distributions $d\sigma(e^+e^- \to Q + X)/dO_Q$, where O_Q is some observable associated with Q. We will come back to this point in chapters 4 and 5.

3.1.1 Contributions from $Q\bar{Q}$, $Q\bar{Q}g$, $Q\bar{Q}gg$, and $Q\bar{Q}q\bar{q}$ final states

We start with the $Q\bar{Q}$ contributions. Figure 3.1 shows representative Feynman diagrams for this two-parton final state up to α_s^2.

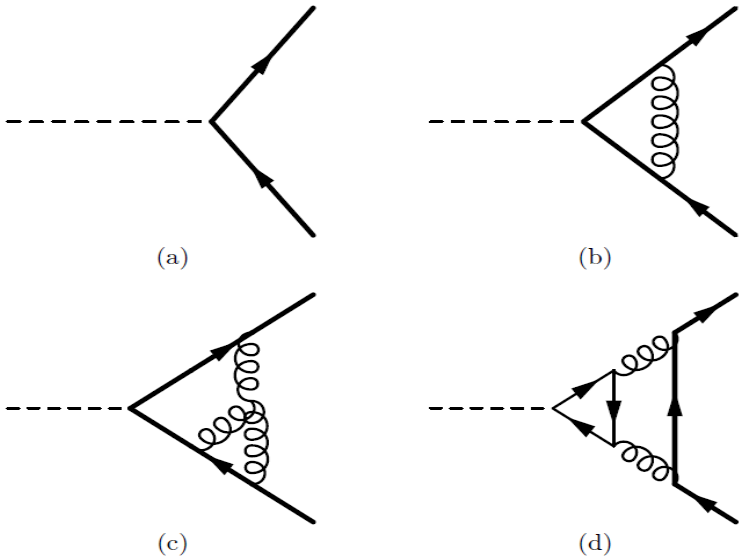

Figure 3.1: Examples of diagrams that contribute to the $Q\bar{Q}$ final state to order α_s^2. The dashed line represents the electroweak neutral current, that is, the virtual photon or Z boson, the thick line the massive Q quark, and the thin line any of the six quarks. The triangle diagrams (d) are summed over the six quark flavors. Here the the vector current contributions are zero due to Furry's theorem.

According to the terminology used in [175–177], the two-loop diagram figure 3.1c belongs to the type-A two-loop contributions where the external current couples to to $Q\bar{Q}$. This diagram and the one-loop diagram fig. 3.1c are also examples of so-called *universal QCD corrections* because the same electroweak couplings as in the lowest order diagram fig. 3.1a are involved. Figure 3.1d is an example of the so-called type-B two-loop contributions where a fermion triangle

loop is involved. Since in fig. (3.2d) it is not necessarily the heavy quark Q that is coupled to the electroweak current, it is an example for the so-called *non-universal QCD corrections* to the lowest order $Q\bar{Q}$ production amplitude.

Examples of diagrams associated with the $Q\bar{Q}g$ final state that lead to contributions of order α_s and as^2 to the differential cross section of (3.1) are displayed in fig. 3.2. The diagrams fig. 3.2a,b and fig. 3.2c belong to the universal and non-universal QCD corrections, respectively.

The four-parton final-state diagrams of fig. 3.3 contribute at order α_s^2 to the differential cross section. An example of a diagram corresponding to the final state $Q\bar{Q}gg$ is shown in fig. 3.3a, while two of the four diagrams associated with $Q\bar{Q}q\bar{q}$ ($q \neq Q$) are exhibited in fig. 3.3b,c. The square of the $Q\bar{Q}gg$ diagrams and the square of fig. 3.3a lead to universal QCD corrections while the square of fig. 3.3c and the interference of figs. 3.3b and 3.3c belong to the non-universal QCD corrections.

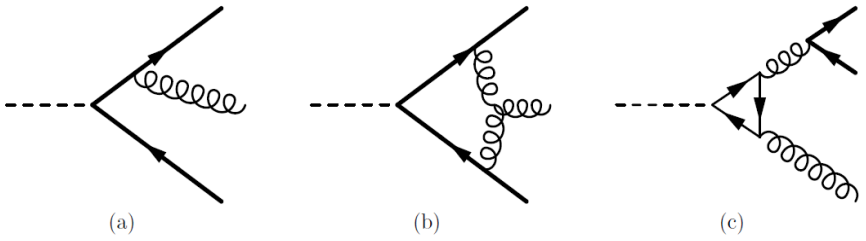

Figure 3.2: Examples of diagrams that contribute to the $Q\bar{Q}g$ final state to order α_s^2. The assignment of the lines is as in figure 3.1.

For our computation of the b-quark forward-backward asymmetry in section 5.3 and comparison of our results with previous ones for massless b quarks [90] it is useful to group the various contributions into the following three classes.

i) **Triangle contributions:** This class refers to those contributions associated with two-parton, three-parton, and four-parton final states where a fermion triangle is involved. These contributions are ultraviolet and infrared finite by themselves. To be specific, this set consists of the interference between the diagrams in figure 3.1a and 3.1d, between the diagrams in figure 3.2a and 3.2c, and between the diagrams in figure 3.3b and 3.3c.

The triangle interferences involve a sum over three generations of quarks. We neglect the masses of the u, d, c, s quarks, which is an excellent approximation for our purposes, i.e., the computation of differential cross sections at or above the Z resonance. After pairing up triangle contributions from two quarks in one SU(2)-doublet, the only non-vanishing one comes from the third generation due to the mass-splitting between the b and t quark. The triangle contributions are part of the non-universal corrections to the leading-order $Q\bar{Q}$ cross section because they involve electroweak couplings of quarks $q \neq Q$.

ii) **Flavor singlet contributions:** The square of diagrams where the observed final-state heavy quark Q is produced by the splitting of a gluon radiated off a quark rather than via a virtual photon or Z boson belong to the so-called singlet contributions. Here the $Q\bar{Q}$ pair is produced in a definite state of charge conjugation, namely in a C-even state. The square of the diagrams in figure 3.3c belong to this class. Obviously these are non-universal corrections. There is an additional singlet contribution from the $Q\bar{Q}Q\bar{Q}$ final state as will be discussed in the next subsection. This contribution belongs to the universal QCD corrections.

iii) **Flavor non-singlet contributions:** All the remaining contributions that are not in the above two classes are classified as non-singlet contributions. Here the observed final-state heavy quark Q is coupled to the electroweak current. All the two-parton diagrams in figure 3.1 other than the so-called type-B two-loop diagrams represented by figure 3.1d, belong to this class. Non-singlet contributions from the three-parton final state are shown in figure 3.2a and 3.2b. All the diagrams that correspond to the $Q\bar{Q}gg$ final state (cf. figure 3.3a) and the square of $Q\bar{Q}q\bar{q}$ ($q \neq Q$) diagram figure 3.3b are in this class. There are also contributions from the $Q\bar{Q}Q\bar{Q}$ final state, see the next subsection 3.1.2. The non-singlet contributions lead to universal QCD corrections to the lowest-order $Q\bar{Q}$ cross section.

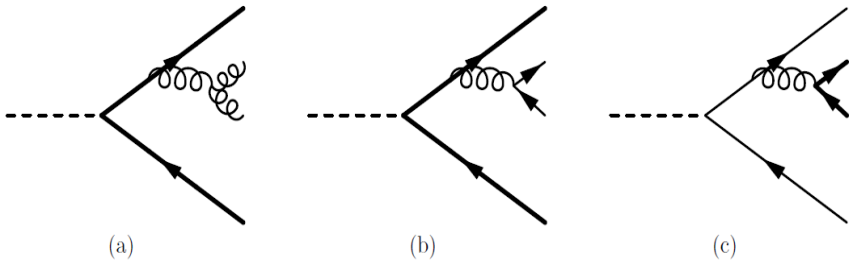

Figure 3.3: (a): Examples of diagrams that contribute to the $Q\bar{Q}gg$ final state at order α_s^2. (b,c): Two of the four diagrams that contribute to the $Q\bar{Q}q\bar{q}$ ($q \neq Q$) final state at order α_s^2.

3.1.2 The $Q\bar{Q}Q\bar{Q}$ final state

The $Q\bar{Q}Q\bar{Q}$ final state contributes to the heavy quark-pair cross section above the $4m_Q$ threshold. At order α_s^2 there are eight diagrams shown in figure 3.4 associated with this final state because it contains two identical (anti)quarks. Notice that the multiplicity factor associated with these diagrams depends on which observable is calculated. In the case of the total cross section for $e^+e^- \to$ hadrons the multiplicity factor is one. However, in the case of (differential) inclusive cross sections for a heavy quark Q these diagrams count twice because there are two quarks Q in the final state. This will be further discussed in chapters 4 and 5 where we compute inclusive b quark distributions and the b-quark forward-backward asymmetry. In the case of top quark production, we limit ourselves to center-mass energy below four-top threshold.

In section 5.3.2, we shall compute the b-quark forward-backward asymmetry in the limit $m_b \to 0$ for the purpose of comparing with the massless result of [90]. Due to a subtlety of A_{FB} for massless quarks (which is actually not well defined at order α_s^2 as as will be explained in section 5.3.2, it is useful to partition the square of the eight $Q\bar{Q}Q\bar{Q}$ diagrams into different groups, following the conventions of [90]. For definiteness we specify in the remainder of this subsection the heavy quark Q to be the bottom quark. Ref. [90] distinguishes between group-(i) contributions that are identical to those of $b\bar{b}q\bar{q}$ shown in figs. 3.3b and 3.3c, but with q being replaced by that b quark that is not triggered on, and group-(ii) genuine interference terms that arise from the fact that there are two indistinguishable (anti)quarks in the final state. Group-(ii), which is called the E-term in [127], is the color subleading part of the squared $b\bar{b}b\bar{b}$ S-matrix

element.

In the following we denote by $\mathcal{D}_i$ the sum of the two diagrams shown in figure 3.4 and $D_{ij} = 2\mathrm{Re}(\mathcal{D}_i^* \mathcal{D}_j)$. Then the E-term is given by the sum of the following interferences:

$$D_{12},\ D_{13},\ D_{24},\ D_{34}\,. \tag{3.2}$$

Ref. [90] considers the E-term to be part of the non-singlet contributions. Group-(i) can be partitioned into non-singlet, singlet, and triangle contributions. By convention we denote the momentum of the triggered b-quark with k_1. The singlet terms refer to those where the b quark that is observed is produced by a gluon. Then the singlet contribution is given by the sum of the terms

$$D_{33} \text{ and } D_{44}\,. \tag{3.3}$$

The triangle interferences are given by the sum of the terms

$$D_{14} \text{ and } D_{23}\,. \tag{3.4}$$

These are interferences between diagrams where the b quark with momentum k_1 couples to the weak current and to the gluon, respectively.

The remaining contributions to group (i) are non-singlet contributions where the triggered b-quark with momentum k_1 is coupled to the electroweak current.

We come back to this classification in section 5.3.2 when comparing our computation of the b-quark forward-backward asymmetry in the limit $m_b \to 0$ with that of [90].

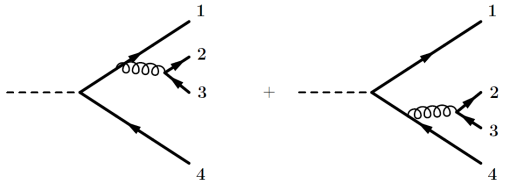

(a) Amplitudes $\mathcal{D}_i$, $i = 1, \ldots, 4$.

Label	$\mathcal{D}_1$	$\mathcal{D}_2$	$\mathcal{D}_3$	$\mathcal{D}_4$
1	k_1	k_1	k_3	k_3
2	k_3	k_3	k_1	k_1
3	k_4	k_2	k_4	k_2
4	k_2	k_4	k_2	k_4

(b) Labeling of the quark momenta

Figure 3.4: Contributions to $e^+e^- \to Q\overline{Q}\,Q\overline{Q}$

3.2 The differential cross section at LO and NLO QCD

In this subsection we outline all the basic ingredients and formulae involved in the computation of the differential cross section for $e^+e^- \to Q\bar{Q} + X$ at order α_s within the antenna subtraction method. Here Q denotes a massive quark, for instance, the bottom or top quark. We work in QCD with n_f massless quarks q and one massive quark Q. In our application to top-quark pair production, $n_f = 5$. When we apply the general formulae of section 3 to $b\bar{b}$ production at the Z-boson resonance we use four massless quarks (i.e., put $n_f = 4$) and a massive b quark. In this case the top-quark is decoupled from its contribution to the 1-loop gluon self-energy (which contributes to the 2-loop type-A $b\bar{b}$ final-state diagrams) because we use the QCD coupling α_s in the $\overline{\text{MS}}$ scheme with 5 flavors, but the top quark contribution to the 2-loop type-B diagrams fig. 3.1d and to the 1-loop triangle diagrams figure 3.2c has to be taken into account.

All S-matrix elements in this and in the following subsection 3.3 refer to UV-renormalized matrix elements. The mass of Q, denoted by m_Q, is renormalized in the on-shell scheme while the QCD coupling α_s, as aleady mentioned, is renormalized in the $\overline{\text{MS}}$ scheme. The renormalization constants of this hybrid renormalization scheme that we need are collected in Appendix A.2. Dimensional regularization (DR) is used to regularize both UV and IR singularities that appear in intermediate steps of perturbative calculations. In the following the differential cross section for $Q\bar{Q}$ productions at order α_s^2 is written schematically as

$$d\sigma = d\sigma_{LO} + d\sigma_1 + d\sigma_2 \,, \tag{3.5}$$

where $d\sigma_{LO}$, $d\sigma_1$, and $d\sigma_2$ denote the LO, NLO, and NNLO QCD contribution, respectively.

3.2.1 LO QCD

To zeroth order in α_s we consider

$$e^-(p_1)\; e^+(p_2) \to \gamma^*, Z^*(q) \to Q(k_1)\; \bar{Q}(k_2) \,, \tag{3.6}$$

where Q denotes a massive quark. The corresponding leading-order (LO) (differential) cross section for unpolarized e^+e^- collisions is given by

$$\int d\sigma_{LO} = \mathcal{N}\, N_c \int d\Phi_2\, \mathcal{F}_2^{(2)}(k_1, k_2) \left|\mathcal{M}_2^0(1_Q, 2_{\bar{Q}})\right|^2, \quad \mathcal{N} = \frac{1}{8s}\,, \tag{3.7}$$

where $N_c = 3$ denotes the number of quark colors and $\mathcal{M}_2^0(1_Q, 2_{\bar{Q}})$ is the two-parton color-stripped Born-level amplitude which is defined in eq. Eq.(3.14) below. Here and in the following, summation over polarizations and colors of the partons in the final state is implicit. The factor $\mathcal{N}$ contains the incident flux factor, $1/(2s) = 1/(2(p_1 + p_2)^2)$ and the spin averaging factor $1/4$ for the initial state. The phase-space measure $d\Phi_n$ in $D = 4 - 2\epsilon$ dimensions for n particles in the final state is defined in Appendix A. We use here and below symbolic labels i_X in order to denote the type X and the four-momentum k_i of a final-state parton in the (color-stripped) S-matrix elements. For example, the symbol 1_Q denotes a massive quark with momentum k_1 while $3_{\bar{q}}$ labels a massless anti-quark with momentum k_3.

The infrared-safe jet-defining function or measurement function is denoted by $\mathcal{F}_n^{(m)}(k_j)$. It must fulfill the conditions (2.7) and (2.8). Here it refers to a n-jet observable constructed out of a pair of heavy quarks $Q, \bar{Q}$ and $(m-2)$ massless partons in the final state. All the computations done in this thesis involve only observables associated with Q and/or $\bar{Q}$. Hence for definiteness we put $n = 2$ in (3.7) and in the following formulae. But we emphasize that the formalism presented below applies to any infrared-safe observable.

3.2.2 NLO QCD

The NLO QCD correction $d\sigma_1$ to the LO differential cross section Eq.(3.7) consists of the interference of the Born and one-loop $Q\bar{Q}$ amplitude and the squared tree-level real radiation amplitude of the three-parton final state

$$e^-(p_1)\; e^+(p_2) \to \gamma^*, Z^*(q) \to Q(k_1)\; \bar{Q}(k_2) + g(k_3)\,. \tag{3.8}$$

Based on what has been discussed in the preceding chapters, in a subtraction method for

handling the IR divergences the NLO correction to the LO cross section or to a differential distribution can be rewritten as follows:

$$\int d\sigma_1 = \int_{\Phi_3} \Big[\Big(d\sigma^R_{Q\bar{Q}g} \Big)_{\epsilon=0} - \Big(d\sigma^S_{Q\bar{Q}g} \Big)_{\epsilon=0} \Big] + \int_{\Phi_2} \Big[d\sigma^V_{Q\bar{Q}} + \int_1 d\sigma^S_{Q\bar{Q}g} \Big]_{\epsilon=0} , \tag{3.9}$$

where $\epsilon = (4-D)/2$ is the regulator parameter of the dimensional regularization scheme and the subscripts Φ_n denote n-particle phase-space integrals defined in $D = 4$ space-time dimensions. Throughout this thesis, the symbol $\int_n$ indicates the analytic integration over the phase space of n unresolved partons in $D \neq 4$ dimensions. The second term in the first and second square bracket of Eq.(3.9) is the unintegrated and integrated IR subtraction term that renders the difference, respectively the combination of the terms in the square brackets finite in $D = 4$ dimensions. We address the construction of NLO subtraction terms required in Eq. (3.9) within the antenna subtraction framework below in Eqs. (3.16), (3.17).

The NLO real and virtual corrections to the LO cross section, Eq.(3.7), $d\sigma^R_{Q\bar{Q}g}$ and $d\sigma^V_{Q\bar{Q}}$, are given by

$$d\sigma^R_{Q\bar{Q}g} = \mathcal{N}\,(4\pi\alpha_s)\left(N_c^2-1\right) d\Phi_3\, \mathcal{F}_2^{(3)}(k_1,k_2,k_3)\left|\mathcal{M}_3^0(1_Q,3_g,2_{\bar{Q}})\right|^2 , \tag{3.10}$$

$$d\sigma^V_{Q\bar{Q}} = \mathcal{N}\left(\frac{\alpha_s}{2\pi}\right)\bar{C}(\epsilon)\left(N_c^2-1\right) d\Phi_2\, \mathcal{F}_2^{(2)}(k_1,k_2)\,\delta\mathcal{M}_2^1(1_Q,2_{\bar{Q}}) , \tag{3.11}$$

where

$$\bar{C}(\epsilon) = 8\pi^2 C(\epsilon) = (4\pi)^\epsilon e^{-\epsilon\gamma_E} \tag{3.12}$$

and $\gamma_E = 0.5772156649\ldots$ denotes the Euler–Mascheroni constant. As before summation over polarizations and colors of final states is not exhibited. To ease the work of typing, we use the following shorthand notation for the interference of the color-stripped tree-level and one-loop two-parton amplitude:

$$\delta\mathcal{M}_2^1\big(i_Q,j_{\bar{Q}}\big) = 2\mathrm{Re}\left[\mathcal{M}_2^{0*}\big(i_Q,j_{\bar{Q}}\big)\,\mathcal{M}_2^1\big(i_Q,j_{\bar{Q}}\big)\right] . \tag{3.13}$$

In the formulas Eq.(3.7), Eq.(3.10), and Eq.(3.13) we have introduced color stripped partial

amplitudes $\mathcal{M}_2^0$, $\mathcal{M}_2^1$, and $\mathcal{M}_3^0$ where the QCD coupling factor is taken out, but electroweak couplings are kept. These quantities are related to the tree-level and the renormalized one-loop matrix elements of $e^-e^+ \to Q\bar{Q}$ and the tree-level matrix element of $e^-e^+ \to Q\bar{Q}g$ via projecting them onto the appropriately normalized color decomposition basis. For the sake of easy reference in the next section we give here the color decomposition of S-matrix elements of these processes to NNLO QCD:

$$\begin{aligned} M(e^-e^+ \to Q\,\bar{Q}) &= \delta_{i_1 i_2}\,\mathcal{M}_2^0\big(1_Q, 2_{\bar{Q}}\big) \\ &+ \left(\frac{\alpha_s}{2\pi}\right)\bar{C}(\epsilon)\,2C_F\,\delta_{i_1 i_2}\,\mathcal{M}_2^1\big(1_Q, 2_{\bar{Q}}\big) \\ &+ \left(\frac{\alpha_s}{2\pi}\right)^2\big(\bar{C}(\epsilon)\big)^2\,\delta_{i_1 i_2}\,\mathcal{M}_2^2\big(1_Q, 2_{\bar{Q}}\big) + \mathcal{O}\big(\alpha_s^3\big)\,, \end{aligned} \tag{3.14}$$

$$\begin{aligned} M(e^-e^+ \to Q\bar{Q}g) &= g_s\,\sqrt{2}\,T^{a_3}_{i_1 i_2}\left\{\mathcal{M}_3^0\big(1_Q, 3_g, 2_{\bar{Q}}\big) + \left(\frac{\alpha_s}{2\pi}\right)\bar{C}(\epsilon)\right. \\ &\times\left[N_c\,\mathcal{M}_3^{1,\mathrm{lc}}\big(1_Q, 3_g, 2_{\bar{Q}}\big) - \frac{1}{N_c}\,\mathcal{M}_3^{1,\mathrm{sc}}\big(1_Q, 3_g, 2_{\bar{Q}}\big)\right. \\ &\left.\left. + n_f\mathcal{M}_3^{1,f}\big(1_Q, 3_g, 2_{\bar{Q}}\big) + \mathcal{M}_3^{1,F}\big(1_Q, 3_g, 2_{\bar{Q}}\big) + \mathcal{M}_3^{1,\mathrm{tr}}\big(1_Q, 3_g, 2_{\bar{Q}}\big)\right] \right. \\ &\left. + \mathcal{O}\big(\alpha_s^2\big)\right\}, \end{aligned} \tag{3.15}$$

where i_1 (i_2) denotes the color index of the heavy quark (antiquark) in the fundamental representation, a_3 is the color index of the gluon in the ajoint representation, $g_s = \sqrt{4\pi\alpha_s}$, $C_F = \frac{N_c^2-1}{2N_c}$, and the generators of $\mathrm{SU}(3)_c$ are normalized according to $\mathrm{tr}(T^aT^b) = T_R\delta_{ab}$ with $T_R = \frac{1}{2}$. As already mentioned at the beginning of sec. 3.2, the number of massless quarks is denoted by n_f which will be set to 4 for bottom-quark production at the Z-pole and to 5 for top-quark production. The renormalized two-loop two-parton amplitude $\mathcal{M}_2^2$, which consists of contributions with different color structures, and the renormalized 1-loop three-parton amplitude in the square bracket of Eq.(3.15) are required in the next section. The $\mathcal{M}_2^2$ are computed by using the heavy quark vector, axial vector, and anomaly form factors known to NNLO in QCD [175–177]. All other one-loop and tree-level amplitudes are computed using standard procedures. The one-loop two- and three-parton amplitudes are calculated by performing a Passarino-Veltman

reduction to scalar one-loop integrals in D dimensions of the respective Born times one-loop interference terms. The scalar one-loop integrals are known in analytic fashion. The labels 'lc' and 'sc' in Eq.(3.15) refer to leading-order and subleading-order term in the color factor N_c, respectively. The terms $\mathcal{M}_3^{1,f}$ and $\mathcal{M}_3^{1,F}$ are the contributions from the massless and massive quark loop, respectively, that enter via the renormalization of the quark-quark-gluon vertex in QCD. The term $\mathcal{M}_3^{1,\mathrm{tr}}$ denotes the contribution from fig. 3.2c, where the axial current couples to quark triangles, summed over all quark flavors (u_i, d_i), which disintegrate into a real and virtual gluon that splits into $Q\bar{Q}$. This term, which is both ultraviolet- and infrared-finite by itself, involves weak couplings of $q \neq Q$ and constitutes, as already mentioned in sec. 3.1, a non-universal correction to the leading-order $Q\bar{Q}$ cross section. We recall from sec. 3.1 that there are also non-universal corrections contained in the two-loop two-parton amplitude $\mathcal{M}_2^2$ – the type-B contributions – and also from four-parton amplitudes that will be discussed in the following subsection.

We continue with the discussion of the formulae for the differential NLO cross section in the antenna subtraction method. The squared tree-level S-matrix element $\left|\mathcal{M}_3^0\right|^2$ of the real radiation correction Eq.(3.10) becomes singular when the gluon momentum k_3 becomes soft. Within the antenna method this soft singularity is subtracted by constructing a local subtraction term that approaches Eq.(3.10) in this soft region. This NLO local subtraction term, which involves a term called quark-antiquark antenna A_3^0, and its integrated form (integrated over the phase space of the unresolved single gluon) are:

$$\begin{aligned} d\sigma^S_{Q\bar{Q}g} &= \mathcal{N}\,(4\pi\alpha_s)\left(N_c^2-1\right) d\Phi_3(k_1,k_2,k_3;q)\,\mathcal{F}_2^{(2)}\Big(\widetilde{k_{13}},\widetilde{k_{32}}\Big) \\ &\quad \times A_3^0\big(1_Q,3_g,2_{\bar{Q}}\big)\,\Big|\,\mathcal{M}_2^0\Big(\widetilde{(13)}_Q,\widetilde{(32)}_{\bar{Q}}\Big)\Big|^2\,, \end{aligned} \tag{3.16}$$

$$\begin{aligned} \int_1 d\sigma^S_{Q\bar{Q}g} &= \mathcal{N}\left(\frac{\alpha_s}{2\pi}\right)\bar{C}(\epsilon)\,\left(N_c^2-1\right) d\Phi_2(k_1,k_2;q)\,\mathcal{F}_2^{(2)}(k_1,k_2) \\ &\quad \times \mathcal{A}_3^0\big(\epsilon,\mu^2/s;y\big)\,\big|\,\mathcal{M}_2^0\big(1_Q,2_{\bar{Q}}\big)\big|^2\,, \end{aligned} \tag{3.17}$$

where μ is the dimensionful parameter of DR, and

$$y=\frac{1-\beta}{1+\beta}\,,\quad \beta=\sqrt{1-4m_Q^2/s}\,. \tag{3.18}$$

The three-parton tree-level massive quark-antiquark antenna function A_3^0 describes a single unresolved gluon radiation between a (massive) quark-antiquark pair at tree-level. Obviously this antenna function $A_3^0(1_Q, 3_g, 2_{\bar{Q}})$ encapsulates all single unresolved limits of this radiation process. We recall that in the antenna picture, the color-ordered $(m+1)$-parton tree-level S-matrix element factorises, in the unresolved IR limits, into a product of the well known soft eikonal factor when the gluon is soft, or Altarelli-Parisi splitting functions when two massless partons are collinear, and a reduced color-ordered m-parton tree-level S-matrix element with the unresolved parton removed but keeping same color-ordering among the remainders. This antenna function $A_3^0(1_Q, 3_g, 2_{\bar{Q}})$ can be obtained via appropriately normalizing the squared tree-level color-stripped S-matrix element for the process $\gamma^* \to Q\bar{Q}g$. The normalization is done with respect to the color-stripped two-parton S-matrix element of $\gamma^* \to Q\bar{Q}$ which is the remaining hard skeleton of $\gamma^* \to Q\bar{Q}g$ when the gluon is soft. The normalization is necessary if we want this antenna function $A_3^0(1_Q, 3_g, 2_{\bar{Q}})$ to have the correct limiting form, a (color-stripped) soft eikonal factor squared, when 3_g is soft. Thus it is given by

$$A_3^0(1_Q, 3_g, 2_{\bar{Q}}) = \frac{|\mathcal{M}_3^{0,\gamma^*}(1_Q, 3_g, 2_{\bar{Q}})|^2}{|\mathcal{M}_2^{0,\gamma^*}(1_Q, 2_{\bar{Q}})|^2} \,. \tag{3.19}$$

Summation over the spins in the numerator and denominator of (3.19) is understood.

The explicit form of this antenna function and its integrated counterpart $\mathcal{A}_3^0$ were derived first in [178,179]. The integrated quark-antiquark antenna function $\mathcal{A}_3^0$ contains an explicit IR pole $\propto 1/\epsilon$ that cancels the corresponding IR pole in the one-loop function contained in $d\sigma_{Q\bar{Q}}^V$. The integrated antenna function $\mathcal{A}_3^0$ on y involves to order ϵ^0, which is sufficient for the NLO computation of the cross section, only logarithms and dilogarithms. The order ϵ terms of $\mathcal{A}_3^0$, which is needed for the NNLO calculation, contains also harmonic polylogarithms (HPL) [180], which can be evaluated using the codes of refs. [181,182].

As already alluded to in section 2.4, the matrix element $\mathcal{M}_2^0$ and the measurement function $\mathcal{F}_2^{(2)}$ in Eq. (3.16) must be evaluated with redefined on-shell momenta $\widetilde{k_{13}}$, $\widetilde{k_{32}}$ that are obtained from k_1, k_2, k_3 by an appropriate phase-space mapping [172]. The point of this mapping is to guarantee that the partial integration over the unresolved radiation in the subtraction term in Eq. (3.16), which is done in numerical manner, is exactly the same as the integration in

Eq. (3.17) done analytically. This is essential for the cancellation of contributions from these purely unphysical terms when they are combined.
Our method to construct the mapped momenta $\widetilde{k_{13}}$, $\widetilde{k_{32}}$, which can be used for observables associated with Q and/or $\bar{Q}$, is given in Appendix B.

3.3 The differential cross section at NNLO QCD

The second-order correction $d\sigma_2$ in the expansion in powers of α_s of the differential cross section of Eq. (3.1), $d\sigma = d\sigma_{LO} + d\sigma_1 + d\sigma_2 + \mathcal{O}(\alpha_s^3)$, receives the following contributions, organized according to the number of partons in the final states:

i) the double virtual correction $d\sigma^{VV}_{\rm NNLO}$ associated with the (renormalized) S-matrix element of $e^+e^- \to Q\bar{Q}$ to order α_s^2 (i.e., 2-loop times Born and 1-loop squared),

ii) the real-virtual cross section $d\sigma^{RV}_{\rm NNLO}$ associated with the S-matrix element of $e^+e^- \to Q\bar{Q}g$ to order α_s^2 (1-loop times Born),

iii) the double real contribution $d\sigma^{RR}_{\rm NNLO}$ associated with the squared Born amplitudes $e^+e^- \to Q\bar{Q}gg$, $e^+e^- \to Q\bar{Q}q\bar{q}$ (where q denotes a massless quark).

Above the $4Q$ threshold, the channel $e^+e^- \to Q\bar{Q}Q\bar{Q}$ is open. This contribution is IR finite as long as we consider massive quarks and is of no concern to us for the purpose of this section. Each of the contributions listed in the above three subsets of is IR divergent.
Within the antenna subtraction method, the IR-subtracted second order correction $d\sigma_2$, where the different pieces are separately finite, is constructed schematically as follows:

$$\begin{aligned}\int d\sigma_2 = \; & \int_{\Phi_4} \left(d\sigma^{RR}_{\rm NNLO} - d\sigma^{S}_{\rm NNLO}\right) + \int_{\Phi_3} \left(d\sigma^{RV}_{\rm NNLO} - d\sigma^{T}_{\rm NNLO}\right) \\ & + \left(\int_{\Phi_2} d\sigma^{VV}_{\rm NNLO} + \int_{\Phi_3} d\sigma^{T}_{\rm NNLO} + \int_{\Phi_4} d\sigma^{S}_{\rm NNLO}\right) . \end{aligned} \tag{3.20}$$

The integrands $d\sigma^{S}_{\rm NNLO}$ and $d\sigma^{T}_{\rm NNLO}$ denote the double-real subtraction terms (for $Q\bar{Q}q\bar{q}$ and $Q\bar{Q}gg$) and the real-virtual subtraction term, respectively. The construction of these terms involves various antenna functions which can be derived from appropriately normalized physical

color-ordered partial amplitudes of certain subprocesses responsible for the unresolved radiation. Due to the much more involved IR singular structure at NNLO compared to NLO, the construction of $d\sigma^S_{\rm NNLO}$ will intertwine with that of $d\sigma^T_{\rm NNLO}$. In addition, individual NNLO IR-subtraction terms introduced and worked out for a specific IR singular region (constructed such that they do a good job there) can produce unwanted extra IR singularities in other singular regions where the IR singularity of the unsubtracted squared S-matrix element is already taken care of by another IR-subtraction term. This leads to the so-called over-subtracted singularities, which must be carefully compensated when constructing NNLO subtraction terms.
We now discuss in turn the various terms in Eq. (3.20) in some detail. It is a good strategy to start with the IR subtraction terms for the processes with the largest particle multiplicity.

3.3.1 Double real-radiation corrections

In this subsection we discuss the computation of $\left(d\sigma^{RR}_{\rm NNLO} - d\sigma^S_{\rm NNLO}\right)$ on the right-hand side of the first line in Eq. (3.20) within the antenna subtraction framework.

The $Q\bar{Q}q\bar{q}$ final state:

First we start with the reaction

$$e^-(p_1)e^+(p_2) \to \gamma^*, Z^*(q) \to Q(k_1)\ \bar{Q}(k_2) + q(k_3)\ \bar{q}(k_4)\,, \tag{3.21}$$

where q denotes a massless quark. The corresponding tree-level amplitude, decomposed into color-stripped partial amplitudes with the QCD coupling factored out explicitly, is given by

$$M\left(e^+e^- \to Q\bar{Q}q\bar{q}\right) \;=\; (4\pi\alpha_s)\left(\delta_{i_1i_4}\delta_{i_3i_2} - \frac{1}{N_c}\,\delta_{i_1i_2}\delta_{i_3i_4}\right)\left(\mathcal{M}_4^Q + \mathcal{M}_4^q\right). \tag{3.22}$$

The colors of the quarks and antiquarks are labeled by $i_1, \ldots, i_4$. The $\mathcal{M}_4^Q$ ($\mathcal{M}_4^q$) corresponds to the color-ordered partial amplitudes where the massless (massive) quark-antiquark pair is produced by the splitting of the virtual gluon radiated off one of the quarks produced by the virtual photon or Z boson. These amplitudes still contain the corresponding electroweak couplings. Squaring the matrix element Eq. (3.22) yields the unsubtracted differential cross

section summed over colors and summed/averaged over all spins:

$$\begin{aligned}\sum_q d\sigma_{\rm NNLO}^{Q\bar{Q}q\bar{q}} &= \mathcal{N}\,(4\pi\alpha_s)^2\left(N_c^2-1\right)d\Phi_4\,\mathcal{F}_2^{(4)}(k_1,k_2,k_3,k_4)\\ &\quad\times\left\{n_f\left|\mathcal{M}_4^Q\right|^2+\sum_q\left|\mathcal{M}_4^q\right|^2+\sum_q 2\,\mathrm{Re}\left[\left(\mathcal{M}_4^Q\right)^*\mathcal{M}_4^q\right]\right\},\end{aligned}\tag{3.23}$$

where the sum is over all n_f massless quark flavors. The factor $\mathcal{N}$ is given in Eq. (3.7). The second and third term in the second line of Eq. (3.23) contain the electroweak couplings of the massless quarks q and contribute to the non-universal QCD corrections to the leading-order differential $Q\bar{Q}$ cross section. As long as Q is massive the propagator factors in the second term cannot become singular in the four-parton phase space. The third term has a singularity which integrable with respect to phase-space integration. Therefore neither of these two terms requires an IR subtraction in the four-parton phase space – only the first term in the second line of Eq. (3.23) does.

As mentioned before, instead of finding a single monolithic NNLO IR subtraction in one go, the task is divided into constructing several pieces, each of which is supposed to perform the IR subtraction in a certain IR singular region.

The fully subtracted IR-finite differential cross section for the process (3.21) reads as follows:

$$d\sigma_{\rm NNLO}^{{\rm sub},Q\bar{Q}q\bar{q}}=\sum_q\left(d\sigma_{\rm NNLO}^{Q\bar{Q}q\bar{q}}-d\sigma_{\rm NNLO}^{S,a,Q\bar{Q}q\bar{q}}-d\sigma_{\rm NNLO}^{S,b,2,Q\bar{Q}q\bar{q}}-\sigma_{\rm NNLO}^{S,b,1,Q\bar{Q}q\bar{q}}\right).\tag{3.24}$$

where the NNLO IR subtraction consists of three pieces, $d\sigma_{\rm NNLO}^{S,a,Q\bar{Q}q\bar{q}}$, $d\sigma_{\rm NNLO}^{S,b,2,Q\bar{Q}q\bar{q}}$, $\sigma_{\rm NNLO}^{S,b,1,Q\bar{Q}q\bar{q}}$. By construction the sum of the three subtraction terms is such that it coincides with Eq. (3.23) in all single and double unresolved limits, i.e., when the massless quarks become collinear and/or soft. Thus, Eq. (3.24) is, as a whole, free of IR divergences and can be integrated over the four-parton phase space numerically in $D=4$ dimensions.

In order to understand the cancellation pattern of the IR singularities among the four terms in Eq. (3.24) in all IR-singular regions of the four-parton phase space, it is advantageous to start with the double-unresolved configurations. The subtraction term for removing the singularities

of Eq. (3.23) due to the double unresolved configuration, where both q and $\bar{q}$ become soft, is

$$d\sigma_{\rm NNLO}^{S,b,2,Q\bar{Q}q\bar{q}} = \mathcal{N}\,(4\pi\alpha_s)^2\left(N_c^2-1\right)d\Phi_4 \times\; B_4^0(1_Q,3_q,4_{\bar{q}},2_{\bar{Q}})\left|\mathcal{M}_2^0\left(\widetilde{(134)}_Q,\widetilde{(342)}_{\bar{Q}}\right)\right|^2\mathcal{F}_2^{(2)}\left(\widetilde{k_{134}},\widetilde{k_{342}}\right)\,. \tag{3.25}$$

The tree-level four-parton antenna function B_4^0 is given in [183], which is obtained via appropriately normalizing the squared tree-level color-ordered (partial) S-matrix element of the process $\gamma^* \to Q(k_1)\bar{Q}(k_2)q(k_3)\bar{q}(k_4)$. (The initial state γ^* is chosen by convention.) The normalization is done with respect to the color-stripped two-parton S-matrix element of $\gamma^* \to Q\bar{Q}$ which is the remaining hard skeleton when both massless quarks are soft. Thus,

$$B_4^0(1_Q,3_q,4_{\bar{q}},2_{\bar{Q}}) = \frac{|\mathcal{M}_4^{Q,\gamma^*}(1_Q,3_q,4_{\bar{q}},2_{\bar{Q}})|^2}{|\mathcal{M}_2^{0,\gamma^*}(1_Q,2_{\bar{Q}})|^2}\,, \tag{3.26}$$

where summation over the spins in the numerator and denominator of (3.26) is understood. The tree-level color-ordered S-matrix element $\mathcal{M}_2^0$ is defined in Eq. (3.14). The momenta $\widetilde{k_{ikl}}$ and $\widetilde{k_{jkl}}$ are linear combinations of the momenta k_i, k_j, k_k, k_l obtained from a $4 \to 2$ mapping, cf. Appendix B.2. It is thus relatively easy to see the $d\sigma_{\rm NNLO}^{S,b,2,Q\bar{Q}q\bar{q}}$ does manage to remove the IR singularities of $d\sigma_{\rm NNLO}^{Q\bar{Q}q\bar{q}}$ in the double-unresolved region. Moreover, it is constructed in a way that facilitates the analytic integration over the double-unresolved phase space in D dimensions.

However, $d\sigma_{\rm NNLO}^{S,b,2,Q\bar{Q}q\bar{q}}$ itself is not able to properly approximate the $d\sigma_{\rm NNLO}^{Q\bar{Q}q\bar{q}}$ in the single unresolved region, which is clearly shown by the appearance of the hard skeleton $\mathcal{M}_2^0\left(\widetilde{(134)}_Q,\widetilde{(342)}_{\bar{Q}}\right)$ in Eq. (3.25). We notice that the hard skeleton of $d\sigma_{\rm NNLO}^{Q\bar{Q}q\bar{q}}$ in the single unresolved region is the (squared) S-matrix element of a $2 \to 3$ process like $e^+e^- \to Q\bar{Q}g$ which in general is not simply proportional to the squared matrix element of $e^+e^- \to Q\bar{Q}$ by a constant factor in the whole 3-particle phase-space. Thus we conclude that $d\sigma_{\rm NNLO}^{S,b,2,Q\bar{Q}q\bar{q}}$ given in Eq. (3.25) is unable to remove the IR singularities of $d\sigma_{\rm NNLO}^{Q\bar{Q}q\bar{q}}$ in the single unresolved region. We have to introduce an additional subtraction term for doing this job.

The term $d\sigma_{\rm NNLO}^{S,a,Q\bar{Q}q\bar{q}}$ is introduced to remove the singularities of the unsubtracted differential cross section $d\sigma_{\rm NNLO}^{Q\bar{Q}q\bar{q}}$ associated with the single unresolved configurations. Within the antenna

method, it is given by

$$
\begin{aligned}
d\sigma_{\mathrm{NNLO}}^{S,a,Q\bar{Q}q\bar{q}} = \mathcal{N}\,(4\pi\alpha_s)^2\left(N_c^2-1\right)d\Phi_4(k_1,k_2,k_3,k_4;q) \\
\times\Bigg[\frac{1}{2}E_3^0(1_Q,3_q,4_{\bar{q}})\left|\mathcal{M}_3^0\left(\widetilde{(13)}_Q,\widetilde{(34)}_g,2_{\bar{Q}}\right)\right|^2\mathcal{F}_2^{(3)}\left(\widetilde{k_{13}},\widetilde{k_{34}},k_2\right) \\
+\frac{1}{2}E_3^0(2_{\bar{Q}},3_q,4_{\bar{q}})\left|\mathcal{M}_3^0\left(1_Q,\widetilde{(34)}_g,\widetilde{(42)}_{\bar{Q}}\right)\right|^2\mathcal{F}_2^{(3)}\left(k_1,\widetilde{k_{34}},\widetilde{k_{42}}\right)\Bigg].
\end{aligned}
\tag{3.27}
$$

The three-parton tree-level quark-gluon antenna function E_3^0 with a massive (anti)quark radiator describes a tree-level radiation process where a pair of massless quarks and a massive quark are present in the final state. Note that this antenna becomes singular in the single unresolved collinear region and in the double soft region. The explicit form of this antenna function is given in [178].

The color-stripped tree-level $Q\bar{Q}g$ matrix element $\mathcal{M}_3^0$ is defined in Eq. (3.15). As in Eq. (3.16), the momenta $\widetilde{k_{ij}}$ and $\widetilde{k_{jk}}$ are redefined on-shell momenta, constructed from linear combinations of the momenta k_i, k_j and k_k [172, 184]. The structure of $d\sigma_{\mathrm{NNLO}}^{S,a,Q\bar{Q}q\bar{q}}$ in Eq. (3.27) makes it clear that it is suitable to be analytically integrated over the single unresolved phase space in D dimensions.

Despite the fact that both $d\sigma_{\mathrm{NNLO}}^{S,b,2,Q\bar{Q}q\bar{q}}$ and $d\sigma_{\mathrm{NNLO}}^{S,a,Q\bar{Q}q\bar{q}}$ are able to do a good job in their respective realm, the double and single unresolved region, both of them produce additional unwanted IR singularities in regions which they were not designed for in the first place. To be more specific about this, $d\sigma_{\mathrm{NNLO}}^{S,b,2,Q\bar{Q}q\bar{q}}$ is IR singular in the single unresolved region where the IR divergences of $d\sigma_{\mathrm{NNLO}}^{Q\bar{Q}q\bar{q}}$ are removed by $d\sigma_{\mathrm{NNLO}}^{S,a,Q\bar{Q}q\bar{q}}$, and $d\sigma_{\mathrm{NNLO}}^{S,a,Q\bar{Q}q\bar{q}}$ is also singular in the double unresolved region where the IR divergences of $d\sigma_{\mathrm{NNLO}}^{Q\bar{Q}q\bar{q}}$ are taken care of by $d\sigma_{\mathrm{NNLO}}^{S,b,2,Q\bar{Q}q\bar{q}}$. To eliminate these so-called over-subtracted singularities, we must introduce an additional subtraction term. The construction of such an additional term is easiest if we examine the limiting form of the IR subtraction term $d\sigma_{\mathrm{NNLO}}^{S,a,Q\bar{Q}q\bar{q}}$ in the double unresolved region, that is, when both k_3 and k_4 become soft simultaneously. Following the procedure how the NLO IR subtraction term Eq. (3.16) for Eq. (3.8) is constructed in the single unresolved region, it is not hard to arrive at the following

expression for this compensating term, which we call $d\sigma_{\rm NNLO}^{S,b,1,Q\bar{Q}q\bar{q}}$:

$$
\begin{aligned}
d\sigma_{\rm NNLO}^{S,b,1,Q\bar{Q}q\bar{q}} = -\mathcal{N}\,(4\pi\alpha_s)^2\left(N_c^2-1\right)d\Phi_4(k_1,k_2,k_3,k_4;q)\\
\times\Bigg[\frac{1}{2}E_3^0(1_Q,3_q,4_{\bar{q}})\,A_3^0\Big(\widetilde{(13)}_Q,\widetilde{(34)}_g,2_{\bar{Q}}\Big)\left|\mathcal{M}_2^0\left((\widetilde{(\widetilde{13})(\widetilde{34})})_Q,(\widetilde{(\widetilde{34})2})_{\bar{Q}}\right)\right|^2\\
\times\mathcal{F}_2^{(2)}\left(\widetilde{k_{(\widetilde{13})(\widetilde{34})}},\widetilde{k_{(\widetilde{34})2}}\right)\\
+\frac{1}{2}E_3^0\big(2_{\bar{Q}},4_{\bar{q}},3_q\big)\,A_3^0\Big(1_Q,\widetilde{(34)}_g,\widetilde{(42)}_{\bar{Q}}\Big)\left|\mathcal{M}_2^0\left((1\widetilde{(\widetilde{34})})_Q,(\widetilde{(\widetilde{34})(\widetilde{42})})_{\bar{Q}}\right)\right|^2\\
\times\mathcal{F}_2^{(2)}\left(\widetilde{k_{1(\widetilde{34})}},\widetilde{k_{(\widetilde{34})(\widetilde{42})}}\right)\Bigg]\,. \qquad (3.28)
\end{aligned}
$$

The arguments of the antenna functions A_3^0 are mapped momenta obtained by the $3 \to 2$ mappings. The arguments of the Born matrix elements and of the measurement functions in Eq. (3.28) are obtained by two consecutive $3 \to 2$ mappings, see Appendix B.2. These two iterated $3 \to 2$ mappings are necessary for the same reason as given before, i.e., in order to be able to perform the integration over the unresolved antenna phase-space in analytic fashion and obtain the integrated subtraction term defined in Eq. (3.47) below.

It is not hard to check that the subtraction term given in Eq. (3.28) manages to eliminate, apart from the unwanted IR singularities of $d\sigma_{\rm NNLO}^{S,a,Q\bar{Q}q\bar{q}}$ in the double unresolved region, also the IR singularities $d\sigma_{\rm NNLO}^{S,b,2,Q\bar{Q}q\bar{q}}$ in the single unresolved region. To appreciate this, we recall how the tree-level four-parton antenna function B_4^0 is constructed, namely it is closely connected to the physical S-matrix-element of $\gamma^* \to Q(k_1)\bar{Q}(k_2)q(k_3)\bar{q}(k_4)$. In fact, the relation between $d\sigma_{\rm NNLO}^{S,b,1,Q\bar{Q}q\bar{q}}$ and $d\sigma_{\rm NNLO}^{S,b,2,Q\bar{Q}q\bar{q}}$ closely resembles, as far as their structure is concerned, the relation between $d\sigma_{\rm NNLO}^{S,a,Q\bar{Q}q\bar{q}}$ and $d\sigma_{\rm NNLO}^{Q\bar{Q}q\bar{q}}$. A close examination of $d\sigma_{\rm NNLO}^{S,b,1,Q\bar{Q}q\bar{q}}$ given in Eq. (3.28) confirms that this term approaches $d\sigma_{\rm NNLO}^{S,b,2,Q\bar{Q}q\bar{q}}$ but not $d\sigma_{\rm NNLO}^{S,a,Q\bar{Q}q\bar{q}}$ in the single unresolved limit. Thus $d\sigma_{\rm NNLO}^{S,b,2,Q\bar{Q}q\bar{q}}$ does not approach $d\sigma_{\rm NNLO}^{Q\bar{Q}q\bar{q}}$ in this limit, i.e., is unable to cancel the singularities of the unsubtracted squared S matrix element in this region. In summary, we see that the functionality of the compensating term $d\sigma_{\rm NNLO}^{S,b,1,Q\bar{Q}q\bar{q}}$ is twofold, namely to eliminate spurious IR singularities produced by $d\sigma_{\rm NNLO}^{S,a,Q\bar{Q}q\bar{q}}$ in the double unresolved region and to eliminate spurious IR singularities produced by $d\sigma_{\rm NNLO}^{S,b,2,Q\bar{Q}q\bar{q}}$ in the single unresolved region.

Due to a subtlety associated with angular correlations in the antenna subtraction frame-

work [145, 172], Eq. (3.24) is not yet the appropriate expression for efficient numerical evaluation. The origin of the problem is that the collinear limit of the S-matrix-element maintains the information about the polarization of the splitting parent particle in $g^* \to q\bar{q}, gg$. This spin/polarization dependence of the collinear factorization thus gives rise to a dependence of the collinear limit of the S-matrix-element on the azimuthal angle in the transverse plane of the collinear direction. In the case at hand the gluon radiated off a Q or $\bar{Q}$ that splits into $q\bar{q}$ leads to angular correlations in the unsubtracted S-matrix element squared. However, the term $d\sigma_{\mathrm{NNLO}}^{S,a,Q\bar{Q}q\bar{q}}$ in Eq. (3.27) that was constructed to take care of the single unresolved limit of the squared matrix element when the q and $\bar{q}$ become collinear, is composed of two products, each of which contains a spin-averaged three-parton antenna function and a three-parton Born matrix element. That is, the subtraction term with label 'a' does not contain these angular terms and, therefore, does not have the same local singular behavior as the unsubtracted squared S-matrix element. The four-parton antenna function B_4^0 and thus the term $d\sigma_{\mathrm{NNLO}}^{S,b,2,Q\bar{Q}q\bar{q}}$ Eq. (3.25) contain these angular correlations, simply because the way B_4^0 is constructed. The angular correlations are absent also in the compensating term $d\sigma_{\mathrm{NNLO}}^{S,b,1,Q\bar{Q}q\bar{q}}$ constructed in Eq. (3.28). However, these angular correlations in $d\sigma_{\mathrm{NNLO}}^{Q\bar{Q}q\bar{q}}$ and in the subtraction term $d\sigma_{\mathrm{NNLO}}^{S,b,2,Q\bar{Q}q\bar{q}}$ are averaged out after integration over the azimuthal angles of the spatial parts of the light-like momenta k_3, k_4. (This is also why these angular-correlation terms are no longer present in the integrated antenna functions that will be introduced in sections 3.3.2 and 3.3.3.) These azimuthal angles are defined in the plane orthogonal to the spatial part of the collinear direction $k = k_3 + k_4$. A precise definition is given in Appendix C.

As shown in [171] and in Appendix C, the functional dependence on ϕ of the squared matrix element in the collinear limit is proportional to $\cos(2\phi + \alpha)$. Here ϕ denotes the azimuthal angle of either $\mathbf{k}_3$ or $\mathbf{k}_4$. This suggests [171, 172] that the angular correlations can be averaged out by combining, for each 'point' k_1, k_2, k_3, k_4 in the four-particle phase-space, two kinematic configurations with azimuthal angles ϕ_j and $\phi_j + \pi/2$, $j = 3, 4$.

Thus in our numerical implementation of the subtracted squared matrix element, we evaluate $\left|\mathcal{M}_4^Q\right|^2$ in Eq. (3.23) and the subtraction term $d\sigma_{\mathrm{NNLO}}^{S,b,2,Q\bar{Q}q\bar{q}}$ containing B_4^0 for each set of momenta k_1, k_2, k_3, k_4 also for k_1, k_2, k_{3r}, k_{4r} and take the average. The 4-momenta k_{3r}, k_{4r} are

obtained by rotating k_3, k_4 by an angle $\pi/2$ around the collinear axis $\mathbf{k} = \mathbf{k_3} + \mathbf{k_4}$ following the prescription described in Appendix C. Hence in our formula (3.24) for the subtracted squared matrix element, the respective terms on the right hand side are replaced by the corresponding averages. Let us denote the unsubtracted differential cross section with the averaged $\left|\mathcal{M}_4^Q\right|^2$ by $d\overline{\sigma}_{\rm NNLO}^{Q\bar{Q}q\bar{q}}$ and the sum of the three subtraction terms in (3.24) with the averaged $d\sigma_{\rm NNLO}^{S,b,2,Q\bar{Q}q\bar{q}}$ by $d\overline{\sigma}_{\rm NNLO}^{\text{antennna, } Q\bar{Q}q\bar{q}}$. We sampled the phase space in regions where $k_3 \cdot k_4/s \leq 10^{-7}$ and we found that the ratio

$$\left| \frac{d\overline{\sigma}_{\rm NNLO}^{Q\bar{Q}q\bar{q}}}{d\overline{\sigma}_{\rm NNLO}^{\text{antennna, } Q\bar{Q}q\bar{q}}} - 1 \right| \leq 10^{-6} \,. \tag{3.29}$$

Therefore, this procedure leads to a very good agreement between the unsubtracted S-matrix element squared and the complete subtraction term in the single unresolved and, of course, also in the double unresolved region.

Obviously, no matter what we have introduced here in order to get a IR-finite $d\sigma_{\rm NNLO}^{\text{sub},Q\bar{Q}q\bar{q}}$, the subtraction terms must be exactly canceled (after integration over the unresolved phase space) by their integrated counterparts which are incorporated with opposite signs into the virtual contributions. To be more specific, the analytically integrated version of $d\sigma_{\rm NNLO}^{S,b,2,Q\bar{Q}q\bar{q}}$ over the double unresolved phase-space will be added back to the two-parton virtual corrections, cf. sec. 3.3.3 below. The term $d\sigma_{\rm NNLO}^{S,a,Q\bar{Q}q\bar{q}}$, together with $d\sigma_{\rm NNLO}^{S,b,1,Q\bar{Q}q\bar{q}}$, will be added to the three-parton one-loop corrections once they are integrated analytically over the single unresolved phase-space, see sec. 3.3.2. As already mentioned above, the above angular correlations are averaged out in these integrated IR subtraction terms, just as in the virtual loop corrections.

The $Q\bar{Q}gg$ final state:

The construction of the NNLO antenna subtraction terms for the $Q\bar{Q}gg$ final state follows in essence the above derivation for the $Q\bar{Q}q\bar{q}$ final state. Yet, here the construction of the subtraction terms is more laborious due to the slightly more involved IR singular regions and the fact that there are now two identical particles in the final state.

We consider the reaction

$$e^-(p_1)e^+(p_2) \to \gamma^*, Z^*(q) \to Q(k_1)\bar{Q}(k_2) + g(k_3)g(k_4) \,. \tag{3.30}$$

The corresponding tree-level S-matrix element can be decomposed into color-ordered partial amplitudes as follows:

$$\begin{aligned} M(e^+e^- \to Q\bar{Q}gg) &= (4\pi\alpha_s)\, 2\left[(T^{a_3}T^{a_4})_{i_1 i_2}\, \mathcal{M}_4^g(1_Q, 3_g, 4_g, 2_{\bar{Q}})\right. \\ &\quad \left. + (T^{a_4}T^{a_3})_{i_1 i_2}\, \mathcal{M}_4^g(1_Q, 4_g, 3_g, 2_{\bar{Q}})\right] . \end{aligned} \tag{3.31}$$

The unsubtracted differential cross section, summed over all colors and summed/averaged over all polarizations, is given by

$$\begin{aligned} d\sigma_{\rm NNLO}^{Q\bar{Q}gg} &= \frac{1}{2}\mathcal{N}\,(4\pi\alpha_s)^2\left(N_c^2-1\right) d\Phi_4(k_1,k_2,k_3,k_4;q)\, \mathcal{F}_2^{(4)}(k_1,k_2,k_3,k_4) \\ &\quad \times\left[N_c\big(|\mathcal{M}_4^g(1_Q,3_g,4_g,2_{\bar{Q}})|^2 + |\mathcal{M}_4^g(1_Q,4_g,3_g,2_{\bar{Q}})|^2\big) - \frac{1}{N_c}\,\mathcal{M}_{\rm sc}\right] , \end{aligned} \tag{3.32}$$

where the subleading color term is given by the square of a sum of two partial amplitudes with different orderings,

$$\mathcal{M}_{\rm sc} = \left|\mathcal{M}_4^g(1_Q,3_g,4_g,2_{\bar{Q}}) + \mathcal{M}_4^g(1_Q,4_g,3_g,2_{\bar{Q}})\right|^2 . \tag{3.33}$$

The factor 1/2 in Eq. (3.32) is due to Bose symmetry. The subleading color term $\mathcal{M}_{\rm sc}$ is obviously symmetric under exchange of 3_g and 4_g and is photon-like. That is to say, no non-abelian gluon vertices are involved. Hence, when the two gluons become collinear, this term does not become singular, just like in QED.

A subtracted IR-finite differential cross section is introduced, in analogy to Eq. (3.24), by subtracting three terms from Eq. (3.32):

$$d\sigma_{\rm NNLO}^{{\rm sub},Q\bar{Q}gg} = d\sigma_{\rm NNLO}^{Q\bar{Q}gg} - d\sigma_{\rm NNLO}^{S,a,Q\bar{Q}gg} - d\sigma_{\rm NNLO}^{S,b,2,Q\bar{Q}gg} - d\sigma_{\rm NNLO}^{S,b,1,Q\bar{Q}gg} . \tag{3.34}$$

This expression is by construction free of IR divergences and can be integrated over the four-parton phase space numerically in $D = 4$ dimensions. Similar to the $Q\bar{Q}q\bar{q}$ case, $d\sigma_{\rm NNLO}^{S,\,a\,Q\bar{Q}gg}$ and $d\sigma_{\rm NNLO}^{S,\,b,2\,Q\bar{Q}gg}$ are introduced to subtract the IR singularities of Eq.(3.32) that arise from single-unresolved and double-unresolved configurations, respectively. But notice that here there are

more IR singular regions than in the $Q\bar{Q}q\bar{q}$ case. As in the $Q\bar{Q}q\bar{q}$ case we need an extra compensating term $d\sigma_{\rm NNLO}^{S,b,1,Q\bar{Q}gg}$ to eliminate the spurious IR singularities of $d\sigma_{\rm NNLO}^{S,\,b,2\;Q\bar{Q}gg}$ in the single unresolved limits and of $d\sigma_{\rm NNLO}^{S,\,a\;Q\bar{Q}gg}$ in the double unresolved limit

. Within the antenna subtraction method, these three subtraction terms are given by

$$
\begin{aligned}
d\sigma_{\rm NNLO}^{S,a,Q\bar{Q}gg} = \frac{1}{2}\mathcal{N}\,(4\pi\alpha_s)^2\left(N_c^2-1\right)d\Phi_4(k_1,k_2,k_3,k_4;q)\\
\times\Bigg\{ N_c\Bigg[d_3^0(1_Q,3_g,4_g)\left|\mathcal{M}_3^0\Big(\widetilde{(13)}_Q,\widetilde{(34)}_g,2_{\bar{Q}}\Big)\right|^2\mathcal{F}_2^{(3)}\Big(\widetilde{k_{13}},\widetilde{k_{34}},k_2\Big)\\
+ d_3^0(1_Q,4_g,3_g)\left|\mathcal{M}_3^0\Big(\widetilde{(14)}_Q,\widetilde{(43)}_g,2_{\bar{Q}}\Big)\right|^2\mathcal{F}_2^{(3)}\Big(\widetilde{k_{14}},\widetilde{k_{43}},k_2\Big)\\
+ d_3^0(2_{\bar{Q}},3_g,4_g)\left|\mathcal{M}_3^0\Big(1_Q,\widetilde{(43)}_g,\widetilde{(32)}_{\bar{Q}}\Big)\right|^2\mathcal{F}_2^{(3)}\Big(k_1,\widetilde{k_{43}},\widetilde{k_{32}}\Big)\\
+ d_3^0(2_{\bar{Q}},4_g,3_g)\left|\mathcal{M}_3^0\Big(1_Q,\widetilde{(34)}_g,\widetilde{(42)}_{\bar{Q}}\Big)\right|^2\mathcal{F}_2^{(3)}\Big(k_1,\widetilde{k_{34}},\widetilde{k_{42}}\Big)\Bigg]\\
-\frac{1}{N_c}\Bigg[A_3^0(1_Q,3_g,2_{\bar{Q}})\left|\mathcal{M}_3^0\Big(\widetilde{(13)}_Q,4_g,\widetilde{(32)}_{\bar{Q}}\Big)\right|^2\mathcal{F}_2^{(3)}\Big(\widetilde{k_{13}},k_4,\widetilde{k_{32}}\Big)\\
+ A_3^0(1_Q,4_g,2_{\bar{Q}})\left|\mathcal{M}_3^0\Big(\widetilde{(14)}_Q,3_g,\widetilde{(42)}_{\bar{Q}}\Big)\right|^2\mathcal{F}_2^{(3)}\Big(\widetilde{k_{14}},k_3,\widetilde{k_{42}}\Big)\Bigg]\Bigg\}
\end{aligned}
\tag{3.35}
$$

for subtracting IR divergences of (3.32) in the single unresolved regions and

$$
\begin{aligned}
d\sigma_{\rm NNLO}^{S,b,2,Q\bar{Q}gg} = \frac{1}{2}\mathcal{N}\,(4\pi\alpha_s)^2\left(N_c^2-1\right)d\Phi_4(k_1,k_2,k_3,k_4;q)\\
\times\Bigg\{ N_c\Bigg[A_4^0(k_1,k_3,k_4,k_2)\left|\mathcal{M}_2^0\left(\widetilde{(134)}_Q,\widetilde{(342)}_{\bar{Q}}\right)\right|^2\mathcal{F}_2^{(2)}\Big(\widetilde{k_{134}},\widetilde{k_{342}}\Big)\\
+ A_4^0(k_1,k_4,k_3,k_2)\left|\mathcal{M}_2^0\left(\widetilde{(143)}_Q,\widetilde{(432)}_{\bar{Q}}\right)\right|^2\mathcal{F}_2^{(2)}\Big(\widetilde{k_{143}},\widetilde{k_{432}}\Big)\Bigg]\\
-\frac{1}{N_c}\tilde{A}_4^0(1_Q,3_g,4_g,2_{\bar{Q}})\left|\mathcal{M}_2^0\left(\widetilde{(134)}_Q,\widetilde{(342)}_{\bar{Q}}\right)\right|^2\mathcal{F}_2^{(2)}\Big(\widetilde{k_{134}},\widetilde{k_{342}}\Big)\Bigg\}
\end{aligned}
\tag{3.36}
$$

for subtracting the IR divergences of (3.32) in the double unresolved region. The compensating

subtraction term is given by

$$
\begin{aligned}
d\sigma_{\rm NNLO}^{S,b,1,Q\bar{Q}gg} = &-\frac{1}{2}\mathcal{N}\,(4\pi\alpha_s)^2\left(N_c^2-1\right)d\Phi_4(k_1,k_2,k_3,k_4;q)\\
&\times\Bigg\{ N_c\Bigg[d_3^0(1_Q,3_g,4_g)\,A_3^0\Big(\widetilde{(13)}_Q,\widetilde{(34)}_g,2_{\bar{Q}}\Big)\left|\mathcal{M}_2^0\left(\widetilde{(\widetilde{(13)}\widetilde{(34)})}_Q,\widetilde{(\widetilde{(34)}2)}_{\bar{Q}}\right)\right|^2\mathcal{F}_2^{(2)}\left(\widetilde{k_{\widetilde{(13)}\widetilde{(34)}}},\widetilde{k_{\widetilde{(34)}2}}\right)\\
&+ d_3^0(1_Q,4_g,3_g)\,A_3^0\Big(\widetilde{(14)}_Q,\widetilde{(43)}_g,2_{\bar{Q}}\Big)\left|\mathcal{M}_2^0\left(\widetilde{(\widetilde{(14)}\widetilde{(43)})}_Q,\widetilde{(\widetilde{(43)}2)}_{\bar{Q}}\right)\right|^2\mathcal{F}_2^{(2)}\left(\widetilde{k_{\widetilde{(14)}\widetilde{(43)}}},\widetilde{k_{\widetilde{(43)}2}}\right)\\
&+ d_3^0(2_{\bar{Q}},3_g,4_g)\,A_3^0\Big(1_Q,\widetilde{(43)}_g,\widetilde{(32)}_{\bar{Q}}\Big)\left|\mathcal{M}_2^0\left(\widetilde{(1\widetilde{(43)})}_Q,\widetilde{(\widetilde{(43)}\widetilde{(32)})}_{\bar{Q}}\right)\right|^2\mathcal{F}_2^{(2)}\left(\widetilde{k_{1\widetilde{(43)}}},\widetilde{k_{\widetilde{(43)}\widetilde{(32)}}}\right)\\
&+ d_3^0(2_{\bar{Q}},4_g,3_g)\,A_3^0\Big(1_Q,\widetilde{(34)}_g,\widetilde{(42)}_{\bar{Q}}\Big)\left|\mathcal{M}_2^0\left(\widetilde{(1\widetilde{(34)})}_Q,\widetilde{(\widetilde{(34)}\widetilde{(42)})}_{\bar{Q}}\right)\right|^2\mathcal{F}_2^{(2)}\left(\widetilde{k_{1\widetilde{(34)}}},\widetilde{k_{\widetilde{(34)}\widetilde{(42)}}}\right)\Bigg]\\
&-\frac{1}{N_c}\Bigg[A_3^0(1_Q,3_g,2_{\bar{Q}})\,A_3^0\Big(\widetilde{(13)}_Q,4_g,\widetilde{(32)}_{\bar{Q}}\Big)\left|\mathcal{M}_2^0\left(\widetilde{(\widetilde{(13)}4)}_Q,\widetilde{(4\widetilde{(32)})}_{\bar{Q}}\right)\right|^2\mathcal{F}_2^{(2)}\Big(\widetilde{k_{\widetilde{(13)}4}},\widetilde{k_{4\widetilde{(32)}}}\Big)\\
&+ A_3^0(1_Q,4_g,2_{\bar{Q}})\,A_3^0\Big(\widetilde{(14)}_Q,3_g,\widetilde{(42)}_{\bar{Q}}\Big)\left|\mathcal{M}_2^0\left(\widetilde{(\widetilde{(14)}3)}_Q,\widetilde{(3\widetilde{(42)})}_{\bar{Q}}\right)\right|^2\mathcal{F}_2^{(2)}\Big(\widetilde{k_{\widetilde{(14)}3}},\widetilde{k_{3\widetilde{(42)}}}\Big)\Bigg]\Bigg\}\,.
\end{aligned}
\tag{3.37}
$$

The tree-level massive quark-gluon antenna function $d_3^0(1_Q,3_g,4_g)$ is given in [178]. It is employed to capture the singular behavior due to the unresolved radiation of a gluon with momentum k_3 between a massive quark Q and a hard resolved gluon of momentum k_4. Notice that the radiation of the two gluons in this antenna function is color-ordered and $d_3^0(1_Q,3_g,4_g)$ is not symmetric with respect to 3_g and 4_g. The component that is anti-symmetric in 3_g and 4_g vanishes by integration over the unresolved antenna phase space. The leading-color four-parton $Q\bar{Q}gg$ antenna function A_4^0 and the subleading color function $\tilde{A}_4^0$, which were derived in [174], govern the color-ordered and non-ordered (photon-like) radiations between a pair of massive radiator quarks, respectively. They are given by

$$
A_4^0(1_Q,3_g,4_g,2_{\bar{Q}})| = \frac{|\mathcal{M}_4^{g,\gamma^*}(1_Q,3_g,4_g,2_{\bar{Q}})|^2}{|\mathcal{M}_2^{0,\gamma^*}(1_Q,2_{\bar{Q}})|^2}\,, \tag{3.38}
$$

$$
\tilde{A}_4^0(1_Q,3_g,4_g,2_{\bar{Q}})| = \frac{\left|\mathcal{M}_4^{g,\gamma^*}(1_Q,3_g,4_g,2_{\bar{Q}})+\mathcal{M}_4^{g,\gamma^*}(1_Q,4_g,3_g,2_{\bar{Q}})\right|^2}{|\mathcal{M}_2^{0,\gamma^*}(1_Q,2_{\bar{Q}})|^2}\,. \tag{3.39}
$$

Summation over the spins in the numerator and denominator of these ratios is understood. The mapped momenta denoted by a tilde and double tilde in Eq. (3.35) – Eq. (3.37) are obtained

from $3 \to 2$, $4 \to 2$, and two iterated $3 \to 2$ mappings, respectively, in completely analogous fashion as in the $Q\bar{Q}q\bar{q}$ case, cf. Appendix B.

The previous remarks on the angular correlations due to gluon splitting in the collinear limit made below eq. Eq. (3.28) apply also here, where the angular correlations in the unsubtracted squared S matrix element are now due to $g \to gg$ and they are present only in the leading color part. As far as the subtraction terms are concerned, these correlations are present only in the leading-color part of the subtraction term Eq. (3.36). Recall that the subleading color parts do not contain a non-abelian vertex.

In analogy to the $Q\bar{Q}q\bar{q}$ case these leading-color terms are evaluated for each set of momenta k_1, k_2, k_3, k_4 and for k_1, k_2, k_{3r}, k_{4r} and then their average is taken. Also here, a very good numerical agreement was found between the averaged $d\sigma_{\rm NNLO}^{Q\bar{Q}gg}$ and the sum of the subtraction terms in the single and double unresolved region characterized by $k_3 \cdot k_4/s \leq 10^{-7}$. We sampled the phase space in this region and found that

$$\left| \frac{d\overline{\sigma}_{\rm NNLO}^{Q\bar{Q}gg}}{d\overline{\sigma}_{\rm NNLO}^{\text{antennna, } Q\bar{Q}gg}} - 1 \right| \leq 10^{-5}\,, \tag{3.40}$$

where the notation in (3.40) is analogous to the notation used in (3.29).

3.3.2 Real-virtual corrections

This subsection is devoted to the computation of the antenna-subtracted order α_s^2 contribution of the $Q\bar{Q}g$ final state,

$$e^-(p_1)e^+(p_2) \to \gamma^*, Z^*(q) \to Q(k_1)\bar{Q}(k_2) + g(k_3)\,, \tag{3.41}$$

to the differential massive quark-pair production cross section. In the schematic formula (3.20) this contribution corresponds to the second term on the right-hand side of the first line of this equation.

The unsubtracted real-virtual cross section:

This contribution is generated by the interference between the tree-level and one-loop $Q\bar{Q}g$

final-state amplitude. Using the conventions of Eq. (3.15) the unsubtracted $\mathcal{O}(\alpha_s^2)$ correction, summed over colors and summed/averaged over spins, is given by

$$\begin{aligned} d\sigma_{\rm NNLO}^{RV,Q\bar{Q}g} &= \mathcal{N}\,(4\pi\alpha_s)^2\left(N_c^2-1\right)C(\epsilon)d\Phi_3(k_1,k_2,k_3;q)\,\mathcal{F}_2^{(3)}(k_1,k_2,k_3) \\ &\quad\times\Bigg[N_c\,\delta\mathcal{M}_3^{1,\rm lc}\big(1_Q,3_g,2_{\bar{Q}}\big)-\frac{1}{N_c}\,\delta\mathcal{M}_3^{1,\rm sc}\big(1_Q,3_g,2_{\bar{Q}}\big)+n_f\delta\mathcal{M}_3^{1,f}\big(1_Q,3_g,2_{\bar{Q}}\big) \\ &\quad+\delta\mathcal{M}_3^{1,F}\big(1_Q,3_g,2_{\bar{Q}}\big)+\delta\mathcal{M}_3^{1,\rm tr}\big(1_Q,3_g,2_{\bar{Q}}\big)\Bigg]. \end{aligned} \tag{3.42}$$

The factor $C(\epsilon)$ is defined in Eq.(3.12). We have introduced the shorthand notation

$$\delta\mathcal{M}_3^{1,X}\big(1_Q,3_g,2_{\bar{Q}}\big)=2\,\mathrm{Re}\left[\big(\mathcal{M}_3^0\big(1_Q,3_g,2_{\bar{Q}}\big)\big)^*\,\mathcal{M}_3^{1,X}\big(1_Q,3_g,2_{\bar{Q}}\big)\right], \tag{3.43}$$

with $X\in\{\mathrm{lc},\mathrm{sc},f,F,\mathrm{tr}\}$. We recall that $\mathcal{M}_3^1$ is the UV-renormalized one-loop amplitude which we computed using the hybrid renormalization scheme defined at the beginning of section 3.2 and in Appendix A.2. The analytic computation of Eq. (3.42) is standard and our computation was sketched below Eq. (3.15). The term $\delta\mathcal{M}_3^{1,\rm tr}$ involves a triangle fermion loop and is free of UV and IR singularities. As already mentioned above, this term belongs to the so-called non-universal QCD corrections because it contains electroweak couplings of quarks other than the external heavy quark. The other contributions to the unsubtracted cross section contain explicit IR poles (single and double poles in $1/\epsilon$) from the IR region in the loop integration. In addition, in the region where the external gluon becomes soft, Eq. (3.42) develops additional IR singularities which would lead to additional poles in ϵ after phase-space integration in D dimensions. We call these singularities of Eq. (3.42) in the limit $k_3\to 0$ implicit IR singularities. Both the explicit and implicit IR singularities must be subtracted with appropriate terms in order that the integration over the three-parton phase space can be performed numerically in 4 dimensions.

Subtraction of explicit infrared poles:

The explicit IR poles (in the DR regulator ϵ) of Eq. (3.42) are canceled by adding the IR subtraction terms Eq. (3.27) and Eq. (3.35), integrated over the phase space of one unresolved

parton:

$$
\begin{aligned}
d\sigma^{T,a,Q\bar{Q}g}_{\rm NNLO} &= -\int_1 d\sigma^{S,a,Q\bar{Q}gg}_{\rm NNLO} - \sum_q \int_1 d\sigma^{S,a,Q\bar{Q}q\bar{q}}_{\rm NNLO} \\
&= -\mathcal{N}\,(4\pi\alpha_s)^2\left(N_c^2-1\right) C(\epsilon) d\Phi_3(k_1,k_2,k_3;q)\,\mathcal{F}_2^{(3)}(k_1,k_2,k_3) \\
&\quad \times \Bigg[\frac{N_c}{2}\Big(\mathcal{D}_3^0\big(\epsilon,\mu^2/k_{13}^2;z_{13}\big) + \mathcal{D}_3^0\big(\epsilon,\mu^2/k_{23}^2;z_{23}\big)\Big) - \frac{1}{N_c}\mathcal{A}_3^0\big(\epsilon,\mu^2/k_{12}^2;y_{12}\big) \\
&\quad + \frac{n_f}{2}\Big(\mathcal{E}_3^0\big(\epsilon,\mu^2/k_{13}^2;z_{13}\big) + \mathcal{E}_3^0\big(\epsilon,\mu^2/k_{23}^2;z_{23}\big)\Big)\Bigg] \big|\mathcal{M}_3^0\big(1_Q,3_g,2_{\bar{Q}}\big)\big|^2 . \qquad (3.44)
\end{aligned}
$$

The integrated quark-gluon antenna functions $\mathcal{D}_3^0$ and $\mathcal{E}_3^0$, which are the integrated versions of the tree-level quark-gluon antenna functions d_3^0 and E_3^0, respectively, can be found in [178,179]. The explicit poles in ϵ of these functions and of $\mathcal{A}_3^0$ cancel[1] the explicit IR poles in Eq. (3.42). The kinematic invariants that appear in the arguments of these functions are

$$
k_{ij}^2 = (k_i+k_j)^2, \quad z_{ij} = \frac{m_Q}{\sqrt{k_{ij}^2}}, \quad \beta_{ij} = \sqrt{1-4z_{ij}^2}, \quad y_{ij} = \frac{1-\beta_{ij}}{1+\beta_{ij}}\,. \qquad (3.45)
$$

The one-loop single-unresolved subtraction term:

The subtraction term (3.44) takes care of the explicit $1/\epsilon^2$ and $1/\epsilon$ IR poles of the unsubtracted 3-parton matrix element. As mentioned above, the matrix element in the square bracket of (3.42) develops, in addition, IR singularities in the 3-parton phase space when the external gluon becomes soft. These implicit singularities (using the above terminology) can be canceled with the following subtraction term:

$$
\begin{aligned}
d\sigma^{T,b,Q\bar{Q}g}_{\rm NNLO} &= \mathcal{N}\,(4\pi\alpha_s)^2\left(N_c^2-1\right) C(\epsilon) d\Phi_3(k_1,k_2,k_3;q)\,\mathcal{F}_2^{(2)}\Big(\widetilde{k_{13}},\widetilde{k_{32}}\Big) \\
&\quad \times \Bigg(N_c\Bigg[A_3^1\big(1_Q,3_g,2_{\bar{Q}}\big)\left|\mathcal{M}_2^0\Big(\widetilde{(13)}_Q,\widetilde{(32)}_{\bar{Q}}\Big)\right|^2 \\
&\qquad + A_3^0\big(1_Q,3_g,2_{\bar{Q}}\big)\,\delta\mathcal{M}_2^1\Big(\widetilde{(13)}_Q,\widetilde{(32)}_{\bar{Q}}\Big)\Bigg]
\end{aligned}
$$

[1] The function $\mathcal{D}_3^0$ has poles of order $1/\epsilon^2$ and $1/\epsilon$, while $\mathcal{E}_3^0$ and $\mathcal{A}_3^0$ have poles of order $1/\epsilon$.

$$
\begin{aligned}
&- \frac{1}{N_c}\Bigg[\tilde{A}_3^1(1_Q,3_g,2_{\bar{Q}})\left|\mathcal{M}_2^0\Big(\widetilde{(13)}_Q,\widetilde{(32)}_{\bar{Q}}\Big)\right|^2 \\
&\qquad + A_3^0(1_Q,3_g,2_{\bar{Q}})\,\delta\mathcal{M}_2^1\Big(\widetilde{(13)}_Q,\widetilde{(32)}_{\bar{Q}}\Big)\Bigg] \\
&+\Big(n_f\,\hat{A}_{3,f}^1(1_Q,3_g,2_{\bar{Q}})+\hat{A}_{3,F}^1(1_Q,3_g,2_{\bar{Q}})\Big)\left|\mathcal{M}_2^0\Big(\widetilde{(13)}_Q,\widetilde{(32)}_{\bar{Q}}\Big)\right|^2\Big). \qquad (3.46)
\end{aligned}
$$

The massive one-loop quark-antiquark antenna functions A_3^1, $\tilde{A}_3^1$, $\hat{A}_{3,f}^1$, and $\hat{A}_{3,F}^1$ were first computed in [78] and A_3^0 is given in [178,179]. The two-parton Born times one-loop interference term $\delta\mathcal{M}_2^1$ is defined in Eq.(3.13). All these terms, except A_3^0 and $\hat{A}_{3,F}^1$, contain poles in ϵ.

The compensation term for oversubtracted poles:

We recall that the sum of $d\sigma_{\rm NNLO}^{S,\,a\;Q\bar{Q}ij}$ and $d\sigma_{\rm NNLO}^{S,\,b,2\;Q\bar{Q}ij}$ fails to exactly approach the differential cross section $d\sigma_{\rm NNLO}^{Q\bar{Q}ij}$ (where $ij = gg$ or $q\bar{q}$) in the IR singular regions due to the spurious IR singularities produced by these subtraction terms (although each of them works fine separately in the IR singular region for which they were constructed in the first place). This mismatch called for an additional compensating term $d\sigma_{\rm NNLO}^{S,\,b,1\;Q\bar{Q}ij}$.

Here we have a similar situation. The explicit IR poles in ϵ of (3.42) are canceled by those of (3.44) in the whole 3-parton phase space, and the implicit singularities of (3.42) in the limit $k_3 \to 0$ are canceled by those of (3.46). But the subtraction term (3.46) has also explicit IR poles which are contained in the 1-loop antenna functions and in the 1-loop matrix element $\delta\mathcal{M}_2^1$. Therefore, we need an additional compensating term with explicit IR poles in ϵ that cancel those of Eq.(3.46) exactly in the whole 3-parton phase-space and whose term of order ϵ^0 has the same singular behavior as (3.44) when the external gluon becomes soft.

Since the integrals of $d\sigma_{\rm NNLO}^{S,\,b,1\;Q\bar{Q}gg}$ and $d\sigma_{\rm NNLO}^{S,\,b,1\;Q\bar{Q}q\bar{q}}$ (introduced in sec. 3.3.1) over the phase space of one unresolved parton must be included in the three-parton corrections, it is not too hard to convince oneself that the following expression plays the role of compensation needed here [78]:

$$
d\sigma_{\rm NNLO}^{T,c,Q\bar{Q}g} = -\int_1 d\sigma_{\rm NNLO}^{S,b,1,Q\bar{Q}gg} - \int_1 d\sigma_{\rm NNLO}^{S,b,1,Q\bar{Q}q\bar{q}}\ . \qquad (3.47)
$$

The integrands are given in Eq.(3.28) and Eq.(3.37), respectively. The integration over the phase space of one unresolved parton yields

$$\begin{aligned} d\sigma_{\rm NNLO}^{T,c,Q\bar{Q}g} &= \mathcal{N}\,(4\pi\alpha_s)^2\left(N_c^2-1\right)C(\epsilon)d\Phi_3(k_1,k_2,k_3;q)\,\left|\mathcal{M}_2^0\Big(\widetilde{(13)}_Q,\widetilde{(32)}_{\bar{Q}}\Big)\right|^2\mathcal{F}_2^{(2)}(\widetilde{p_{13}},\widetilde{p_{32}}) \\ &\quad\times\Bigg[\frac{N_c}{2}\Big(\mathcal{D}_3^0\big(\epsilon,\mu^2/k_{13}^2;z_{13}\big)+\mathcal{D}_3^0\big(\epsilon,\mu^2/k_{23}^2;z_{23}\big)\Big)-\frac{1}{N_c}\mathcal{A}_3^0\big(\epsilon,\mu^2/k_{12}^2;y_{12}\big) \\ &\quad+\frac{n_f}{2}\Big(\mathcal{E}_3^0\big(\epsilon,\mu^2/k_{13}^2;z_{13}\big)+\mathcal{E}_3^0\big(\epsilon,\mu^2/k_{23}^2;z_{23}\big)\Big)\Bigg]A_3^0\big(1_Q,3_g,2_{\bar{Q}}\big)\ . \end{aligned} \tag{3.48}$$

In summary, the pattern of cancellation or matching of IR singularities among the four terms $d\sigma_{\rm NNLO}^{RV,Q\bar{Q}g}$, $d\sigma_{\rm NNLO}^{T,a,Q\bar{Q}g}$, $d\sigma_{\rm NNLO}^{T,b,Q\bar{Q}g}$, and $d\sigma_{\rm NNLO}^{T,c,Q\bar{Q}g}$ is as follows. The poles in ϵ of $d\sigma_{\rm NNLO}^{T,a,Q\bar{Q}g}$ cancel exactly those of $d\sigma_{\rm NNLO}^{RV,Q\bar{Q}g}$ everywhere in the three-parton phase space. The same cancellation holds between the ϵ pole terms of $d\sigma_{\rm NNLO}^{T,b,Q\bar{Q}g}$ and that of $d\sigma_{\rm NNLO}^{T,c,Q\bar{Q}g}$. In the region where the external gluon is unresolved – that is, when $k_3 \to 0$ – the ϵ-free part of $d\sigma_{\rm NNLO}^{T,b,Q\bar{Q}g}$ correctly approximates the implicit infrared singularities of Eq.(3.42). In this soft region, the sum of $d\sigma_{\rm NNLO}^{T,a,Q\bar{Q}g}$ and $d\sigma_{\rm NNLO}^{T,c,Q\bar{Q}g}$ is also finite, namely the implicit IR singular pieces contained in these two terms cancel among each other.

The subtracted three-parton cross section at NNLO:

Combining Eqs. (3.42), (3.44), (3.46), and (3.48) yields an expression that is free of both explicit and implicit IR singularities in the entire three-parton phase space in $D = 4$ dimensions:

$$\int_{\Phi_3}\Big[d\sigma_{\rm NNLO}^{RV,Q\bar{Q}g}-d\sigma_{\rm NNLO}^{T,a,Q\bar{Q}g}-d\sigma_{\rm NNLO}^{T,b,Q\bar{Q}g}-d\sigma_{\rm NNLO}^{T,c,Q\bar{Q}g}\Big]_{\epsilon=0}=\text{finite}. \tag{3.49}$$

We recall that the terms $d\sigma_{\rm NNLO}^{T,a,Q\bar{Q}g}$ and $d\sigma_{\rm NNLO}^{T,c,Q\bar{Q}g}$ are counterbalanced by the double-real subtraction terms $d\sigma_{\rm NNLO}^{S,a,Q\bar{Q}ij}$ and $d\sigma_{\rm NNLO}^{S,b,1,Q\bar{Q}ij}$ $(ij = gg, q\bar{q})$, respectively, that were defined in section 3.3.1. Hence, only $d\sigma_{\rm NNLO}^{T,b,2,Q\bar{Q}g}$ integrated over over the gluon phase space has to be added back to the two-parton contribution that will be discussed in the next subsection.

3.3.3 Double virtual corrections

Finally, we are at the stage of discussing how to compute the order α_s^2 contribution of the $Q\bar{Q}$ final state to the differential massive quark-pair production cross section within the antenna framework, that is, the sum of the three terms in the second line of Eq.(3.20).

Unsubtracted real-virtual cross section:

The renormalized two-parton one-loop and two-loop $Q\bar{Q}$ matrix elements defined in Eq. (3.14) yield the following $\mathcal{O}(\alpha_s^2)$ correction to the differential cross section:

$$\begin{aligned} d\sigma_{\mathrm{NNLO}}^{VV,Q\bar{Q}} &= \mathcal{N}\left(\bar{C}(\epsilon)\right)^2\left(\frac{\alpha_s}{2\pi}\right)^2 N_c\, d\Phi_2(k_1,k_2;q)\,\mathcal{F}_2^{(2)}(k_1,k_2)\,\Big\{4C_F^2\left|\mathcal{M}_2^1\big(1_Q,2_{\bar{Q}}\big)\right|^2 \\ &\quad + 2\mathrm{Re}[\mathcal{M}_2^{0*}\big(1_Q,2_{\bar{Q}}\big)\,\mathcal{M}_2^2\big(1_Q,2_{\bar{Q}}\big)]\Big\}. \end{aligned} \tag{3.50}$$

Summation over all colors and spins of the final state is understood. The factor $\bar{C}(\epsilon)$ is defined in Eq.(3.12). The real and imaginary parts of the one-loop vertex functions $VQ\bar{Q}$ ($V=\gamma,Z$), up to and including terms of order ϵ, and the corresponding two-loop vertex form-factors to order ϵ^0 were computed in [175–177]. With these vertex form factors, Eq.(3.50) can be computed in straightforward fashion. The last term on the right-hand side of Eq.(3.50) can be decomposed into different color structures, that is, leading and subleading color contributions, terms that involve a massless and massive quark loop in the gluon vacuum polarization tensor, and fermion-triangle loop contributions summed over all quark flavors. These triangle loop contributions (the type-B contributions, see sec. 3.1.1) which are finite by themselves [177], are non-universal QCD corrections to the leading-order cross section.

The subtraction term:

Recalling the subtraction terms that were introduced above, those that remain to be counterbalanced are $d\sigma_{\mathrm{NNLO}}^{T,b,Q\bar{Q}g}$ (cf. Eq. (3.46)) and $d\sigma^{S,b,2,Q\bar{Q}ij}$ ($ij=q\bar{q},gg$) (cf. Eq. (3.25) and Eq. (3.36)). They have to be integrated over the unresolved one-parton, respectively two-parton phase space in order to serve as counterterm for the IR poles in ϵ of the double-virtual correction Eq.(3.50).

We get

$$
\begin{aligned}
&\int_1 d\sigma_{\rm NNLO}^{T,b,Q\bar{Q}g} + \int_2 d\sigma_{\rm NNLO}^{S,b,2,Q\bar{Q}gg} + \sum_q \int_2 d\sigma_{\rm NNLO}^{S,b,2,Q\bar{Q}q\bar{q}} \\
&= \mathcal{N}\left(\bar{C}(\epsilon)\right)^2 \left(\frac{\alpha_s}{2\pi}\right)^2 \left(N_c^2-1\right) d\Phi_2(k_1,k_2;q)\, \mathcal{F}_2^{(2)}(k_1,k_2) \\
&\quad \times \Bigg\{ N_c \Bigg[\Big(\mathcal{A}_4^0\big(\epsilon,\mu^2/s;y\big) + \mathcal{A}_3^1\big(\epsilon,\mu^2/s;y\big) \Big) \big|\mathcal{M}_2^0\big(1_Q,2_{\bar{Q}}\big)\big|^2 \\
&\qquad\qquad + \mathcal{A}_3^0\big(\epsilon,\mu^2/s;y\big)\, \delta\mathcal{M}_2^1\big(1_Q,2_{\bar{Q}}\big) \Bigg] \\
&\quad - \frac{1}{N_c} \Bigg[\Big(\frac{1}{2}\,\tilde{\mathcal{A}}_4^0\big(\epsilon,\mu^2/s;y\big) + \tilde{\mathcal{A}}_3^1\big(\epsilon,\mu^2/s;y\big) \Big) \big|\mathcal{M}_2^0\big(1_Q,2_{\bar{Q}}\big)\big|^2 \\
&\qquad\qquad + \mathcal{A}_3^0\big(\epsilon,\mu^2/s;y\big)\, \delta\mathcal{M}_2^1\big(1_Q,2_{\bar{Q}}\big) \Bigg] \\
&\quad + 2\,T_R\,n_f \Big(\mathcal{B}_4^0\big(\epsilon,\mu^2/s;y\big) + \hat{\mathcal{A}}_{3,f}^1\big(\epsilon,\mu^2/s;y\big) \Big) \big|\mathcal{M}_2^0\big(1_Q,2_{\bar{Q}}\big)\big|^2 \\
&\quad + 2\,T_R\,\hat{\mathcal{A}}_{3,F}^1\big(\epsilon,\mu^2/s;y\big) \big|\mathcal{M}_2^0\big(1_Q,2_{\bar{Q}}\big)\big|^2 \Bigg\}. \qquad (3.51)
\end{aligned}
$$

The auxiliary variable y is defined in Eq.(3.18). The integrated antenna functions $\mathcal{B}_4^0$, $\mathcal{A}_4^0$, and $\tilde{\mathcal{A}}_4^0$ were computed in [174, 183] and $\mathcal{A}_3^1$, $\tilde{\mathcal{A}}_3^1$, $\hat{\mathcal{A}}_{3,f}^1$, and $\hat{\mathcal{A}}_{3,F}^1$ were determined in [78].

The subtraction term Eq. (3.51) has to be added to Eq. (3.50). In the sum all IR poles cancel analytically.

$$
\int_{\Phi_2} \left[d\sigma_{\rm NNLO}^{VV,Q\bar{Q}} + \int_1 d\sigma_{\rm NNLO}^{T,b,Q\bar{Q}g} + \int_2 d\sigma_{\rm NNLO}^{S,b,2,Q\bar{Q}gg} + \sum_q \int_2 d\sigma_{\rm NNLO}^{S,b,2,Q\bar{Q}q\bar{q}} \right]_{\epsilon=0} = \text{finite}. \qquad (3.52)
$$

After summing these terms and after analytic cancellation of the IR poles, one can take the limit $\epsilon \to 0$ and perform the remaining integration over the two-parton phase space in four dimensions.

Chapter 4

Application to $t\bar{t}$ and $b\bar{b}$ production

In this chapter we apply the formalism developed in the preceding chapter to top-quark pair production in the continuum and to bottom-quark pair production at the Z-boson resonance. In the following sections we present or results for the respective $t\bar{t}$ and $b\bar{b}$ cross sections and several distributions at NNLO QCD. Our results for the t- and b-quark forward-backward asymmetry at NNLO QCD will be discussed separately in chapter 5.

For our numerical computations in this and in the next chapter we use the following Standard Model input parameters. The values of the weak-boson masses and of the total Z-boson decay width are taken from [185]:

$$m_W = 80.385 \text{ GeV}\,, \quad m_Z = 91.1876 \text{ GeV}\,, \quad \Gamma_Z = 2.4952 \text{ GeV}\,. \tag{4.1}$$

For the QCD coupling defined in the $\overline{\text{MS}}$ scheme in 5 flavor QCD we use the value [186]

$$\alpha_s^{(n_f=5)}(\mu = m_Z) = 0.118\,. \tag{4.2}$$

For the masses of the top quark and bottom quark defined in the on-shell scheme we use

$$m_t = 173.34 \text{ GeV}\,, \quad m_b = 4.89 \text{ GeV}\,. \tag{4.3}$$

As to the top quark mass, we have identified the central value of the average of experimental

extractions [7] of the top-quark mass (from fits with templates to the t-quark invariant mass distribution and other variables) with the on-shell or pole mass of this quark. The value (4.3) of the pole mass of the b quark is obtained as follows. The relation between the the pole mass m_b and the $\overline{\rm MS}$ mass $\overline{m}_b(\overline{m}_b)$ is of the form

$$m_b = \overline{m}_b(\overline{m}_b)\ f(n_l, \overline{m}_l, \overline{m}_b, \alpha_s)\,, \tag{4.4}$$

where $n_l = 4$, $\overline{m}_l$ $(l = 1, \ldots, 4)$ are the $\overline{\rm MS}$ masses of the u, d, s, c quarks, and $\alpha_s(\overline{m}_b)$ is the $\overline{\rm MS}$ coupling of 5-flavor QCD which is evaluated at $\mu = \overline{m}_b$. The conversion relation f is known in QCD perturbation theory to order α_s^3 [187–189]. Using this 3-loop relation, the value $\overline{m}_b(\overline{m}_b) = 4.18$ GeV [186], $\overline{m}_c = 1.27$ GeV [186], the 3-loop renormalization group running of α_s with the input value (4.2), and putting the masses of the u, d, s quarks to zero, we obtain the on-shell b-quark mass given in Eq. (4.3).

In the case of top quark production, the other 5 quarks (including the bottom quark) are taken to be massless and $\alpha_s(\mu)$ is computed in 6-flavor QCD using the input value (4.2), the respective matching relation [190] as described in Appendix A.3, and 3-loop renormalization group running. When we consider bottom production at the Z-pole, we work in 5 flavor QCD with α_s given in (4.2). Here we use massless u, d, s, c quarks and and a massive b quark. In QCD with α_s defined in the $\overline{\rm MS}$ renormalization scheme with 5 flavors, the top quark is decoupled from the gluon polarization tensor but is still present in the 1-loop and 2-loop triangle diagrams ('anomaly-type diagrams') shown in figs. 3.2 and 3.1.

We work to lowest order in the electroweak couplings. The sine of the weak mixing angle, $\sin^2\theta_W$, is fixed by $\sin^2\theta_W = 1 - m_W^2/m_Z^2$. For computing the electroweak couplings we use the so-called G_μ scheme [66] where the electromagnetic coupling is given by $\alpha = \sqrt{2} G_\mu m_W^2 s_W^2/\pi = 7.5624 \times 10^{-3}$ with the Fermi-constant $G_\mu = 1.166379 \times 10^{-5}$ GeV^{-2}.

Our approach to computing the cross section of the reaction $e^+e^- \to Q\bar{Q}X$ in the SM is fully differential, that is, we use the respective antenna-subtracted differential cross sections for 2-parton, 3-parton, and 4-parton final states of chapter 3, integrate them over the respective phase-spaces and add them up. Our approach allows to apply arbitrary phase-space cuts.

However, we refrain from applying cuts in the following.

As emphasized above, we work to lowest order in the electroweak couplings. Each of the various contributions to the differential $Q\bar{Q}$ cross section up to and including order α_s^2 is given by the sum of a s-channel γ and Z-boson contribution and a γZ interference term[1]. In practice, it is technically more convenient to reorganize these electroweak components according to the vector and axial vector couplings involved, rather than γ and Z-boson mediators. We denote these contributions to the differential cross section by $d\sigma^{(i,j)}$, where the first index i in the superscript (i,j) labels the final state, i.e., $i = Q\bar{Q}$, $Q\bar{Q}g$, $Q\bar{Q}gg$, $Q\bar{Q}q\bar{q}$, $Q\bar{Q}Q\bar{Q}$ and the second index j refers to the power of the QCD coupling α_s involved. The $d\sigma^{(i,j)}$ can be written as contractions of lepton and hadron tensors. This is schematically illustrated in fig. 4.1. The $d\sigma^{(i,j)}$ have, for unpolarized e^+e^- collisions, the structure

$$d\sigma^{(i,j)} = \frac{1}{8s}\frac{(4\pi\alpha)^2(4\pi\alpha_s)^j}{|D_Z|^2} \sum_{F,(X,Y,X',Y')\in\mathcal{K}} k^{XY}_{F,X'Y'} L^{\mu\nu}_{XY} H^{(i,j),F,X',Y'}_{\mu\nu} d\Phi_i \,, \tag{4.5}$$

where

$$D_Z = s - m_Z^2 + \mathrm{i} m_Z \Gamma_Z \tag{4.6}$$

is the denominator of the Z-boson propagator, and $L^{\mu\nu}_{XY}$ and $H^{(i,j),F,X',Y'}_{\mu\nu}$ are the lepton and the antenna-subtracted, i.e., IR finite hadron tensors. The symbol $\mathcal{K}$ denotes the following index set:

$$\begin{aligned}\mathcal{K} = \{&(V,V,V,V),(V,V,A,A),(A,A,V,V),(A,A,A,A),\\ &(V,A,V,A),(V,A,A,V),(A,V,A,V),(A,V,V,A)\}\,,\end{aligned} \tag{4.7}$$

where V and A label the vector and axial vector couplings proportional to γ^μ and $\gamma^\mu\gamma_5$, respectively, that appear in the electron Z/γ, heavy quark Z/γ, and light quark Z/γ vertices. The first two (last two) labels in (X,Y,X',Y') refer to the two electroweak electron vertices (heavy quark, respectively light quark) vertices, cf. fig. 4.1. The index F in (4.5) refers to the case where the two electroweak vertices in a hadron tensor are associated both with the

[1] In principle, s-channel SM Higgs-boson exchange contributes also to (4.8), but this contribution can be safely neglected because of the tiny Higgs Yukawa coupling to the electron.

heavy quark ($F = QQ$), both with a light quark ($F = qq$), and with a light and a heavy quark ($F = qQ$), respectively. The $k^{XY}_{F,X'Y'}$ are listed in Appendix A.1 and denote sums of products of electroweak vector and axial vector couplings. They involve also factors of s (the denominator of the photon propagator) and D_Z. A sum over the light quark flavors in (4.5) is understood.

The two-loop $Q\bar{Q}$ matrix elements and the integrated antenna subtraction terms contain harmonic polylogarithms (HPL) [180]. We evaluate them with the codes of refs. [181,182]. The integrated antenna functions $\mathcal{A}^1_3$, $\tilde{\mathcal{A}}^1_3$ are expressed in terms of HPL and cyclotomic harmonic polylogarithms [191–193]. We evaluate the cyclotomic HPL numerically by using their Poincaré-iterated integral representations.

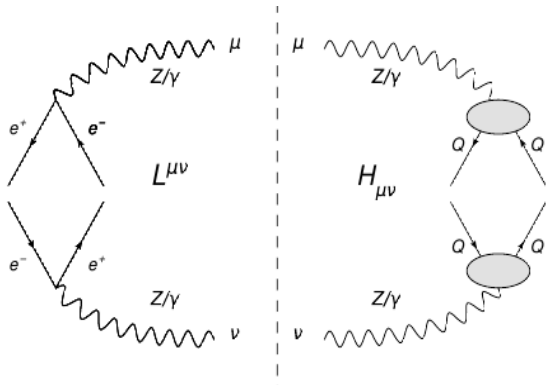

Figure 4.1: The decomposition of the $d\sigma^{(i,j)}$ into a lepton tensor $L^{\mu\nu}$ and a hadron tensor $H_{\mu\nu}$.

4.1 The $t\bar{t}$ cross section above threshold

We consider

$$e^-(p_1)e^+(p_2) \to \gamma^*, Z^*(q) \to t(k_1)\ \bar{t}(k_2) + X\,, \tag{4.8}$$

for unpolarized e^+ and e^- beams and e^+e^- center-of-mass (c.m.) energies $\sqrt{s}$ sufficiently away from the $t\bar{t}$ threshold, where fixed order perturbation theory in the SM couplings, in particular in α_s, is applicable. As already discussed in the introduction, perturbation theory in α_s breaks down close to threshold and one has to use methods of effective field theory [194–197] in order to compute the $t\bar{t}$ production cross section in this kinematic region. For a rather recent state-of-the-art computation of the $t\bar{t}$ production cross section at threshold, see [37].

For center-of-mass (c.m.) energies $\sqrt{s} > 4m_t$, four-top production, i.e., $t\bar{t}t\bar{t}$ production occurs. The order α_s^2 cross section of this process does not contain any IR singularities. It makes only a small contribution to the inclusive $t\bar{t}$ cross section as long as we are not significantly above the four-top threshold. Moreover, the $t\bar{t}t\bar{t}$ final state has a distinct signature and could be experimentally distinguished from $t\bar{t}$ final states. Here we consider c.m. energies $\sqrt{s} \lesssim 4m_t$. Figure 4.2 shows our result for the $e^+e^- \to t\bar{t}$ cross section at LO, NLO, and NNLO QCD for c.m. energies $\sqrt{s} \lesssim 4m_t$. In the case of $\sigma^{t\bar{t}}_{\mathrm{NLO}}$ and $\sigma^{t\bar{t}}_{\mathrm{NNLO}}$ the solid lines represent the values computed with the choice $\mu = \sqrt{s}$ for the renormalization scale. Uncertainties due to undetermined higher-order corrections are conventionally estimated by varying the renormalization-scale μ between $\sqrt{s}/2$ and $2\sqrt{s}$. The upper and lower dashed lines correspond to these scale variations. In order to exhibit the size of the higher order QCD corrections relative to the LO cross section, we represent the $t\bar{t}$ cross section in the form

$$\sigma^{t\bar{t}}_{\mathrm{NNLO}} = \sigma^{t\bar{t}}_{\mathrm{LO}} \left(1 + \Delta_1 + \Delta_2\right). \tag{4.9}$$

The order α_s and α_s^2 corrections Δ_1 and Δ_2 are displayed, for three renormalization scales μ, in figure 4.3 as functions of the c.m. energy $\sqrt{s}$. The changes of Δ_1 and Δ_2 due to scale variations are small, especially for Δ_2. (The logarithmic scale on the y axis of figure 4.3 may give a wrong impression.)

In the computation of $\sigma^{t\bar{t}}_{\mathrm{NNLO}}$, we have included also the non-universal contributions of order $\mathcal{O}(\alpha_s^2)$ that contain the electroweak couplings of quarks $q \neq t$. These contributions are free of divergences and are very small. For instance, at $\sqrt{s} = 500$ GeV they amount to -0.16% of the total second order correction Δ_2 defined in Eq. (4.9), and this fraction decreases further in magnitude for smaller c.m. energies.

Our results displayed in figure 4.3 agree with the calculation of the $t\bar{t}$ cross section in [80] shown for $\mu = \sqrt{s}$ in this reference. In the near threshold regime where the top-quark velocity β is small and where $\alpha_s \ll \beta \ll 1$ holds, the first few terms of the threshold expansion of $\sigma^{t\bar{t}}_{\mathrm{NNLO}}$ are known analytically [198–201]. For the vector current contribution to σ_{NNLO} asymptotic expansions in the region where $m_t^2/s \ll 1$ are also known [73–76]. We have numerically compared our exact NNLO result with these expansions in the respective kinematic regimes and found

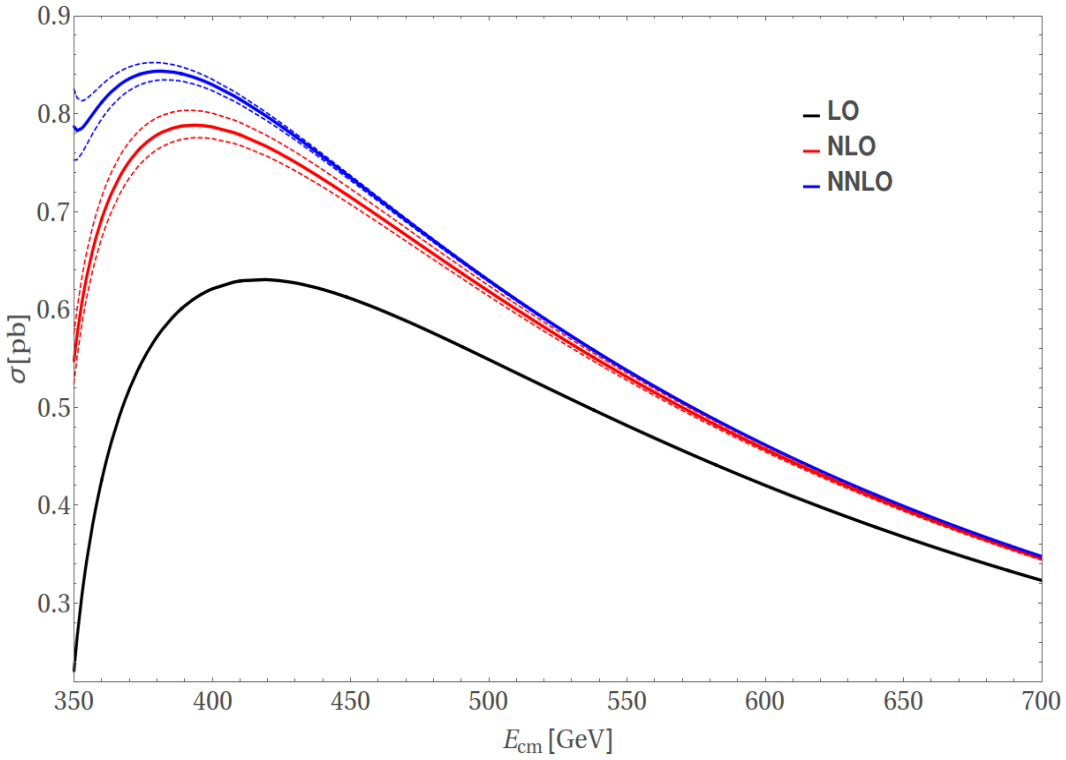

Figure 4.2: The total $t\bar{t}$ cross section at LO, NLO, and NNLO QCD as a function of the c.m. energy. The solid lines that refer to $\sigma^{t\bar{t}}_{\rm NLO}$ and $\sigma^{t\bar{t}}_{\rm NNLO}$ correspond to the choice $\mu = \sqrt{s}$, the dashed lines correspond to $\mu = \sqrt{s}/2$ and $2\sqrt{s}$.

agreement.

From figures 4.2 and 4.3 we can see that the higher order QCD corrections to the $t\bar{t}$ cross sections decrease with increasing c.m. energies $\sqrt{s}$. In the near threshold region, the QCD corrections become rather large. The blue thick line in figure 4.2 representing the total NNLO result already shows a hint of blowing up when $\sqrt{s} \to 2m_t$. This feature of our fixed-order perturbative calculation is due to the well-known Coulomb singularities [74, 202]. In this non-relativistic kinematic region, the behavior of the $t\bar{t}$ cross section can be effectively obtained via the imaginary part of the respective non-relativistic Green function in the presence of a Coulomb potential. Roughly speaking, each exchange of a virtual longitudinal gluon between the two non-relativistic heavy quarks, that is, a re-scattering through the Coulomb potential, results in a single $1/\beta$ enhancement where, as above, β is the velocity of the heavy quark. (In addition, exchanges of transverse gluons are in effect described by a running QCD coupling α_s which should also be taken into account.) The NLO cross section, i.e., the red line in fig. 4.2, does not diverge but goes to a constant for $\beta \to 0$, because it involves only a single

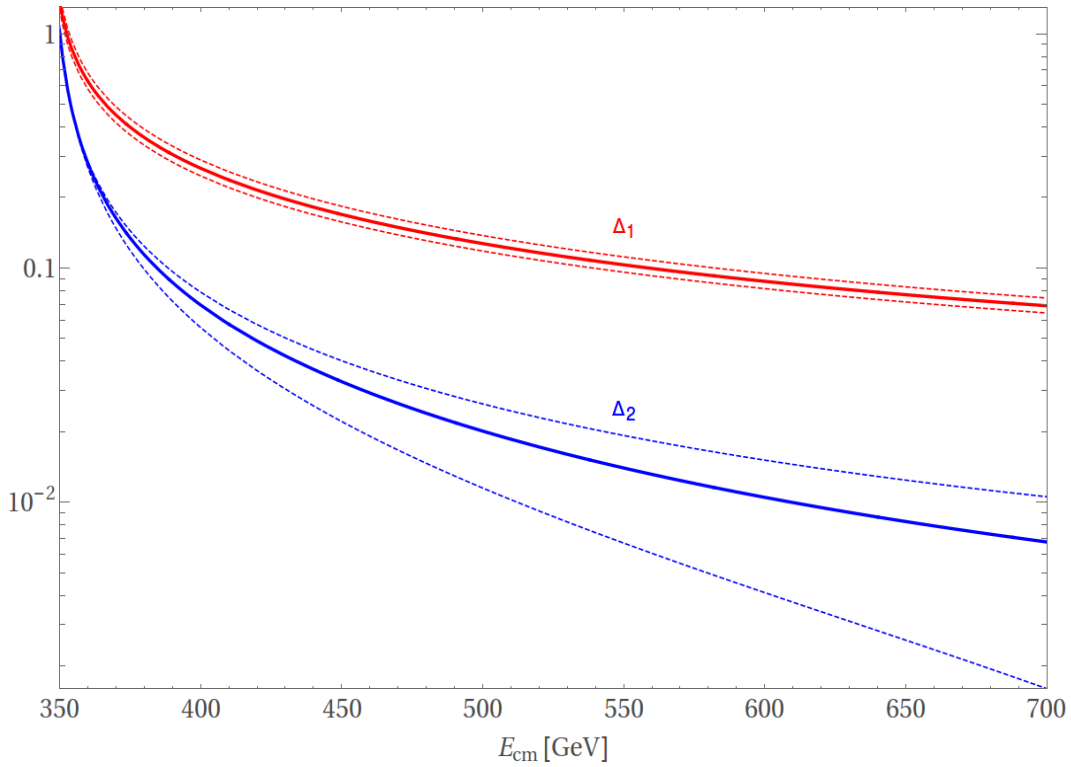

Figure 4.3: The order α_s and α_s^2 corrections Δ_1 and Δ_2 to the LO $t\bar{t}$ cross section defined in Eq. (4.9) as a function of the c.m. energy. The solid lines correspond to the choice $\mu = \sqrt{s}$, the upper and lower dashed lines correspond to $\mu = \sqrt{s}/2$ and $2\sqrt{s}$.

$1/\beta$ Coulomb singularity, (due to one virtual longitudinal gluon exchange) which is completely compensated by the suppression factor β due to the shrinking phase-space. The presence of Coulomb singularities in fixed order perturbative calculations near threshold clearly signifies the break-down of such a calculation. If we still stick to perturbative methods, then one way to improve in the near threshold region is to sum these Coulomb singularities through all perturbative orders, which then leads to a finite result (see, for instance, [197, 202]). This refinement is, however, beyond the scope of this thesis. As emphasized before we confine our calculations to $t\bar{t}$ production in the continuum.

Another point to notice in figure 4.2 is that, in the region where the perturbative calculation is reliable, the scale-variation band at NNLO is narrower than at NLO. This is a common aspect of perturbative calculations. Notice also that the scale-variation bands do not overlap here. Non-overlapping scale-variation bands are not uncommon in higher-order QCD calculations. One should always keep in mind that the scale variation does not correspond to a solid error/uncertainty estimate. It is a convenient ad hoc procedure to estimate the size of the

uncalculated higher order corrections. Moreover, the scale variation does not have to be in the range $\sqrt{s}/2 \leq \mu \leq 2\sqrt{s}$. This is nothing but a rather commonly accepted convention in the case of the total cross section $\sigma(s)$.

Finally we list, for a reference, in table 4.1 the QCD corrections Δ_1 and Δ_2 for selected c.m. energies $\sqrt{s}$ for $\mu = \sqrt{s}$. With the input values given above the cross section $\sigma^{t\bar{t}}_{\rm NNLO}$ reaches its maximum at $\sqrt{s} = 381.3$ GeV. We obtain $\sigma^{t\bar{t}}_{\rm NNLO}(381.3{\rm GeV}) = 0.843$ pb for $\mu = \sqrt{s}$. The numbers in table 4.1 and figure 4.3 suggest that fixed order perturbation theory can be applied for $\sqrt{s} > 360$ GeV.

Table 4.1: The QCD corrections Δ_1 and Δ_2 to the LO $t\bar{t}$ cross section defined in Eq. (4.9) for several c.m. energies and $\mu = \sqrt{s}$.

$\sqrt{s}$ [GeV]	360	381.3	400	500
Δ_1	0.627	0.352	0.266	0.127
Δ_2	0.281	0.110	0.070	0.020

4.2 Top quark distributions

In this section, we present our results for a selected set of top-quark distributions. we consider the distribution of the cosine of the top-quark scattering angle $\theta_t = \angle(t, e^-)$ in the e^+e^- c.m. frame, the transverse momentum p_T^t of the top quark and of the $t\bar{t}$ system, $p_T^{t\bar{t}} = |\mathbf{k_{T,t}} + \mathbf{k_{T,\bar{t}}}|$, with respect to the beam direction, and the $t\bar{t}$ invariant mass distribution $M_{t\bar{t}}$. In the following we use for convenience the shorthand notations LO, NLO, and NNLO for $d\sigma^{t\bar{t}}_{\rm LO}/dO$, $d\sigma^{t\bar{t}}_{\rm NLO}/dO = (d\sigma^{t\bar{t}}_{\rm LO} + d\sigma^{t\bar{t}}_1)/dO$, and $d\sigma^{t\bar{t}}_{\rm NNLO}/dO = (d\sigma^{t\bar{t}}_{\rm LO} + d\sigma^{t\bar{t}}_1 + d\sigma^{t\bar{t}}_2)/dO$, where O denotes one of these observables. We confine ourselves to c.m. energies 400 and 500 GeV where perturbative calculations are reliable and the $t\bar{t}$ cross section is rather large.

Distribution of $\cos\theta_t$: The plots in figure 4.4 display the distribution of $\cos\theta_t$ at $\sqrt{s} = 400$ and 500 GeV at LO, NLO, and NNLO QCD. As expected from the behavior of the total $t\bar{t}$ cross section shown in figure 4.2, the order α_s and order α_s^2 QCD corrections to the LO distribution of this observable decrease if one moves further away from threshold. As the panels in the middle of the plots show, the inclusion of the order α_s^2 correction significantly reduces the

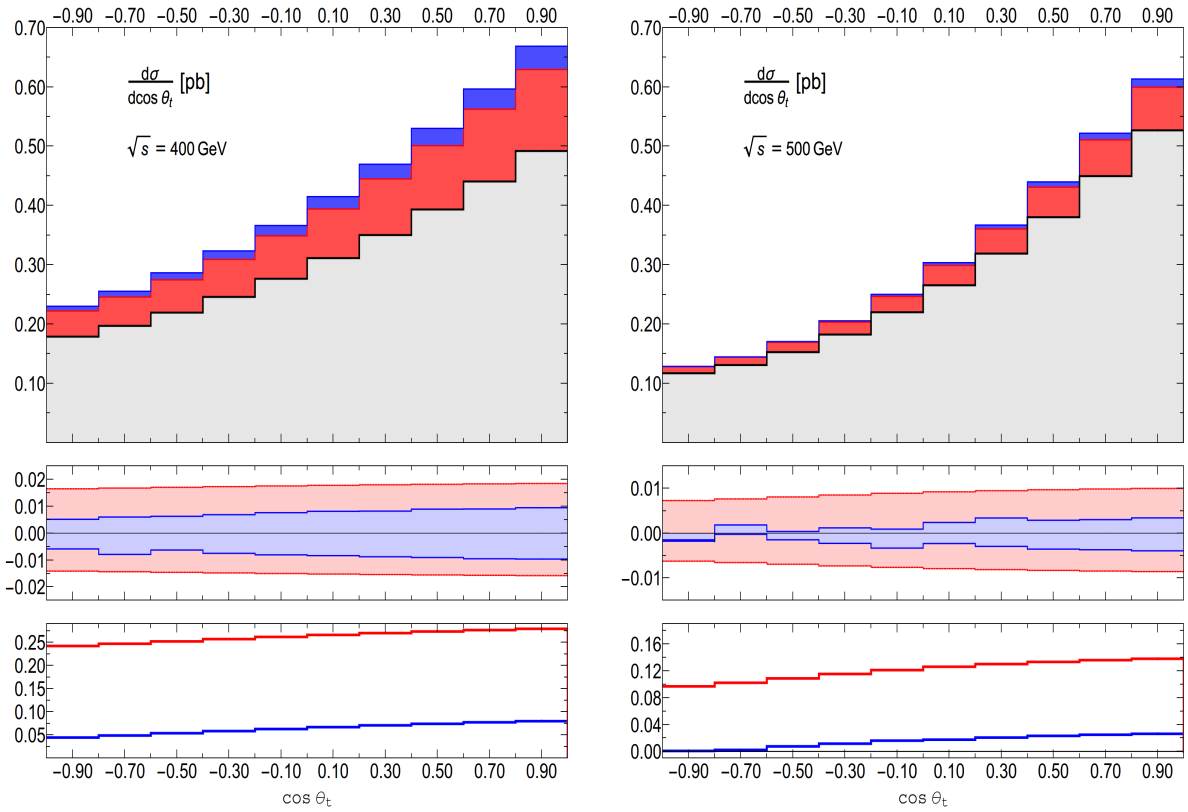

Figure 4.4: The distribution of $\cos\theta_t$ at $\sqrt{s} = 400$ GeV (plots on the left) and 500 GeV (plots on the right). The upper panels show the distribution at LO (grey), NLO (red), and NNLO QCD (blue) for $\mu = \sqrt{s}$. The panels in the middle show the scale variations NLO(μ')/NLO($\mu = \sqrt{s}$) $-$ 1 (red band) and NNLO(μ')/NNLO($\mu = \sqrt{s}$) $-$ 1 (blue band) of the first and second order QCD corrections, where $\sqrt{s}/2 \leq \mu' \leq 2\sqrt{s}$. The lower panels display the ratios $d\sigma_1^{t\bar{t}}/d\sigma_{\rm LO}^{t\bar{t}}$ (red) and $d\sigma_2^{t\bar{t}}/d\sigma_{\rm LO}^{t\bar{t}}$ (blue) for $\mu = \sqrt{s}$.

dependence of the distribution on variations of the scale. The ratios $d\sigma_1^{t\bar{t}}/d\sigma_{\rm LO}^{t\bar{t}}$ and $d\sigma_2^{t\bar{t}}/d\sigma_{\rm LO}^{t\bar{t}}$ for $\sqrt{s} = 400$ GeV and $\mu = \sqrt{s}$ shown in the lower panel of the left plot in figure 4.4 agree with the corresponding result given in [80].

Both the order α_s and order α_s^2 curve in fig. 4.4 follow the same pattern as the leading-order distribution. Since the leading-order contribution dominates over the higher order perturbative corrections at the c.m. energies considered here, the features of the distribution can be understood from the LO contribution which can easily be computed analytically. Working out the contraction of the lepton-tensor $L_{\mu\nu}$ and and leading-order hadron-tensor $H_{\mu\nu}^{(2,0)}$ in Eq. (4.5), we see immediately that the result is a quadratic form in the scattering angle $\cos\theta_t$, which is due to the fact that its orbital part contains a s-wave and a p-wave. The distribution in figure 4.4 are not symmetric in $\cos\theta_t$ around $\cos\theta_t = 0$ because the interaction between the Z boson and

top quark does not conserve the parity P. This leads to parity-odd VA terms in the differential cross section which are anti-symmetric in $\cos\theta_t$, which gives rise to a non-vanishing forward backward asymmetry as we will discuss in detail in the next chapter. The sign of the top-quark forward backward asymmetry is positive. Accordingly, more top-quarks are produced in the forward region ($\cos\theta_t > 0$) than in the backward region ($\cos\theta_t < 0$). When the c.m. energy is lowered towards the near-threshold region, the s-wave in the orbital angular momentum part of $d\sigma$ will become more and more dominant. As a consequence, the distribution will become more and more flat. Indeed, consider just the tree-level S-matrix-element in the near-threshold limit where the p-wave gets squeezed out and only the s-wave remains. Here the distribution in $\cos\theta_t$ becomes flat and the forward-backward asymmetry will become zero. On the other hand, when we go to the high-energy region $s \gg m_t^2$, the orbital p-wave component is no longer suppressed, which leads to a shape of the $\cos\theta_t$ distribution where the central part is reduced compared to the forward and backward regions. This is not visible in the plots of fig. 4.4, because $\sqrt{s} = 500$ GeV does not correspond to the high-energy region for top quark pair production, but it is clearly visible for bottom pair production at the Z-pole which will be discussed in the next section. From the lower panels of fig. 4.4 we see that both the order α_s and order α_s^2 correction to the LO $\cos\theta_t$ distribution show the same pattern: they are larger in the top-quark forward direction than in the backward direction and thus increase the top-quark forward-backward asymmetry, which is the topic of the next chapter.

Distribution of p_T^t: Figure 4.5 displays the distribution of the top-quark transverse momentum p_T^t at the c.m. energies $\sqrt{s} = 400$ GeV and 500 GeV at LO, NLO, and NNLO QCD. As in the case of the $\cos\theta_t$ distribution, the order α_s and α_s^2 corrections become smaller when the c.m. energy is increased from 400 to 500 GeV. Nevertheless, the $\mathcal{O}(\alpha_s^2)$ correction is still $\sim 5\%$ for most of the p_T^t bins. Including the α_s^2 correction reduces the uncertainty due to scale variations for all for all p_T^t bins, as shown in the middle panels of fig. 4.5. The reason why the NNLO scale variations of the p_T^t distribution for $\sqrt{s}$ =500 GeV (shown by the blue curve in the middle panel) fluctuate more than its counterpart at $\sqrt{s}$ =400 GeV is the following: In our computation the same total number of random points were sampled by the Monte Carlo (MC) integration routine for both c.m. energies. Thus, there is, on average, a smaller number of MC

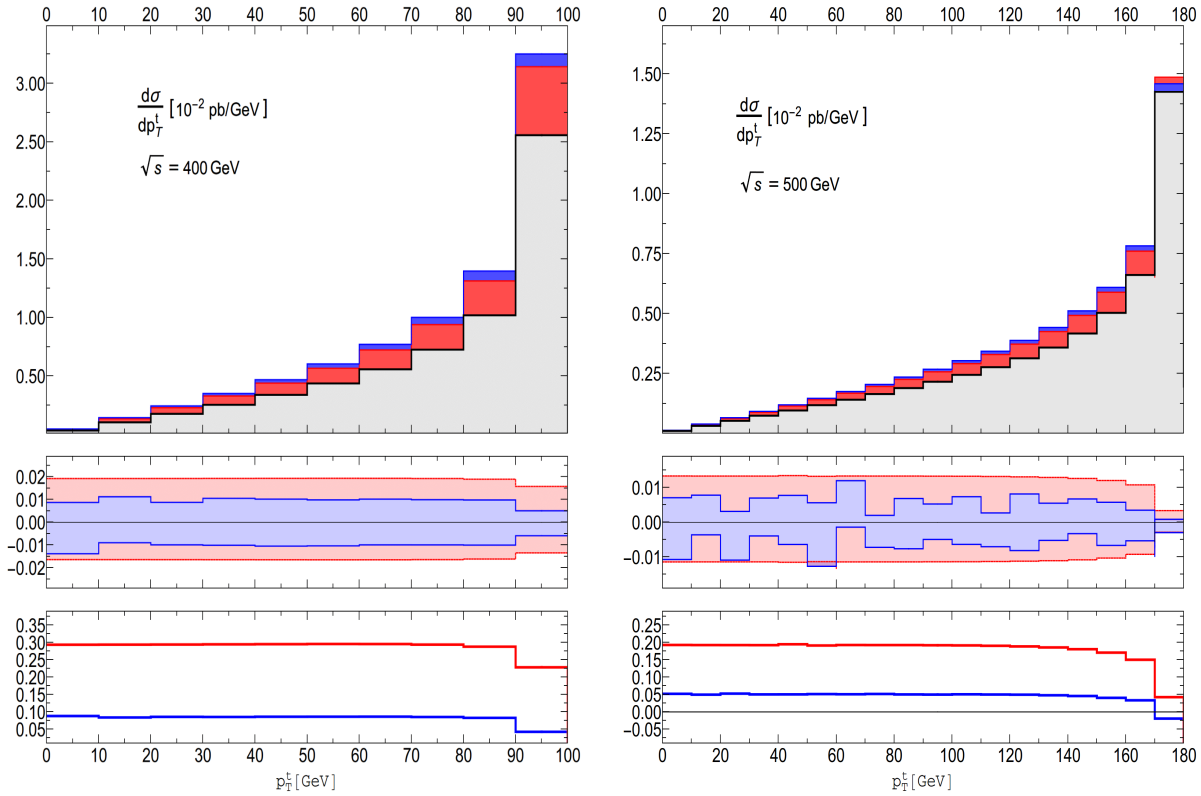

Figure 4.5: The distribution of the transverse momentum p_T^t of the top quark at $\sqrt{s} = 400$ GeV (plots on the left) and 500 GeV (plots on the right). The meaning of the upper, middle, and lower panels is as in figure 4.4.

events distributed into a single p_T^t bin in the 500 GeV case (simply due to the increment in the number of bins). The maximum top-quark transverse momentum is 99.77 GeV (180.15 GeV) at the c.m. energy 400 GeV (500 GeV) for a top-quark mass $m_t = 173.34$ GeV that we use. The rising shape of the transverse momentum distribution, starting from $p_T^t = 0$, can be read off from the LO distribution. A straightforward computation yields

$$\frac{\mathrm{d}\sigma_{LO}^{t\bar{t}}}{\mathrm{d}p_T^t} = \frac{8p_T^t\left((s-4m_t^2)(r_0+r_1+r_2) - 4\left(p_T^t\right)^2(r_1+r_2)\right)}{(s-4m_t^2)^2\sqrt{1-\frac{4\left(p_T^t\right)^2}{s-4m_t^2}}}, \tag{4.10}$$

where the coefficients r_i depend on s, m_t, m_Z, and the electroweak couplings. For small p_T^t the distribution grows linearly.

From the lower panels of fig. 4.5 one sees that α_s and α_s^2 corrections increase the p_T^t distribution, but not necessarily in every p_T^t bin. At $\sqrt{s} = 500$ GeV the order α_s^2 correction is in fact negative in the last bin. This feature becomes more pronounced for larger c.m. energies.

The ratios $d\sigma_1^{t\bar{t}}/d\sigma_{\rm LO}^{t\bar{t}}$ and $d\sigma_2^{t\bar{t}}/d\sigma_{\rm LO}^{t\bar{t}}$ for $\sqrt{s} = 400$ GeV and $\mu = \sqrt{s}$ shown in the lower panel of the left plot in figure 4.5 agree with the corresponding plot displayed in [80], except for the last bin at $(p_T^t)_{\rm max}$. This is apparently due to the fact that a slightly lower value of the top-quark mass was used in [80], which shifts $(p_T^t)_{\rm max}$ at 400 GeV to a value slightly above 100 GeV.

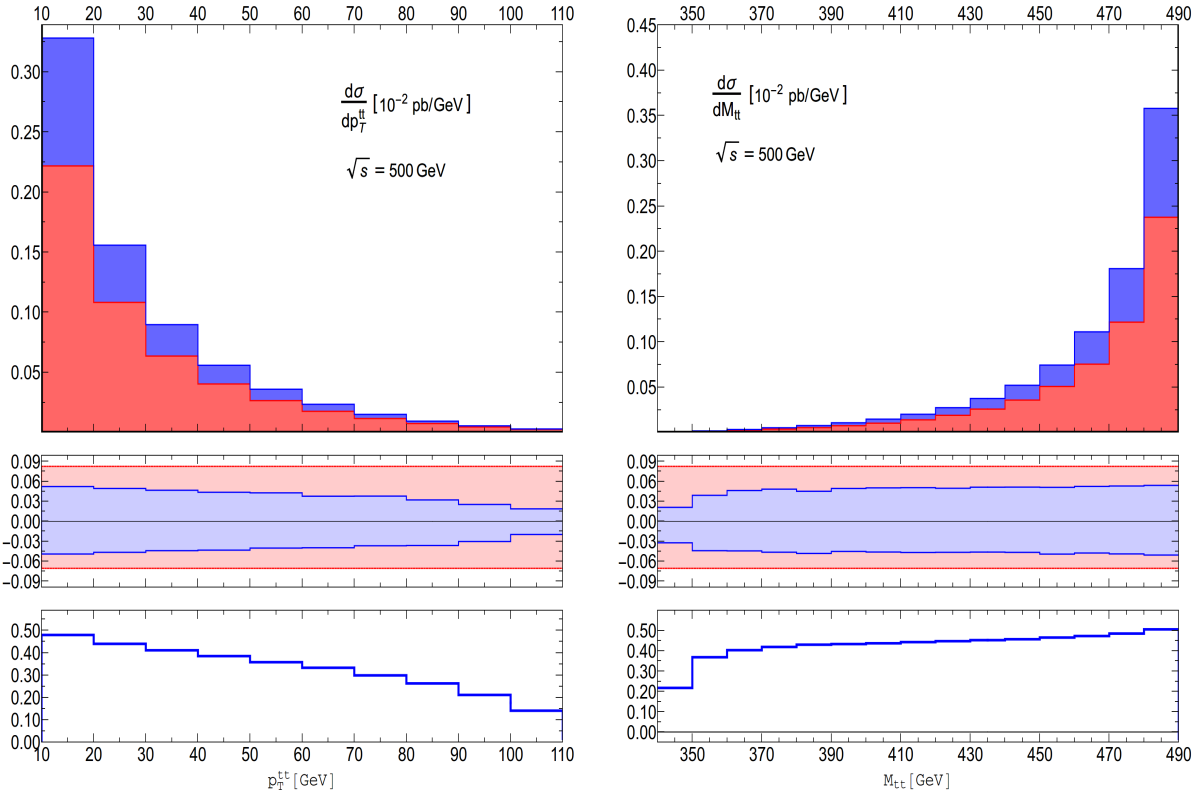

Figure 4.6: The distribution of the transverse momentum $p_T^{t\bar{t}}$ of the $t\bar{t}$ system for events with $p_T^{t\bar{t}} \geq 10$ GeV (plots on the left), and the $t\bar{t}$ invariant mass distribution for events with $M_{t\bar{t}} \leq 490$ GeV (plots on the right) at $\sqrt{s} = 500$ GeV for $\mu = \sqrt{s}$. The upper panels show the distributions at NLO (red) and NNLO QCD (blue). The panels in the middle show the scale variations NLO(μ')/NLO($\mu = \sqrt{s}$) $-$ 1 (red band) and NNLO(μ')/NNLO($\mu = \sqrt{s}$) $-$ 1 (blue band) of the first and second order QCD corrections, where $\sqrt{s}/2 \leq \mu' \leq 2\sqrt{s}$. The lower panels display the ratio $d\sigma_2^{t\bar{t}}/d\sigma_1^{t\bar{t}}$ for $\mu = \sqrt{s}$.

Distributions of $p_T^{t\bar{t}}$ and $M_{t\bar{t}}$: The left plots of figure 4.6 show, for $\sqrt{s} = 500$ GeV, the distribution of the transverse momentum of the $t\bar{t}$ system, $p_T^{t\bar{t}}$, for events with $p_T^{t\bar{t}} \geq 10$ GeV. The right plots show the $t\bar{t}$ invariant mass distribution for events with $M_{t\bar{t}} \leq 490$ GeV. These cuts remove the LO contribution and events with very soft massless parton radiations at order α_s and α_s^2. Clearly, the bins that are removed by these cuts contain most of the $t\bar{t}$ events.

Let us briefly discuss the kinematic range of $p_T^{t\bar{t}}$ distribution. For $t\bar{t}$ final states $p_T^{t\bar{t}} = 0$. For $t\bar{t}g$ final states $p_T^{t\bar{t}}$ becomes maximal for the following configuration: the t and $\bar{t}$ move parallel and

in a plane perpendicular to the electron positron beam and the momentum is balanced by the gluon moving in the opposite direction. For $\sqrt{s} = 500$ GeV the maximum $p_T^{t\bar{t}}$ is 129.81 GeV, but events with $p_T^{t\bar{t}}$ near this value are very rare. For the four-partion final states $t\bar{t}gg$ and $t\bar{t}q\bar{q}$ the maximum $p_T^{t\bar{t}}$ can be at most as large as for the three-parton final state. The kinematic range of the $M_{t\bar{t}}$ distribution is $2m_t \leq M_{t\bar{t}} \leq \sqrt{s}$.

The decrease of the $p_T^{t\bar{t}}$ distribution and the rise of the $M_{t\bar{t}}$ distribution towards their respective endpoints shown in figure 4.6 is a consequence of the fact that it is more preferable to radiate gluons with small energy rather than large energy.

The NNLO QCD correction to the NLO result increases significantly towards small $p_T^{t\bar{t}}$ in the left plots, respectively towards large $M_{t\bar{t}}$ in the right plots of figure 4.6. In the bin 10 GeV $\leq p_T^{t\bar{t}} \leq$ 20 GeV the order α_s^2 correction is almost 50% of the NLO contribution. This is due to logarithmic enhancement in the variable $p_T^{t\bar{t}}$ in the soft radiation region which is a feature of the fixed order perturbative calculation. In fact this is not uncommon for observables for which there exists a kinematic configuration where virtual ("non-radiative") corrections are favored over the real radiative corrections contributing at the same perturbative order, and hence a balance between these two types of corrections is spoiled. In such a kinematic region, one type of correction is effectively singled out and becomes dominant (usually the virtual non-radiative one). The we find that in this special region the fixed order perturbative corrections get enhanced, i.e., become relatively large. For example, consider a jet observable calculated at a fixed perturbative order. Such a fixed-order calculation becomes unreliable when we try to approach the parameter region where the jet defining parameters such as jet mass or jet angular width are chosen to be very small. In fact, this can also happen to the p_T^t distributions shown in figure 4.5. Imagine a p_T^t bin sitting right at the $(p_T^t)_{\max}$ with very small bin width. Then diagrammatically, the contributing diagrams are only the virtual loop-diagrams with reduced (radiation-free) kinematics and the real-radiation diagrams where the energy carried away by the radiation is very very small. Although the sum of these contributions is still free of IR singularities, a logarithmic enhancement will remain which makes the fixed order perturbative calculations unreliable. If we insist on examining these special kinematic regions but still stick to perturbative methods, then we must refine the results by resuming

these large logarithmic terms that show up in all of the subsequent perturbative orders. Coming back to the $p_T^{t\bar{t}}$ distribution shown in the left plot of figure 4.6 this means one would have to sum these logarithmic enhancement terms in the small $p_T^{t\bar{t}}$ region, but this is beyond the scope of this paper. An analogous statement applies to the $M_{t\bar{t}}$ distribution shown in the right plot of figure 4.6. Here the dangerous region are the $M_{t\bar{t}}$ bins close to the c.m. energy.

4.3 The $b\bar{b}$ cross section at the Z resonance

In this section, we move to analyzing bottom quark pair production in e^+e^- collisions at the Z resonance,

$$e^+e^- \to Z \to b\bar{b} + X\,, \tag{4.11}$$

to second order in the QCD coupling α_s. Because at the Z pole, the contribution to $d\sigma^{b\bar{b}}$ of Z-boson exchange, $Z-\gamma$ interference, and γ exchange is of order 1, order α, and order α^2 with respect to the electroweak interactions, and because we work to lowest order in the electroweak couplings, we neglect in this section the contributions of γ exchange and $Z-\gamma$ interference to the (differential) $b\bar{b}$ cross section. (In fact, right at $\sqrt{s} = m_Z$ the $Z-\gamma$ interference term vanishes.) To order α_s^2 the cross section of the reaction (4.11) receives contributions from the two-parton $b\bar{b}$ final state (at Born level, to order α_s, and to order α_s^2), the three-parton final state $b\bar{b}g$ (to order α_s and to order α_s^2), and the four-parton final states $b\bar{b}gg$, $b\bar{b}q\bar{q}$, and $b\bar{b}b\bar{b}$. The $b\bar{b}b\bar{b}$ diagrams discussed in section 3.1.2 are taken into account with a multiplicity factor one in the computation of the $b\bar{b}$ cross section. This corresponds to an exclusive definition of the cross section [90], that is the cross section for events containing at least one b quark. The inclusive b cross section, where the $b\bar{b}b\bar{b}$ diagrams are taken into account with a multiplicity factor two, is the cross section where each b quark is contributing once.

Our computational framework is the same as in the case of $t\bar{t}$ production, i.e., the antenna method described in section 3. Here we work, as already emphasized above, in QCD with massless u, d, s, c quark and a massive b quark with its on-shell mass values given in Eq. (4.3). The top quark enters only in the UV and IR finite 1-loop and 2-loop triangle diagrams, cf.

section 3. The QCD coupling that we use here is given in (4.2). Analogous to the $t\bar{t}$ case we use here the notation $d\sigma^{b\bar{b}}_{\rm NLO} = d\sigma^{b\bar{b}}_{\rm LO} + d\sigma^{b\bar{b}}_1$ and $d\sigma^{b\bar{b}}_{\rm NNLO} = d\sigma^{b\bar{b}}_{\rm NLO} + d\sigma^{b\bar{b}}_2$.

Our results for the $b\bar{b}$ cross section at LO, NLO, and NNLO QCD at $\sqrt{s} = m_Z$ are given in table 4.2 for three renormalization scales. Moreover, this table contains also the order α_s and order α_s^2 QCD corrections Δ^b_1 and Δ^b_2 to the LO $b\bar{b}$ cross section defined by writing the NNLO cross section in the form

$$\sigma^{b\bar{b}}_{\rm NNLO} = \sigma^{b\bar{b}}_{\rm LO}\,(1 + \Delta^b_1 + \Delta^b_2)\,. \tag{4.12}$$

Table 4.2: The $b\bar{b}$ cross section at LO, NLO, and NNLO QCD at $\sqrt{s} = m_Z$, and the QCD corrections Δ^b_1 and Δ^b_2 to the LO $b\bar{b}$ cross section defined in Eq. (4.12) for three renormalization scales μ.

	$\sigma^{b\bar{b}}_{LO}$ [pb]	$\sigma^{b\bar{b}}_{NLO}$ [pb]	$\sigma^{b\bar{b}}_{NNLO}$ [pb]	Δ^b_1	Δ^b_2
$\mu = m_Z$	8742.84	9119.93	9152.29	4.31×10^{-2}	3.7×10^{-3}
$\mu = 2m_Z$	8742.84	9084.25	9141.60	3.90×10^{-2}	6.6×10^{-3}
$\mu = m_Z/2$	8742.84	9164.18	9157.60	4.82×10^{-2}	-7.5×10^{-4}

The numbers given in table 4.2 show that, at $\sqrt{s} = m_Z$, the QCD corrections to the LO $b\bar{b}$ are small and that inclusion of the NNLO QCD correction significantly reduces the uncertainty associated with scale variations.

4.4 Bottom-quark distributions

Our set-up allows to compute the distribution of any IR-finite b-quark observable at NNLO QCD. Our main interest in $b\bar{b}$ production at the Z pole is, however, the computation of the forward-backward asymmetry for massive b quarks at NNLO QCD, which was so far not available in the literature. We determine this asymmetry from the distributions of the b-quark and oriented thrust directions. Besides these distributions we consider here for the sake of brevity only the distribution of the b-quark transverse momentum p^b_T.

At this point a remark on the four-b diagrams discussed in section 3.1.2 is in order. By convention, we have taken them into account with a multiplicity factor one in the above computation of $\sigma^{b\bar{b}}_{\rm NNLO}$. It is however not entirely clear how the four-b final states were treated in e^+e^- collider

experiments in the past. As mentioned in [90] one finds vague statements in the experimental literature, for instance "a four-b final state is more likely to be tagged than a two-b one, but less than twice as likely". Thus if a calculation should match a respective measurement one has to understand whether experiments have used (or use) the same or different tagging efficiencies for the $b\bar{b}$ and $b\bar{b}b\bar{b}$ final states. In principle, in the computation of the (differential) inclusive b cross section $d\sigma(e^+e^- \to b + X)/dO_b$, where O_b is some b-quark observable, the four-b diagrams count twice, because there are two b quarks in the final state. We have used this multiplicity factor in the computation of the distributions of this section. (Numerically, the difference between using multiplicity factors one or two is very small.)

Distribution of p_T^b: Our results for the distribution of the b-quark transverse momentum p_T^b are shown in fig. 4.7. In the kinematic region where p_T^b is close to maximal, which corresponds to the last bin in fig. 4.7, the order α_s and α_s^2 QCD corrections are due to one-loop or two-loop contributions from $b\bar{b}$ final states and real radiation diagrams with soft gluon(s) or soft $q\bar{q}$. Thus, we expect large logarithmic enhancements from these corrections. Let's consider the vicinity of the maximally allowed p_T^b determined by the $b\bar{b}$ final state where these two partons are in the plane transverse to the beam. The real radiation corrections deplete this region of the p_T^b distribution and increase the number of b quarks with smaller transverse momentum. This may explain qualitatively why the net higher order QCD corrections are negative in the vicinity of the maximally allowed p_T^b.

Distribution of b-quark and thrust direction: Next we consider the distributions of the b-quark direction of flight and of the oriented thrust axis. The forward-backward asymmetries corresponding to these directions will be discussed in the next chapter. If the b-quark direction of flight is chosen, then $\theta_b = \angle(\mathbf{k}_1, \mathbf{p}_1)$, where $\mathbf{k}_1$ and $\mathbf{p}_1$ are the three-momenta of the b quark and of the electron, respectively, in the e^+e^- c.m. frame. However, an accurate determination of the b-quark momentum is contaminated by quark fragmentation and decay. In the past experimental analyzes often used the thrust axis as reference axis. Before we present the plots for both distributions, let us quickly recapitulate the definition of thrust. Thrust is one of the widely used global observables (meaning that all final state particles of a given event contribute), called event shapes. For a given n-parton event described by a collection of final-state four-

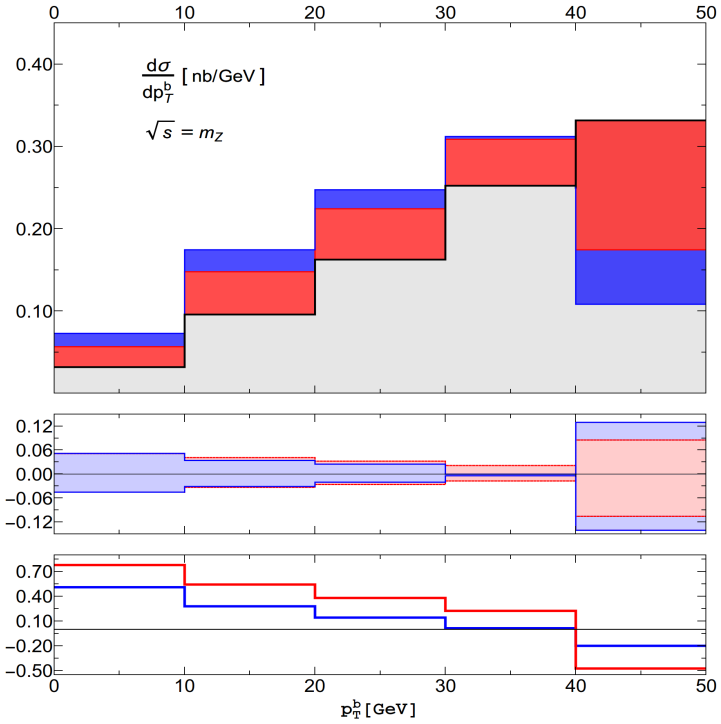

Figure 4.7: The distribution of the transverse momentum p_T^b of the b quark at $\sqrt{s} = m_Z$. The upper panels show the distribution at LO (grey), NLO (red), and NNLO QCD (blue) for $\mu = m_Z$. The panels in the middle show the scale variations NLO(μ')/NLO($\mu = m_Z$) $-$ 1 (red band) and NNLO(μ')/NNLO($\mu = m_Z$) $-$ 1 (blue band) of the first and second order QCD corrections, where $m_Z/2 \leq \mu' \leq 2m_Z$. The lower panels display the ratios $d\sigma_1^{b\bar{b}}/d\sigma_{\rm LO}^{b\bar{b}}$ (red) and $d\sigma_2^{b\bar{b}}/d\sigma_{\rm LO}^{b\bar{b}}$ (blue) for $\mu = m_Z$.

momenta $\{k_i\}_{i=1}^n$ (related by momentum conservation), the thrust axis is the direction $\mathbf{n}_T$ that maximizes the thrust T defined by [203, 204]:

$$T = \max_{\mathbf{n}_T} \frac{\sum_{i=1}^{n} |\mathbf{k}_i \cdot \mathbf{n}_T|}{\sum_{i=1}^{n} |\mathbf{k}_i|}, \qquad |\mathbf{n}_T| = 1. \tag{4.13}$$

It can be shown [205] that

$$\mathbf{n}_T \parallel \sum_i \varepsilon_i \mathbf{k}_i, \qquad \varepsilon_i \in \{0, \pm 1\}, \tag{4.14}$$

which implies that (4.13) is equivalent to the finite maximization problem:

$$T = \max_{\varepsilon_i} \frac{|\sum_i \varepsilon_i \mathbf{k}_i|}{\sum_i |\mathbf{k}_i|}. \tag{4.15}$$

This formula determines $\mathbf{n}_T$ up to a sign. Its orientation is fixed by requiring $\mathbf{n}_T \cdot \mathbf{k}_1 > 0$. A geometric interpretation can be given to thrust: it is the ratio between the longest of all sides and diagonal lines of all possible polygons constructed out of a given set of 3-vectors ($\{\mathbf{k}_i\}$) to the perimeter fixed by this chosen set of vectors. Thus, if the thrust axis is chosen as reference axis, the forward hemisphere is defined by $\mathbf{n}_T \cdot \mathbf{p}_1 > 0$. Therefore, in this case $\theta_T = \angle(\mathbf{n}_T, \mathbf{p}_1)$. The possible directions of the oriented thrust axis $\mathbf{n}_T$ are shown in figure 4.8 for the 3-parton final state $b(k_1)\bar{b}(k_2)g(k_3)$. According to the above formulas the oriented thrust axis is

$$\mathbf{n}_T \parallel \mathbf{k}_1 \qquad \text{if } |\mathbf{k}_1| > |\mathbf{k}_2|,\ |\mathbf{k}_3|\,, \tag{4.16}$$

$$\mathbf{n}_T \parallel -\mathbf{k}_2 \qquad \text{if } |\mathbf{k}_2| > |\mathbf{k}_1|,\ |\mathbf{k}_3|\,, \tag{4.17}$$

$$\mathbf{n}_T \parallel -\mathbf{k}_3 \qquad \text{if } |\mathbf{k}_3| > |\mathbf{k}_1|,\ |\mathbf{k}_2|\,. \tag{4.18}$$

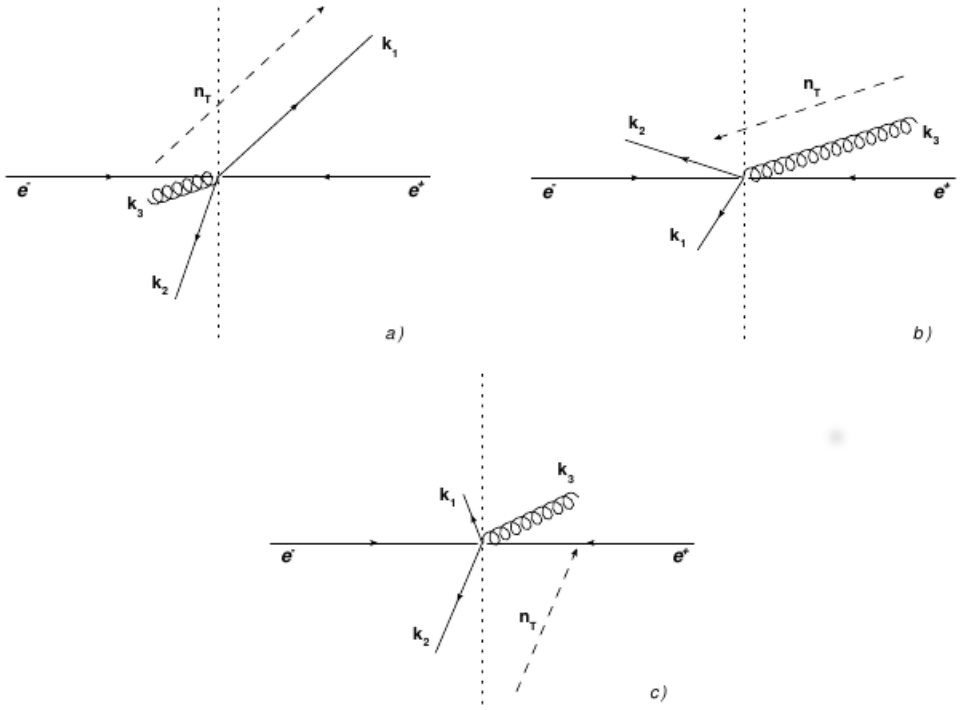

Figure 4.8: The possible directions of the oriented thrust axis in case of a 3-parton $Q\bar{Q}g$ final state.

In the case of a four-parton final state, $\mathbf{n}_T$ is an element of the following set:

$$\mathbf{n}_T \in \{\mathbf{k}_1, \pm\mathbf{k}_2, \pm\mathbf{k}_3, \pm\mathbf{k}_4, \pm(\mathbf{k}_1+\mathbf{k}_2), \pm(\mathbf{k}_1+\mathbf{k}_3), \pm(\mathbf{k}_1+\mathbf{k}_4)\}\,, \tag{4.19}$$

and the sign is fixed by the requirement $\mathbf{n}_T \cdot \mathbf{k}_1 > 0$. Normalization of the thrust vector is understood. The type-a antenna subtraction terms involve mapped momenta that arise from $3 \to 2$ phase-space mappings (see section 3.3.1). In this case the thrust vector is an element of the set

$$\widetilde{\mathbf{n}}_T \in \{\pm\widetilde{\mathbf{k}}_{ij}, \pm\widetilde{\mathbf{k}}_k, \pm\mathbf{k}_l\}\,, \qquad i \neq j \neq k \neq l \in \{1, \ldots, 4\}\,, \tag{4.20}$$

Again, the sign is fixed by the condition $\widetilde{\mathbf{n}}_T \cdot \mathbf{k}_1 > 0$.

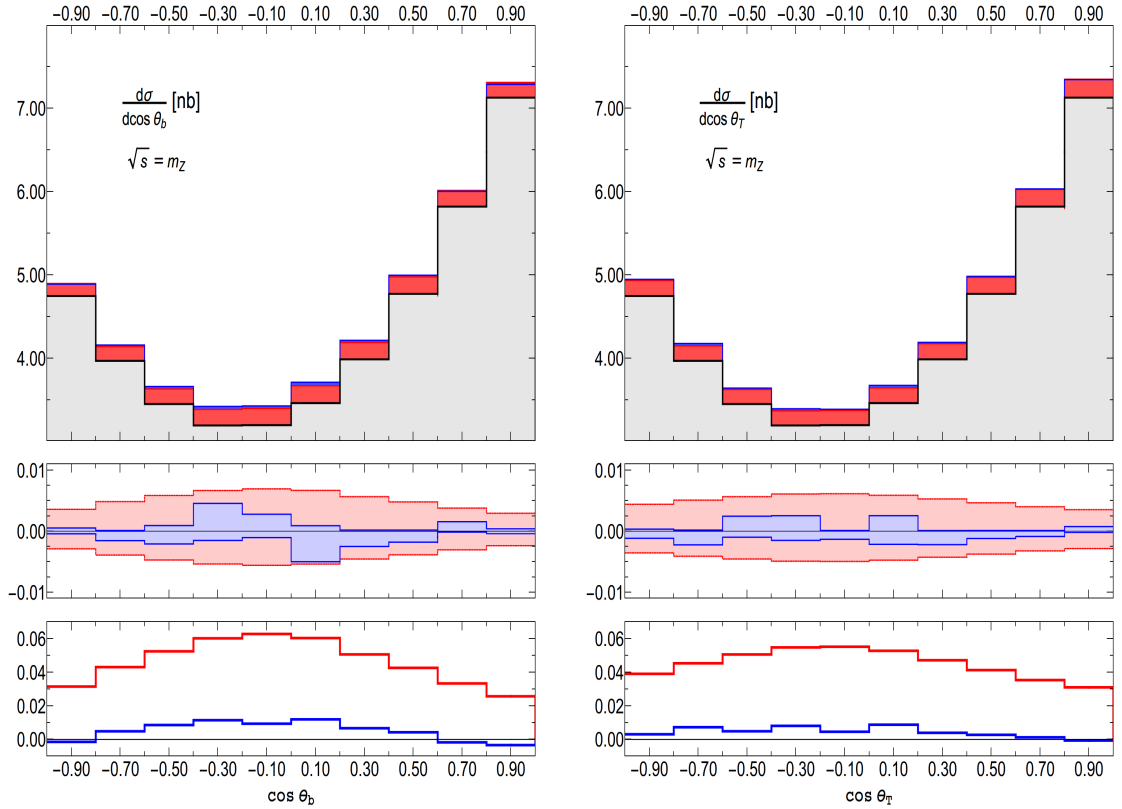

Figure 4.9: The distribution of $\cos\theta_b$ (plots on the left) and of $\cos\theta_T$ (plots on the right) at $\sqrt{s} = m_Z$. The upper panels show the respective distribution at LO (grey), NLO (red), and NNLO QCD (blue) for $\mu = m_Z$. The panels in the middle display the scale variations $\mathrm{NLO}(\mu')/\mathrm{NLO}(\mu = m_Z) - 1$ (red band) and $\mathrm{NNLO}(\mu')/\mathrm{NNLO}(\mu = m_Z) - 1$ (blue band) of the first and second order QCD corrections, where $m_Z/2 \leq \mu' \leq 2m_Z$. The lower panels show the ratios $d\sigma_1^{b\bar{b}}/d\sigma_{\mathrm{LO}}^{b\bar{b}}$ (red) and $d\sigma_2^{b\bar{b}}/d\sigma_{\mathrm{LO}^{b\bar{b}}}$ (blue) for $\mu = m_Z$.

In figure 4.9 we display the distributions of $\cos\theta_b$ and $\cos\theta_T$ to order α_s^2, where θ_b (θ_T) is the angle between the b-quark direction (oriented thrust direction) and the electron beam. The first thing to notice is that, in comparison to the top-quark $\cos\theta_t$ distribution shown in figure 4.4, for bottom production at the Z-pole the orbital p-wave component of the S matrix element is much more dominant. This is because at $\sqrt{s} = m_Z$ we are in the high-energy region

of b-quark production. Both plots show qualitatively the well-known LO p-wave $(1 + \cos^2\theta)$ angular dependence which is modulated by a term linear in $\cos\theta$ resulting from the parity-odd contributions.

The plots in the second panels of fig. 4.9 show that incorporating the order α_s^2 corrections helps to reduce the scale variation uncertainties both for the $\cos\theta_b$ and the $\cos\theta_T$ distribution.

From the third panels of fig. 4.9 we see that with increasing θ_b or θ_T, that is, when going from the backward to the forward direction, the order α_s and α_s^2 QCD corrections do not steadily grow – unlike the case of top-quark production, see fig. 4.4. Thus in the case of bottom production at $\sqrt{s} \gg m_b$, the higher order QCD corrections do not necessarily increase the b-quark forward-backward asymmetry.

Chapter 5

The top- and bottom-quark forward-backward asymmetry

As already mentioned in the introduction, forward-backward asymmetries are precision observables for the determination of the neutral current couplings of leptons and quarks f in the reactions $e^+e^- \to f\bar{f}X$. In this chapter we compute the respective forward-backward asymmetries for $t\bar{t}$ and $b\bar{b}$ production to second order in α_s.

The forward-backward asymmetry A_{FB} in fermion antifermion pair production, in particular in $Q\bar{Q}$ production is defined by[1]

$$A_{FB} \equiv \frac{N_F - N_B}{N_F + N_B}\,, \tag{5.1}$$

where N_F (N_B) is the number of quarks produced in the forward (backward) direction. The identification of the forward/backward direction involves a choice of reference axis. The definition of the reference axis must be such that the resulting forward-backward asymmetry is an infrared safe (IR-safe) quantity so that it can be reliably calculated and subsequently compared with experimental measurements. Common choices include the direction of flight of the heavy quark and the oriented thrust axis defined by a certain thrust-finding algorithm, both of which will be considered in this thesis for the bottom quark. The definition of the thrust axis is given

[1]Here and in the following, we refrain from putting an index Q on A_{FB}. Thus in sections 5.2 and 5.3 the notation A_{FB} refers to the top-quark and bottom-quark asymmetry, respectively.

in Eq. (4.14) in section 4.4. The two-fold ambiguity inherent in this definition is resolved by singling out the direction which is closer to the flavored quark in question. For $t\bar{t}$ production we will consider only the t-quark direction of flight as reference axis for computing A_{FB}, because this direction can be well reconstructed in $t\bar{t} \to$ leptons plus jets events where the top-quark decays hadronically, $t \to bq\bar{q}'$.

Both choices of reference axes are infrared and collinear safe for massive quarks. However they no longer keep this IR-safe property when a masssless quark flavor is considered. Intuitively this fact can be understood by recalling that the notion of "the number of massless quarks of a specific flavor or number of gluons" is not an IR-safe quantity in QCD. This point is already clear in QED: considering the number of soft photons produced in the soft photon region $E_\gamma \to 0$ is physically not meaningful. Technically, A_{FB} for massless quarks of a specific flavor – consider, for definiteness, massless b quarks — suffers from some uncanceled logarithmic divergences due to the involvement of the $b\bar{b}b\bar{b}$ final state (section 3.1.2) where the particle-multiplicity $n_b \neq 1$ of these 4-b final states spoils the cancellation of all IR singularities [90]. It turns out that it is the denominator of Eq. (5.1), the total number of massless b quarks produced, that contains uncanceled collinear divergences while the difference $N_F - N_B$ in the numerator of (5.1) happens to remain finite. We will come back to this in more detail in section 5.3.2. What is always legal to ask is the number of flavored jets produced according to an IR-safe jet definition. An infrared-safe definition of a flavored quark jet for a massless quark was given in [206]. Based on this jet algorithm a definition of the forward-backward asymmetry based on the jet axis was given in [91] that is IR finite in the limit $m_b \to 0$,

Before we proceed it is useful to pause for a moment and discuss why there is a non-vanishing A_{FB} in the process under consideration. The asymmetry A_{FB} is generated by those terms in the squared S-matrix elements of the reactions $e^+e^- \to Q\bar{Q}X$ which are odd under the interchange of Q and $\bar{Q}$ while the initial state is kept fixed. Thus, as already emphasized in the introduction, $A_{FB} \neq 0$ is not a sign of a symmetry violation. In particular, it has a priori nothing to do with parity violation. For instance, in pure Quantum Electrodynamics (QED) an non-zero A_{FB} is generated at order α^3 in $e^+e^- \to Q\bar{Q}X$. The following QED contributions generate a non-zero asymmetry [207]: i) the interference of the 1-loop $Q\bar{Q}$ box diagrams and

the Born diagram and ii) the interference of real photon radiation from the initial and the final state. Both i) and ii) contain even and odd terms with respect to $Q \leftrightarrow \bar{Q}$.

This QED contribution is a gauge-invariant part of the higher-order electroweak contributions and will not be considered in the following because, as emphasized repeatedly, we consider here $e^+e^- \to Q\bar{Q}X$ only to lowest order in the electroweak couplings, i.e., the s-channel γ and Z-boson exchange matrix elements. Those terms in these squared matrix elements that are odd with respect to $Q \leftrightarrow \bar{Q}$ are also parity-odd, i.e., are generated by the interference of vector and axial vector couplings. Below we calculate the QCD-induced correction factors to these lowest-order asymmetries.

A further remark concerns the so-called charge asymmetry. The initial state $|e^+(-\mathbf{p}_1)e^-(\mathbf{p}_1)\rangle$ is a CP eigenstate in the e^+e^- frame. If the interactions that affect $e^+e^- \to Q\bar{Q}X$ are CP-invariant then A_{FB} is equal to the charge asymmetry A_C that is defined by the number of quarks Q minus the number of antiquarks $\bar{Q}$ in the forward direction divided by the total number of produced $Q\bar{Q}$ pairs.

5.1 A_{FB} to second order in α_s

We recall the definition of the differential inclusive cross section for the production of a (massive) quark flavor Q, i.e., $d\sigma(e^+e^- \to Q+X)/dx_Q d\cos\theta$, where θ is the angle between the the electron three-momentum $\mathbf{p_1}$ and the axis defining the forward hemisphere, $x_Q = 2E_Q/\sqrt{s}$, and E_Q is the energy of Q. Both θ and E_Q are defined in the e^+e^- c.m. frame. With this distribution one can define forward and backward cross sections

$$\sigma_F = \int_0^1 d\cos\theta \int_{x_0}^1 dx_Q \frac{d\sigma}{dx_Q d\cos\theta}\,, \quad \sigma_B = \int_{-1}^0 d\cos\theta \int_{x_0}^1 dx_Q \frac{d\sigma}{dx_Q d\cos\theta}\,, \tag{5.2}$$

and the symmetric and antisymmetric cross section σ_S and σ_A,

$$\sigma_S = \sigma_F + \sigma_B\,, \quad \sigma_A = \sigma_F - \sigma_B\,. \tag{5.3}$$

In (5.2) the parameter $x_0 = 2m_Q/\sqrt{s}$. With (5.3) the forward-backward asymmetry (5.1) can be expressed as

$$A_{\rm FB} = \frac{\sigma_A}{\sigma_S}\,. \tag{5.4}$$

We emphasize again that above the threshold for $Q\bar{Q}Q\bar{Q}$ production the Feynman diagrams associated with this process contribute with a multiplicity factor two both to σ_S and σ_A because this final state contains two quarks Q.

The forward-backward asymmetry belongs to the class of observables that can be computed at the level of unresolved partons. We consider now the individual contributions to (5.4) to second order in α_s. These contributions are understood to be regulated, as in the previous chapters, with antenna subtraction terms. To order α_s^2 the symmetric and antisymmetric cross sections receive the following contributions from unresolved partons:

$$\sigma_{A,S} = \sigma_{A,S}^{(2,0)} + \sigma_{A,S}^{(2,1)} + \sigma_{A,S}^{(3,1)} + \sigma_{A,S}^{(2,2)} + \sigma_{A,S}^{(3,2)} + \sigma_{A,S}^{(4,2)} + \mathcal{O}(\alpha_s^3)\,, \tag{5.5}$$

where the first number in the superscripts (i, j) denotes the number of final-state partons associated with the respective term and the second one the order of α_s.

5.1.1 Unexpanded asymmetry

Inserting (5.5) into (5.4) we get the unexpanded version of $A_{\rm FB}$ to first and to second order in α_s:

$$A_{\rm FB}(\alpha_s) = \frac{\sigma_A^{(2,0)} + \sigma_A^{(2,1)} + \sigma_A^{(3,1)}}{\sigma_S^{(2,0)} + \sigma_S^{(2,1)} + \sigma_S^{(3,1)}} \equiv A_{\rm FB}^{\rm LO}\; C_1\,, \tag{5.6}$$

$$A_{\rm FB}(\alpha_s^2) = \frac{\sigma_A^{(2,0)} + \sigma_A^{(2,1)} + \sigma_A^{(3,1)} + \sigma_A^{(2,2)} + \sigma_A^{(3,2)} + \sigma_A^{(4,2)}}{\sigma_S^{(2,0)} + \sigma_S^{(2,1)} + \sigma_S^{(3,1)} + \sigma_S^{(2,2)} + \sigma_S^{(3,2)} + \sigma_S^{(4,2)}} \equiv A_{\rm FB}^{\rm LO}\; C_2\,, \tag{5.7}$$

where

$$A_{\rm FB}^{\rm LO} = \frac{\sigma_A^{(2,0)}}{\sigma_S^{(2,0)}}\,, \tag{5.8}$$

is the forward-backward asymmetry at Born level. The factors C_1 and C_2 defined by the respective ratio on the left of Eq. (5.6) and (5.7) are the unexpanded first-order and second-order QCD correction factors.

5.1.2 Expanded asymmetry

Taylor expansion of Eq. (5.6) to first order and of (5.7) to second order in α_s gives

$$A_{\rm FB}^{\rm NLO} = A_{\rm FB}^{\rm LO}\,[1 + A_1] \;+\; \mathcal{O}(\alpha_s^2)\,, \tag{5.9}$$

$$A_{\rm FB}^{\rm NNLO} = A_{\rm FB}^{\rm LO}\;[1 \;+\; A_1 \;+\; A_2] \;+\; \mathcal{O}(\alpha_s^3)\,, \tag{5.10}$$

where A_1 and A_2 are the QCD corrections of $\mathcal{O}(\alpha_s)$ and $\mathcal{O}(\alpha_s^2)$, respectively.

$$A_1 = \sum_{i=2,3} \Big[\frac{\sigma_A^{(i,1)}}{\sigma_A^{(2,0)}} \;-\; \frac{\sigma_S^{(i,1)}}{\sigma_S^{(2,0)}}\Big]\,, \tag{5.11}$$

$$A_2 = \sum_{i=2,3,4} \Big[\frac{\sigma_A^{(i,2)}}{\sigma_A^{(2,0)}} \;-\; \frac{\sigma_S^{(i,2)}}{\sigma_S^{(2,0)}}\Big] - \frac{\sigma_S^{(2,1)} + \sigma_S^{(3,1)}}{\sigma_S^{(2,0)}}\,A_1\,. \tag{5.12}$$

Eqs. (5.9) and (5.10) are the expanded versions of the forward-backward asymmetry at NLO and NNLO QCD.

The unexpanded and expanded first and second-order forward-backward asymmetries differ by terms of order α_s^2 and order α_s^3, respectively. Below we shall evaluate both versions of the asymmetry for top and bottom quarks. The differences between the two versions may be considered as an estimate of the theory uncertainties.

As to the expanded version (5.10) of the forward-backward asymmetry, we recall that the two-parton and the sum of the three- and four-parton contributions to A_2 are separately infrared (IR) finite, cf. [88, 90, 201]. The $Q\bar{Q}$ contribution to A_2 is determined by the one-loop [59] and two-loop [175–177] QCD vertex form factors γ^*, $Z^* \to Q\bar{Q}$ and it was calculated in [201] for massive b and top quarks.

The three- and four-parton contributions to A_2 may be computed with any NLO method for handling the IR divergences, for example, with the dipole subtraction method [128, 130]. Let us

briefly discuss why with such a method subtracted three- and four-parton contributions to A_2 can be computed that are separately finite. We recall the generalized eikonal-like factorization property of QCD amplitudes in the soft limit [97, 101, 128]. The only hard skeleton of our $Q\bar{Q}$ amplitudes at NNLO QCD that survive in the double soft limit (which is the only double unresolved region for heavy quark pair production in e^+e^-collisions) is the $2 \to 2$ tree-level amplitude $e^+e^- \to Q\bar{Q}$. The key point to realize is that neither the (generalized) eikonal factors or soft currents nor their integrated forms have any knowledge about the structure of this hard skeleton, for instance of the scattering angle of the heavy quark w.r.t. the electron beam. On the other hand, it is precisely the structure of this hard skeleton that determines the forward-backward asymmetry. This implies that in the double-soft region $\sigma_A^{(i,2)}$ and $\sigma_S^{(i,2)}$ are proportional to $\sigma_A^{(2,0)}$ and $\sigma_S^{(2,0)}$, respectively, with the same IR singular proportionality factor. This holds separately for $i = 2, 3, 4$. Therefore, in the double soft-region each of the three differences $\left[\sigma_A^{(i,2)}/\sigma_A^{(2,0)} - \sigma_S^{(i,2)}/\sigma_S^{(2,0)}\right]$ $(i = 2, 3, 4)$ that appear in A_2 (cf. Eq. (5.12)) is infrared finite. In other words, these differences do not require a NNLO infrared subtraction. Yet, this difference becomes IR singular for $i = 3, 4$ in the single unresolved region, but they can be separately regularized with an NLO subtraction scheme [208], such that the sum of the differences for $i = 3$ and $i = 4$ is IR finite.

However, for the calculation of the numerator and denominator of the unexpanded asymmetry (5.7) an NNLO IR method is required. We calculate both versions of the b-quark forward-backward asymmetry at NNLO with the NNLO antenna subtraction set-up outlined in the previous chapters.

5.1.3 Leading-order formulas and $\sin^2\theta_W^{eff}$

It is useful to recall the analytic formula for the forward-backward asymmetry at lowest order. Neglecting the electron mass the symmetric and antisymmetric LO cross sections for $e^+e^- \to$

$\gamma^*, Z^* \to Q\bar{Q}$ are given by

$$\begin{aligned}\sigma_S^{(2,0)} =& \frac{N_c}{24\pi}\frac{1}{s}\beta\left(v_e^\gamma v_Q^\gamma\right)^2(3-\beta^2) + \frac{N_c}{12\pi}\frac{s}{D_Z}\beta\left(1-\frac{m_Z^2}{s}\right)v_e^\gamma v_Q^\gamma v_e^Z v_Q^Z(3-\beta^2) \\ &+ \frac{N_c}{24\pi}\frac{s}{D_Z}\beta\left[\left(a_e^Z\right)^2+\left(v_e^Z\right)^2\right]\left[2\left(a_Q^Z\right)^2\beta^2+\left(v_Q^Z\right)^2(3-\beta^2)\right], \end{aligned} \tag{5.13}$$

$$\sigma_A^{(2,0)} = \frac{N_c}{4\pi}\frac{s}{D_Z}\beta^2 a_e^Z a_Q^Z\left[v_e^Z v_Q^Z + \frac{1}{2}\left(1-\frac{m_Z^2}{s}\right)v_e^\gamma v_Q^\gamma\right], \tag{5.14}$$

where v_f^γ is the electric charge of the fermion f in units of $e>0$ and v_f^Z, a_f^Z are the vector and axial vector couplings of f to the Z boson defined in Eq. (A.4) of Appendix A.1. Moreover, $\beta = \sqrt{1-4m_Q^2/s}$ is the velocity of Q and D_Z is the numerator of the Z-boson propagator. The leading-order asymmetry $A_{\rm FB}^{\rm LO}$ is given by the ratio (5.8). Near threshold, $\sqrt{s}\to 2m_Q$, the asymmetric cross section, which is generated by the p-wave component of the S matrix element, is suppressed by a factor of β compared to the symmetric cross section and, therefore, the forward-backward asymmetry becomes zero.

Right at the Z resonance, $\sqrt{s}=m_Z$, the couplings to the photon are put to zero if one works at lowest order in the electroweak couplings. Then

$$A_{\rm FB}^{\rm LO} = \frac{6\beta v_e^Z a_e^Z v_Q^Z a_Q^Z}{\left[(a_e^Z)^2+(v_e^Z)^2\right]\left[2\left(a_Q^Z\right)^2\beta^2+\left(v_Q^Z\right)^2(3-\beta^2)\right]}. \tag{5.15}$$

The formulas (5.13) - (5.15) apply to the production of quark and lepton pairs $f\bar{f}$. ($N_c\to 1$ for $f=e,\mu,\tau$.) Neglecting the mass of the final-state fermion f in (5.15), we have

$$A_{\rm FB}^{\rm LO}(m_f=0) = \frac{3}{4}\mathcal{A}_e\mathcal{A}_f\,, \quad \text{where} \quad \mathcal{A}_f = \frac{2v_f^Z a_f^Z}{(v_f^Z)^2+(a_f^Z)^2}\,. \tag{5.16}$$

In the SM the forward-backward asymmetry depends on $s_W^2\equiv\sin^2\theta_W$. The sensitivity of $A_{\rm FB}^{\rm LO}$ to s_W^2 is given by $S_f\equiv\partial A_{\rm FB}^{\rm LO}/\partial s_W^2$. This quantity depends on the charge of the final-state fermion f as is clear from the expression for v_f^Z. We may estimate S_f at the Z pole using $s_W^2=0.23$ as an example. For quarks with $|Q_Q|=1/3$, i.e. for b quarks we get $S_Q=S_b\simeq 5.6$, while for quarks with $|Q_Q|=2/3$, i.e. for c quarks we get $S_Q=S_c\simeq 4.4$. For charged leptons

$S_l \simeq 1.9$. This signifies that at the Z pole the b-quark forward-backward asymmetry has the highest sensitivity to $\sin^2\theta_W$, as was already emphasized in the introduction.

In electroweak precision fits to data at the Z pole the formula for $A_{\rm FB}^{\rm LO}$ is used where the couplings v_f^Z and a_f^Z of the final-state fermions are replaced by effective couplings $v_{f,eff}^Z$ and $a_{f,eff}^Z$. In fact, one goes further and expresses these couplings in terms of an effective weak mixing angle $\sin^2\theta_W^{eff}$ and a normalization factor ρ_f. By convention, these effective couplings incorporate only the genuine weak-interaction corrections (which are IR finite) to $Z \to f\bar{f}$ which are calculated in some renormalization scheme, see for instance [209]. (For the 2-loop weak corrections to $Z \to b\bar{b}$ see [210].) The QED and QCD corrections (in the case of $f = Q$) are taken into by correcting the measured forward-backward asymmetry. This will be outlined in somewhat more detail in sec. 5.3.4.

In this thesis we consider unpolarized e^+e^- collisions. The leading-order formulas for the symmetric and antisymmetric cross sections given above can be straightforwardly extended to the cases where the electron and/or positron beam is longitudinally polarized to some degree. (For explicit formulas, see for instance, [90].) Below we compute the universal and non-universal QCD corrections to order α_s^2 (as defined in section 3.1) to the LO top- and bottom quark asymmetry. The respective universal QCD corrections apply as a multiplicative factor to the LO asymmetry also in the case of $t\bar{t}$ and $b\bar{b}$ production by polarized e^- and/or e^+ beams.

5.2 The top-quark asymmetry above the $t\bar{t}$ threshold

In this section we present our results for the t-quark forward-backward asymmetry at NNLO QCD and lowest order in the electroweak couplings above the $t\bar{t}$ threshold. This observable is of central interest for the top-physics program at future e^+e^- colliders [27].

We consider the top-quark asymmetry for c.m. energies $\sqrt{s} > 2m_t$ where fixed-order perturbation theory in α_s is reliable. For definiteness, we confine ourselves to $\sqrt{s} \lesssim 4m_t$. For $\sqrt{s} > 4m_t$ the $t\bar{t}t\bar{t}$ final state contributes, too. This final state has a signature which is clearly distinct from $t\bar{t}$ events. Thus, the four-top final state may or may not be included in future measurements of the top-quark A_{FB}, depending on experimental strategies.

We consider here the top-quark A_{FB} with respect to the top-quark direction of flight in the e^+e^- c.m. frame. As already mentioned above this axis can be reconstructed in future $t\bar{t}$ data, in particular in $t\bar{t} \to$ lepton + jets events where the top quark decays hadronically, $t \to bq\bar{q}'$. We use for our computation of the top-quark A_{FB} the antenna-subtracted squared matrix elements that correspond to the contributions of the various final states at NNLO QCD. This allows to implement acceptance cuts, although we refrain here from applying cuts. Our results for the top-quark asymmetry given below follow from the computations of the $\cos\theta_t$ distributions at LO, NLO, and NNLO QCD which were presented for two c.m. energies in sec. 4.2. The input values for the top-quark mass, the QCD and electroweak couplings, in particular the value of $sin^2\theta_W$, are those given at the beginning of chapter 4. Our main interest is the determination of the NLO and NNLO QCD correction factors to the LO asymmetry. These factors may be used in the future to extract from the measurement of the top-quark A_{FB} the leading-order asymmetry which contains the information about the neutral-current couplings of the top quark.

Table 5.1 contains our results for the unexpanded version of the top-quark A_{FB} at NLO and NNLO QCD and the associated QCD correction factors C_1 and C_2 defined in Eq. (5.6) and (5.7) for several c.m. energies. This version of computing the asymmetry corresponds to its experimental measurements or its simulation Monte Carlo event generators. The central values refer to the choice of renormalization scale $\mu = \sqrt{s}$ and the given uncertainties are obtained by varying μ simultaneously in the numerator and denominator of Eq. (5.6) and (5.7) between $\sqrt{s}/2 \leq \mu \leq 2\sqrt{s}$. The scale uncertainties are small, but the NNLO uncertainties do not decrease compared to those at NLO QCD. This feature is not uncommon for an observable that is defined as a ratio. The simultaneous scale variation of the numerator and denominator may underestimate the scale uncertainties. A more conservative procedure would be to vary numerator and denominator independently, which is possible in the case of the unexpanded asymmetry.

Table 5.2 contains our results for the expanded version of the top-quark forward-backward asymmetry at NLO and NNLO QCD defined in Eq. (5.9) and (5.10), respectively, and the correction terms A_1 and A_2 given in Eq. (5.11) and (5.12) for several c.m. energies. The central

Table 5.1: The unexpanded version of the top-quark forward-backward asymmetry and the QCD correction factors C_1 and C_2 defined in Eq. (5.6) and (5.7) for several c.m. energies.

$\sqrt{s}$ [GeV]	$A_{\rm FB}^{\rm LO}$ [%]	$A_{\rm FB}(\alpha_s)$ [%]	$A_{\rm FB}(\alpha_s^2)$ [%]	C_1	C_2
360	14.94	$15.31^{+0.02}_{-0.02}$	$15.82^{+0.08}_{-0.06}$	$1.0247^{+0.0013}_{-0.0013}$	$1.0589^{+0.0053}_{-0.0040}$
400	28.02	$28.77^{+0.05}_{-0.04}$	$29.42^{+0.10}_{-0.09}$	$1.0268^{+0.0018}_{-0.0014}$	$1.0500^{+0.0036}_{-0.0032}$
500	41.48	$42.32^{+0.06}_{-0.05}$	$42.83^{+0.08}_{-0.07}$	$1.0203^{+0.0014}_{-0.0012}$	$1.0325^{+0.0019}_{-0.0017}$
700	51.34	$51.78^{+0.03}_{-0.03}$	$52.03^{+0.04}_{-0.04}$	$1.0086^{+0.0006}_{-0.0006}$	$1.0134^{+0.0008}_{-0.0008}$

values and the uncertainties refer to the scales $\mu = \sqrt{s}$ and $\mu = \sqrt{s}/2$ and $2\sqrt{s}$, respectively. Obviously, here we vary μ simultaneously in the σ_S and σ_A of different partonic channels between $\sqrt{s}/2$ and $2\sqrt{s}$. The numbers $\delta A_{\rm FB}^{\rm NNLO}$ in the last column of table 5.2 signify the change of $A_{\rm FB}^{\rm NNLO}$ if our input value for the top-quark mass is changed by ± 0.5 GeV. For a given c.m. energy $A_{\rm FB}^{\rm NNLO}$ increases if the top-quark mass is decreased and vice versa. Simulations indicate that the top-quark mass can be measured with a much smaller uncertainty than ± 0.5 GeV from a $t\bar{t}$ threshold scan at a future e^+e^- collider [27].

Table 5.2: The top-quark forward-backward asymmetry at LO, NLO, and NNLO QCD for several c.m. energies using the expansions Eq. (5.9) and (5.10).

$\sqrt{s}$ [GeV]	$A_{\rm FB}^{\rm LO}$ [%]	$A_{\rm FB}^{\rm NLO}$ [%]	$A_{\rm FB}^{\rm NNLO}$ [%]	A_1 [%]	A_2 [%]	$\delta A_{\rm FB}^{\rm NNLO}$ [%]
360	14.94	$15.54^{+0.05}_{-0.04}$	$16.23^{+0.12}_{-0.10}$	$4.01^{+0.35}_{-0.29}$	$4.58^{+0.46}_{-0.38}$	± 0.59
400	28.02	$28.97^{+0.08}_{-0.07}$	$29.63^{+0.11}_{-0.10}$	$3.41^{+0.29}_{-0.25}$	$2.36^{+0.11}_{-0.11}$	± 0.27
500	41.48	$42.42^{+0.08}_{-0.07}$	$42.91^{+0.08}_{-0.07}$	$2.28^{+0.19}_{-0.16}$	$1.18^{+0.01}_{-0.01}$	± 0.13
700	51.34	$51.81^{+0.04}_{-0.03}$	$52.05^{+0.04}_{-0.04}$	$0.91^{+0.07}_{-0.06}$	$0.47^{+0.01}_{-0.01}$	± 0.06

In the computation of the numbers in table 5.1 and table 5.2, we have included in A_2 also the non-universal contributions that contain the electroweak couplings of quarks $q \neq t$. We remark that the square of the diagrams where γ^*/Z^* couple to $q \neq t$ and the $t\bar{t}$ pair is produced by gluon splitting does not contribute to the antisymmetric cross section, but they do make non-zero contribution to the symmetric cross section. These contributions are pretty small due to the fact that the top-quark mass is not small compared to c.m. energy considered. The ratio $r = A_2^{\rm non}/A_2$ of the non-universal and the total order α_s^2 correction increases with increasing c.m. energy. We find that $r = -0.16\%, -1\%$, and -2.4% for $\sqrt{s} = 400$ GeV, 500 GeV, and

700 GeV, respectively.

The numbers of table 5.2 tell us that close to the $t\bar{t}$ threshold, at $\sqrt{s} \simeq 360$ GeV, fixed order perturbation theory is no longer reliable because the second order correction A_2 to the forward-backward asymmetry is larger than the first order correction A_1. From the numbers given in table 5.1 one can draw the same conclusion. For $\sqrt{s} > 380$ GeV, the ratio $|A_2/A_1|$ becomes smaller than one. Notice that the order α_s^2 correction is significant as compared to the first order one: $|A_2/A_1| \gtrsim 0.5$ for the c.m. energies listed in table 5.2. The uncertainties of $A_{\rm FB}^{\rm NNLO}$ due to scale variations are small, but these uncertainties do not decrease, in the range of c.m. energies given in table 5.2, compared to the scale uncertainties of $A_{\rm FB}^{\rm NLO}$.

As discussed in section 5.1.2, the two-parton, i.e., the $t\bar{t}$ contribution to $A_{\rm FB}$ is separately IR-finite, both at order α_s and at order α_s^2 [201]. In the range of c.m. energies given in table 5.2, the $t\bar{t}$ final state makes the largest contribution both to A_1 and A_2. For $\sqrt{s} \lesssim 500$ GeV it is significantly larger than the respective contribution from the three- and four-parton final states. Here, we have computed the $t\bar{t}$ contribution to A_1 and A_2 with the antenna-subtracted two-parton matrix elements of sections 3.2 and 3.3. It was computed in [208] with an NLO subtraction scheme, namely dipole subtraction with massive quarks [130]. We agree with the results of [208]. The top-quark forward-backward asymmetry at NNLO QCD was computed before in ref. [80] in the unexpanded version with values of m_t and α_s that differ slightly from the ones that we use here. Taking these differences into account we agree with [80]. The method employed in [80] is a mixture of phase-space slicing and NLO dipole subtraction method.

One may take the spread between the values of the unexpanded and expanded versions of A_{FB}, at NLO and NNLO QCD respectively, given in tables 5.1 and 5.2 as an estimate of the uncalculated higher order corrections. Alternatively, one may add the scale uncertainties and the uncertainties due to $\delta m_t = \pm 0.5$ GeV of the expanded version (cf. table 5.2) linearly and take this as residual uncertainty of our prediction of $A_{\rm FB}^{\rm NNLO}$. An uncertainty of 0.4% and 0.2% at $\sqrt{s} = 400$ and 500 GeV, respectively, results in this way. This estimate is in accord with the spread between the expanded and unexpanded results listed in tables 5.1 and 5.2. This uncertainty is significantly smaller than the projected experimental precision of top-quark $A_{\rm FB}$ measurements at future electron-positron colliders [32]. This observable has a high sensitivity

to precisely determine the neutral current couplings of the top quark and probe for anomalous couplings in e^+e^- collisions [32].

5.3 The bottom-quark asymmetry at the Z pole

Finally we determine the b-quark forward-backward asymmetry at the Z resonance to NNLO QCD and lowest order in the electroweak couplings. As in section 4.4 the contributions involving virtual photon exchange are neglected. We compute the b-quark A_{FB} with respect to both the b-quark and the thrust direction. The input values of the Standard Model couplings and masses are specified at the beginning of section 4. In particular we recall that we use α_s defined in 5-flavor QCD and the bottom-quark on-shell mass $m_b = 4.89 \pm 0.04$ GeV. For the mass of the top quark that appears in the triangle-loop diagrams contributing to the non-universal corrections to A_{FB} we use $m_t = 173.34$ GeV. The u, d, c, s quarks are taken to be massless. Although, as explained above, the expanded version of A_{FB} at NNLO QCD can be calculated using a NLO IR subtraction scheme, we employ again the set-up of the NNLO antenna subtraction scheme developed in the previous chapters. First we calculate the b-quark asymmetry without phase-space cuts. In section 5.3.3 we apply a cut on $\cos\theta_b$, respectively on $\cos\theta_T$ and determine the resulting asymmetry.

5.3.1 Massive b quark, quark axis and thrust axis

With the input parameters mentioned above, the Born-level value of the b-quark forward-backward asymmetry at $\sqrt{s} = m_Z$ is $A_{\rm FB}^{\rm LO} = 0.1512$. The value of $A_{\rm FB}^{\rm LO}$ is very sensitive to the input value of s_W^2 but insensitive to the value of m_b within its uncertainty. As in the case of the top quark, we are primarily concerned with the order α_s and α_s^2 QCD corrections to the LO asymmetry, both in the unexpanded and expanded version of the asymmetry. In this subsection we take into account all Feynman diagram contributions discussed in sections 3.1.

First we present for the expanded version of the asymmetry our results for the QCD corrections defined in Eqs. (5.9) - (5.12). Table 5.3 lists the values of the NLO and NNLO correction

Table 5.3: The first- and second-order QCD correction factors defined in (5.9) - (5.12) to the LO b-quark forward-backward asymmetry at the Z peak for the input values given in the text and for $\mu = m_Z$. The numbers in superscript (subscript) refer to the changes if $\mu = 2m_Z$ ($\mu = m_Z/2$) is chosen.

	$1 + A_1$	$1 + A_1 + A_2$	A_1	A_2
quark axis:	$0.9710^{+0.0028}_{-0.0034}$	$0.9587^{+0.0026}_{-0.0028}$	-0.0290	-0.0123
thrust axis:	$0.9713^{+0.0027}_{-0.0026}$	$0.9608^{+0.0022}_{-0.0025}$	-0.0287	-0.0105

factor, both for the quark axis and the thrust axis definition, for the three renormalization scales $\mu = m_Z/2, m_Z, 2m_Z$. Contrary to the case of the top-quark the QCD corrections decrease the asymmetry. The numbers given in this table show that the order α_s^2 corrections are significant. For $\mu = m_Z$ the ratio A_2/A_1 is 43% and 37% for the quark and thrust axis definition, respectively. The scale variations change both the first- and second-order QCD correction factors by about ± 0.003 with respect to their values at $\mu = m_Z$. As already discussed in the preceding section for the top quark case, the fact that inclusion of the second-order correction term A_2 does not reduce the scale uncertainty is not unusual for an observable that is defined as a ratio. Contrary to the case of the top quark for the c.m. energies used in sec. 5.2, the order α_s and α_s^2 corrections A_1 and A_2 are dominated by the contributions from the three-parton and three- and four-parton final states, respectively. In the limit $m_b \to 0$ the $b\bar{b}$ contribution to A_1 and the non-singlet $b\bar{b}$ contribution to A_2 vanish because of the chirality-preserving feature of gauge interactions of massless quark in these diagrams. Because $m_b/m_Z \ll 1$ these 2-parton contributions to A_1 and A_2 turn out to be about two orders of magnitude smaller than the three-parton, respectively three- and four-parton contributions. The $b\bar{b}$ triangle contribution to A_2 (cf. figure 3.1d) is about one order of magnitude larger than the non-singlet $b\bar{b}$ contribution, but an order of magnitude smaller than those from the three- and four-parton final states.

We have included in the computation of $A_{\rm FB}$ the non-universal corrections $A_2^{\rm non-u.}$ of order α_s^2 that contain the vector and axial vector couplings of quarks $q \neq b$. They are significant. For instance, for the quark axis definition and $\mu = m_Z$ we get $A_2^{\rm non-u.} = -0.00310$ which is 25% of the total correction A_2. This number comes about as follows. The two- and the three-parton contribution to $A_2^{\rm non-u.}$, that is, the interference of figure 3.1a and 3.1d and of figure 3.2a and 3.2c, is small: it is +0.00085 and +0.00028, respectively. The dominant part is due to the

non-universal contributions from the $b\bar{b}q\bar{q}$ ($q \neq b$) final state. While the term $\sigma_A^{(4,2)}/\sigma_A^{(2,0)}$ (cf. eq. (5.12)) of this correction is negligibly small, the term $\sigma_S^{(4,2)}/\sigma_S^{(2,0)}$ is significant. As a result the contribution of this term to $A_2^{\text{non-u.}}$ is -0.00423. Notice that the value of $A_2^{\text{non-u.}}$ depends on the value of $\sin^2\theta_W$.

In order to factorize out the dependence of the QCD correction factors on α_s, we now represent the expanded version of the b-quark asymmetry, both for the quark and the thrust axis, in the form:

$$A_{\text{FB}}^{\text{NNLO}} = A_{\text{FB}}^{\text{LO}} \left[1 - a_1 \frac{\alpha_s}{2\pi} - a_2 \left(\frac{\alpha_s}{2\pi}\right)^2\right] . \tag{5.17}$$

Table 5.4 contains the values of the coefficients a_1 and a_2 extracted from the values of A_1 and A_2 of table 5.3. The rather large changes of a_2 with variation of μ is due to the fact that the variation of the complete correction A_2 is small (because of the definition of A_{FB} as an ratio) but the variation of α_s^2 with μ is significant. The numbers given in table 5.4 should be useful for future implementation of our results into simulation programs that use a value of α_s different from ours.

Table 5.4: The values of the first- and second-order coefficients a_1 and a_2 defined in (5.17).

		a_1	a_2
quark axis	$\mu = m_Z/2$:	1.544	26.67
	$\mu = m_Z$:	1.544	34.84
	$\mu = 2m_Z$:	1.544	43.06
thrust axis	$\mu = m_Z/2$:	1.528	21.75
	$\mu = m_Z$:	1.528	29.81
	$\mu = 2m_Z$:	1.528	37.98

Monte-Carlo simulations or measurements of the b-quark forward-backward asymmetry at the Z peak may also be compared with perturbative computations where the ratio $\frac{N_F - N_B}{N_F + N_B}$ is not expanded. In this case the order α_s and order α_s^2 correction factors C_1 and C_2 defined in (5.6) and (5.7) apply. Their values are given in table 5.5.

As in the top quark case, the spread between the second-order expanded and unexpanded correction factors may be viewed, in addition or alternatively to scale variations, as an indication of the order of magnitude of the uncalculated higher-order corrections. The comparison of the values of $1 + A_1 + A_2$ and C_2 for fixed μ given in table 5.3 and 5.5 shows that both for the

Table 5.5: The first- and second-order QCD correction factors C_1 and C_2 associated with the unexpanded version of the b-quark $A_{\rm FB}$.

	C_1	C_2
quark axis:	$0.9722^{+0.0025}_{-0.0031}$	$0.9594^{+0.0026}_{-0.0030}$
thrust axis:	$0.9725^{+0.0025}_{-0.0031}$	$0.9614^{+0.0023}_{-0.0026}$

quark and the thrust axis definition the spread between these correction factors is significantly smaller than the change of these terms due to scale variations.

5.3.2 Approaching the limit $m_b \to 0$

As a check, we want to calculate the b-quark $A_{\rm FB}$ for $m_b \to 0$ and compare with the order α_s^2 results of [89, 90] obtained for $m_b = 0$. To be precise, we compute the second-order QCD correction to the b-quark forward-backward asymmetry for a sequence of decreasing values of m_b and then perform a fit to these numbers which allows us to extrapolate to $m_b = 0$. In order to conform to the calculation of [90] we neglect now, as was done in [90], the so-called singlet and the triangle contributions that were classified in sec. 3.1 in accord with [90]. As a short reminder, flavor singlet contributions consist of diagrams where the bottom quark that is observed is produced via the splitting of an intermediate gluon $g \to b\bar{b}$ rather than by the (electro)weak neutral current. The triangle contributions correspond to two-parton, three-parton, and four-parton cut-diagrams where a triangle fermion loop is involved. The remaining contributions are the so-called non-singlet contributions and they are taken into account when approaching the massless b-quark limit. The non-singlet contributions to the second-order QCD correction A_2 are denoted in the following by A_2^{NS}. Recall that as far as the $b\bar{b}b\bar{b}$ final state is concerned, the E-term given by the interferences listed in Eq. (3.2) contribute to A_2^{NS}.

Note that in the limit $m_b \to 0$, the only non-vanishing two-parton two-loop contributions to A_2 are the triangle contributions, fig. 3.1c. All other diagrams, the non-singlet $b\bar{b}$ contributions, lead to the same QCD correction for the vector and axial-vector coupling of the Z boson, as a consequence of chiral invariance of the massless theory, so that their net contribution to A_2 vanishes. Thus for $m_b = 0$ the non-singlet QCD correction term A_2^{NS} receives only contributions

form 3-parton and 4-parton final states.

In the limit $m_b \to 0$ the second-order QCD correction A_2^{NS} becomes singular. In order to understand this let us decompose the symmetric and antisymmetric non-singlet cross sections as follows [90]:

$$\sigma_{S,NS}(w_E) = \sigma_{S,NS}(w_E = 0) + w_E \sigma_S^{(2,0)} \int E_S \,, \tag{5.18}$$

$$\sigma_{A,NS}(w_E) = \sigma_{A,NS}(w_E = 0) + w_E \sigma_A^{(2,0)} \int E_A \,. \tag{5.19}$$

Here the first terms on the right-hand sides of these equations denote all non-singlet contributions to order α_s^2 except the E term, while $\int E_S$ and $\int E_A$ denote the phase-space integrals of the symmetric and antisymmetric E-term, and w_E is a multiplicity or weight factor. Recall that the inclusive definition of $\sigma_{S,NS}$ and $\sigma_{A,NS}$ corresponds to $w_E = 2$ because there are two b quarks in the $b\bar{b}b\bar{b}$ final state. The corresponding forward-backward asymmetry is $A_{FB,NS}(w_E) = \sigma_{A,NS}(w_E)/\sigma_{S,NS}(w_E)$ and by expansion in α_s one gets A_2^{NS}.

It turns out that the inclusive definition with $w_E = 2$ yields an antisymmetric cross section which is infrared finite to order α_s^2 in the limit $m_b \to 0$, but the symmetric cross section is IR divergent in this limit, even if one considers only the non-singlet component. Thus $A_{FB,NS}(w_E = 2)$ is IR divergent at order α_s^2 for $m_b \to 0$. In fact this holds for any value of $w_E > 0$. For instance, for $w_E = 1$ the symmetric cross section $\sigma_{S,NS}(w_E = 1)$ is IR-finite at order α_s^2 for $m_b \to 0$, while $\sigma_{A,NS}(w_E = 1)$ is not.

Let us try to understand this. The divergences for $m_b \to 0$ in the above non-singlet components are associated with logarithmically enhanced terms $\propto \alpha_s^2 \ln(s/m_b^2)$ that arise in the phase-pace integration of the E-term in the four triple-collinear regions, where three of the four b quarks become simultaneously parallel [90]. What are the consequences of this singularities for (5.18) and (5.19)? The b quark from gluon splitting $g \to b\bar{b}$ does not contribute to $\int E_A$. Therefore only half of the b quarks from the $b\bar{b}b\bar{b}$ final state, those from $Z \to b\bar{b}$, contribute $\int E_A$. This factor 1/2 compensates the factor $w_E = 2$. As a result, for $m_b \to 0$, the divergence in $2\sigma_A^{(2,0)} \int E_A$ is canceled by the respective divergence that arises from the 1-loop $b\bar{b}g$ diagrams that contribute to $\sigma_{A,NS}(w_E = 0)$. On the other hand, for $w_E = 2$ there is a mismatch of sin-

gularities of the symmetric E-term, $2\sigma_S^{(2,0)} \int E_S$, and and of the singularities of $\sigma_{S,NS}(w_E = 0)$. Therefore $\sigma_{S,NS}(w_E = 2)$ and hence $A_{FB,NS}(w_E = 2)$ are IR-singular for $m_b \to 0$. If one would choose $w_E = 1$ then $\sigma_{A,NS}(w_E = 1)$ becomes IR-singular, while $\sigma_{S,NS}(w_E = 1)$ is IR-finite for $m_b \to 0$. (Recall that the multiplicity factor $w_E = 1$ corresponds to the exclusive definition of the cross section. This is also the multiplicity factor with which the $b\bar{b}b\bar{b}$ final state and the other $q\bar{q}q\bar{q}$ final states contribute to the total cross section $e^+E^- \to$ hadrons.)

Refering to the definition of the b-quark forward-backward asymmetry (5.1) which involves the number of b quarks in the forward and backward direction an the total number of b quarks, one has to choose $w_E = 2$. Because $A_{FB,NS}(w_E = 2)$ is IR-divergent at order α_s^2 for $m_b \to 0$, ref. [90] defined an auxiliary variable $\hat{A}_{FB,NS}$ that is IR finite in this limit, namely

$$\hat{A}_{FB,NS} \equiv \frac{\sigma_{A,NS}(w_E = 2)}{\sigma_{S,NS}(w_E = 1)} \,. \tag{5.20}$$

Using (5.18) and (5.19) and expanding the ratio one sees that the physical expression for the asymmetry is

$$A_{FB,NS}(w_E = 2) = \hat{A}_{FB,NS} - A_{\rm FB}^{LO} \int E_S \,. \tag{5.21}$$

In this way, the term $\propto \int E_S$ which becomes singular for $m_b \to 0$ is isolated. Ref. [90] computed $\hat{A}_{FB,NS}$ for massless b quarks and the term $A_{\rm FB}^{LO} \int E_S$ for small, but non-zero m_b.

Now we explicitly expand (5.21) to order α_s^2. Referring to the definition of the first and second-order QCD correction terms A_1 and A_2 in Eq. (5.10) we get analogously for the non-singlet second-order QCD correction term

$$A_2^{NS}(w_E = 2) = \hat{A}_2^{NS} - \int E_S \,. \tag{5.22}$$

The term $\hat{A}_2^{NS}$, which is finite for $m_b = 0$ as emphasized above, was computed for a massless b quark in [89, 90] and [90] for the quark axis and thrust axis definition, respectively. Here we compute $\hat{A}_2^{NS}$, respectively the coefficient

$$\hat{a}_2^{NS} = -\left(\frac{2\pi}{\alpha_s}\right)^{-2} \hat{A}_2^{NS} \tag{5.23}$$

for a sequence of decreasing b-quark mass values between $m_b = 4.89$ GeV and $m_b = 1$ GeV. We choose the renormalization scale to be $\mu = m_Z$. We compute $\hat{a}_2^{NS}$ both for the quark and thrust axis definition of $A_{\rm FB}$. The results are shown by the red solid triangle points in the left

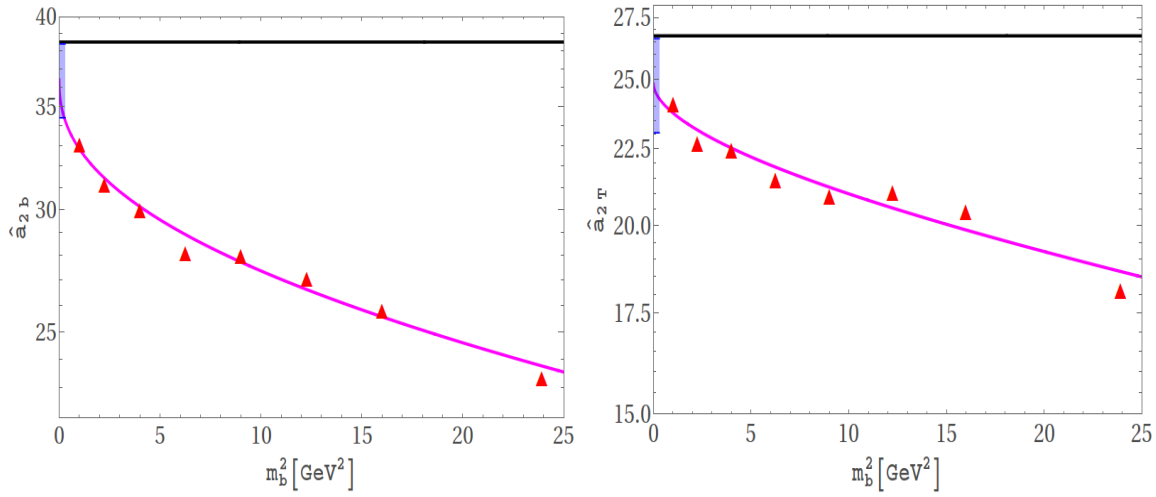

Figure 5.1: Left plot: The solid red triangles are values of the order α_s^2 correction coefficients $\hat{a}_2^{NS}$ defined in (5.23) for the quark axis definition for a sequence of b-quark mass values. The solid red curve is obtained by a fit using the ansatz (5.24). The horizontal solid black line is the value for $m_b = 0$ computed in [89, 90]. The shaded blue vertical line is the 1σ uncertainty of the value of $\hat{a}_2^{NS}$ at $m_b = 0$ resulting form the fit. Right plot: same as left plot, but for the thrust axis definition of $A_{\rm FB}$. The corresponmding value of $\hat{a}_2^{NS}$ at $m_b = 0$ computed in [90] is represented by the solid black line.

and right plots of figure 5.1. In order to extrapolate $\hat{a}_2^{NS}$ to $m_b = 0$ we perform a fit using the ansatz

$$c_0 + c_1 z + c_2 z \ln z^2 \,, \tag{5.24}$$

where $z = (m_b/m_Z)$. The structure of this ansatz is inspired by the analytic form of the high-energy asymptotic expansion of the antisymmetric cross section for massive quark pair production in e^+e^- collisions. (The asymptotic expansion of the symmetric cross section contains only powers of z^2 (and logs).) The coefficient c_0 is our fit value of $\hat{a}_2^{NS}$ at $m_b = 0$. We obtain

$$\text{quark axis: } c_0 = 36.40 \pm 1.70 \,, \qquad \text{thrust axis: } c_0 = 24.83 \pm 1.78 \,, \tag{5.25}$$

which agree within errors with the values

$$\hat{a}_{2b}^{NS}(m_b = 0) = 38.5, \qquad \hat{a}_{2T}^{NS}(m_b = 0) = 26.74 \tag{5.26}$$

for the quark axis [89, 90] and thrust axis [90] definition, respectively. Therefore we conclude that our calculation of the b-quark $A_{\rm FB}$ in the massless b quark limit at the Z pole agrees with [89, 90].

If one wants to compare the size of the QCD corrections to $A_{\rm FB}$ for a massive and a massless b-quark (under the same assumptions), one should compare the massless order α_s^2 correction coefficients of [89,90] with the respective coefficients shown in figure 5.1 for non-zero m_b, rather than comparing with the coefficients a_2 given in table 5.4, because the latter contain also singlet and triangle contributions which are not included in (5.26). Figure 5.1 shows that both for the quark and for the thrust axis definition, the second-order corrections are smaller in magnitude for massive quarks than for massless ones. For $m_b = 4.89$ GeV we obtain

$$\widehat{a}_{2b}(m_b = 4.89\ \text{GeV}) = 23.31, \qquad \widehat{a}_{2T}(m_b = 4.89\ \text{GeV}) = 18.43\,. \tag{5.27}$$

The magnitude of the second-order corrections decreases with increasing quark mass. This holds true also for the first-order corrections, as exemplified by comparing the values of a_1 for $m_b = 4.89$ GeV listed in table 5.4 with the values $a_{1b} = 2$ and $a_{1T} = 1.787$ for $m_b = 0$. This is in accord with the basic physical fact that a massive (anti)quark is more inert than a massless one in radiating off partons, and hence less affected by changes of its direction with respect to the leading-order quark antiquark configuration.

5.3.3 The b-quark asymmetry with a cut

Measurements of the b-quark $A_{\rm FB}$ at the Z pole used quite generally the oriented thrust axis for defining the forward and backward hemispheres [53]. The experiments used acceptance cuts, in particular a cut on $\cos\theta_T$ for selecting $b\bar{b}$ events and extrapolated the b-quark asymmetry determined in the fiducial phase space to the full phase space. On the theoretical side one may compute $A_{\rm FB}$ with cuts, which would perhaps allow a more direct comparison with experimental results. In this subsection we consider the b-quark $A_{\rm FB}$ with respect to the thrust axis definition for $m_b = 4.89$ GeV, apply a cut on $\cos\theta_T$, and compute the first and second-order QCD correction factors.

Inspecting the plots displayed in fig. 4.9 for the $\cos\theta_T$ distribution shows that the QCD corrections are larger in the central region than in the forward and backward regions. Thus we expect that the QCD corrections to $A_{\rm FB}^{LO}$ become larger in magnitude when a cut on $\cos\theta_T$ is applied. For definiteness, we use the cut $|\cos\theta_T| \leq 0.9$. The resulting first and second-order QCD correction factors in the expanded and unexpanded version of the asymmetry are given in table 5.6 for $\mu = m_Z$. Comparing with the numbers listed in table 5.3 and 5.5 one sees that, indeed, a cut on $\cos\theta_T$ increases the magnitude of the QCD corrections. Because they are negative, the QCD correction factors become smaller when a cut on cut on $\cos\theta_T$ is applied.

Table 5.6: The first- and second-order QCD correction factors (expanded and unexpanded) to the LO b-quark forward-backward asymmetry at the Z peak for the thrust axis definition and for the cut $|\cos\theta_T| \leq 0.9$. The renormalization scale $\mu = m_Z$.

$1 + A_1$	$1 + A_1 + A_2$	C_1	C_2
0.9681	0.9572	0.9695	0.9579

5.3.4 Phenomenological consequences

Finally we discuss the phenomenological impact of our order α_s^2 calculation of the b-quark $A_{\rm FB}$ for $m_b \neq 0$. We emphasize, however, that the following discussion is not a full-fledged analysis. Such an analysis would require the knowledge of a number of details about the respective measurements of $A_{\rm FB}$ made in the past which is not the topic of this thesis. The QCD corrections to the b-quark $A_{\rm FB}$ computed above cannot be applied directly to the analysis of experiments. (This holds true also for the calculations of [89, 90] for $m_b = 0$.) In the measurements of the b-quark asymmetry by the experiments at the previous e^+e^- colliders LEP and SLC, which are reviewed in [53–55], the forward and backward hemispheres was defined using the thrust axis. In our computation the thrust axis is defined for partonic final states, but the hadronization of partons causes a smearing of this axis. In addition, a bias in the topology of the events is introduced by the experimental selection and analysis method towards two-jet final states which causes additional uncertainties [211, 212].

A proper discussion of all these issues is certainly beyond the scope of this thesis. In order to get an idea about the impact of the QCD corrections to the lowest order $A_{\rm FB}$ computed

above, we compare them with those QCD corrections that were taken into account in [53–55]. These analyses aimed at extracting a pseudo-observable, namely the so-called bare b-quark Z-pole asymmetry $A_{\rm FB}^{0,b}$ from the measured asymmetry $A_{\rm FB,exp}^{b,T}$. For the determination of this pseudo-observable, a procedure described in [211, 212] was used. First, $A_{\rm FB,exp}^{b,T}$ was corrected for QCD effects. Schematically the procedure is as follows. (A more precise description what was actually done by experiments will be given at the end of this subsection.) Using (5.17) one writes

$$A_{\rm FB,exp}^{b,T} = \left[1 - a_{1T}\frac{\alpha_s}{2\pi} - a_{2T}\left(\frac{\alpha_s}{2\pi}\right)^2\right](A_{\rm FB}^{0,b})_{\rm exp} \equiv (1 - C_{\rm QCD}^{T})(A_{\rm FB}^{0,b})_{\rm exp}\,. \tag{5.28}$$

The QCD corrected "experimental asymmetry" $(A_{\rm FB}^{0,b})_{\rm exp}$ was then further corrected to obtain the experimental value of the pseudo-observable $A_{\rm FB}^{0,b}$, which is defined by

$$A_{\rm FB}^{0,b} = (A_{\rm FB}^{0,b})_{\rm exp} + \delta A_{\rm FB}^{b}\,. \tag{5.29}$$

The corrections $\delta A_{\rm FB}^{b}$ include the energy shift from $\sqrt{s} = 91.26$ GeV (all measured asymmetries were corrected, in a first step, to this energy) to $\sqrt{s} = m_Z$, QED corrections, corrections due to γ exchange and $Z - \gamma$ interference, and due to imaginary parts of effective weak couplings (cf. for instance, [85]). These corrections were computed with the program `ZFITTER` [213]. The value $\delta A_{\rm FB}^{b} = 0.0019 \pm 0.0002$ was obtained [85]. With this correction a value of the bare asymmetry $A_{\rm FB}^{0,b}$ was finally deduced. In this way ref. [55] obtained for the pseudo-observable the experimental value

$$A_{FB}^{0,b} = 0.0992 \pm 0.0016\,, \tag{5.30}$$

where the error refers to experimental and theoretical uncertainties. The pseudo-observable $A_{FB}^{0,b}$ still contains the genuine weak-interaction corrections One may use the concept of the effective weak mixing angle, respectively $\sin^2\theta_{W,eff}$ as discussed in section 5.1.3, with which the leading-order formula for A_{FB}^{LO} can be parametrized. Then a comparison of $A_{FB}^{LO}(\sin^2\theta_{W,eff})$ with (5.30) yields a value for this parameter[2]. Yet, let us stick to the pseudo-observable $A_{\rm FB}^{0,b}$ rather than to $\sin^2\theta_{W,eff}$. The most recent combined SM fit to all precision observables available [56]

[2]The hadronic effective weak mixing angle is actually flavor-dependent due to higher-order weak corrections, see for instance [210].

yields $A_{FB}^{0,b} = 0.1032$. The pull between this value and (5.30) is 2.5σ.

The QCD correction factor defined in (5.28) and used in [55] was obtained as follows [211,212]. For the order α_s correction the value $a_{1T} = 1.54$ was taken[3] that was computed in [87] for $m_b = 4.5$ GeV. For the second-order QCD correction coefficient the value $a_2^T(m_b = 0) = 23.72$ was used. This number is obtained by adding to the massless result of [90] the two-loop $b\bar{b}$ triangle contribution. The QCD correction factor determined in [212] is $(1 - C_{\rm QCD}^T) = 0.9646 \pm 0.0063$ where the error includes estimates of hadronization effects. Our thrust axis correction factor given in table 5.3 is $(1+A_1+A_2) = 0.9608 \pm 0.0025$, where the error is due to scale uncertainties only, agrees with that factor within the uncertainties. Our central value is smaller than 0.9646 by 0.4%. Using Eqs. (5.28) and (5.29) and the value of $\delta A_{\rm FB}^b$ given above we find that our correction changes the value of the pseudo-observable $A_{FB}^{0,b}$ to

$$(A_{FB}^{0,b})_{new} = 0.0996 \pm 0.0016\,. \tag{5.31}$$

Thus our new massive b-quark result of order α_s^2 leads to a slight decrease of the pull between $A_{FB}^{0,b}$ and the SM fit cited above, namely from 2.5σ to 2.2σ.

We recall that our value of the QCD correction factor was obtained by taking into account all second-order QCD contributions discussed in section 3.1. If one neglects the singlet contributions, that is, if one uses the value of $\hat{a}_{2T}(m_b = 4.89\ {\rm GeV})$ given in (5.27) and adds the $b\bar{b}$ and $b\bar{b}g$ triangle contributions, we get for the thrust axis correction factor $(1+A_1+A_2) = 0.9659 \pm 0.0023$. This value is not significantly larger than the correction factor used in [212] and cited above.

At this point we may speculate and assume that the QCD correction factor in the correction procedure (5.28) should not be the factor that was computed in the full phase space but the factor computed in a fiducial phase space. Let's further assume that the cut $|\cos\theta_T| \leq 0.9$ applies. Then one should use in (5.28) the QCD correction factor $(1 + A_1 + A_2) = 0.9572$ given in table 5.6 instead of the factor 0.9659. Then the central value of the pseudo-observable $A_{FB}^{0,b}$ changes from $A_{FB}^{0,b} = 0.0996$ given in (5.31) to $A_{FB}^{0,b} = 0.1000$. Assuming that the error given in (5.31), respectively in (5.30) does not change, the pull between this value and the value

[3] This value is almost the same as the value $a_{1T} = 1.53$ given in table 5.4. We recall that we use a slightly larger b-quark mass. Moreover, we determine the thrust axis by classifying the final states according to the moduli of their three-momenta rather than their energies as in [87].

$A_{FB}^{0,b} = 0.1032$ obtained by the SM fit [56] is then further reduced, namely to 2.0σ.

However, the above discussion of the impact of our new results on the order α_s^2 QCD corrections to the LO b-quark $A_{\rm FB}$ have to have to be taken with a grain of salt. The issue of extracting a value of the pseudo-observable $A_{FB}^{0,b}$ is not so straightforward. The 'old' value given in Eq. (5.30) is an average [55] of quite a number of $A_{FB}^{0,b}$ determinations by a number of experiments that used different methods to measure $A_{\rm FB,exp}^{b,T}$. These methods include b-tagging by high P_T leptons, lifetime-tagged events in combination with jet charge measurements, and selecting b events by specific final states, namely D mesons from B decays. Some of the experiments reviewed in [53] used cuts on $\cos\theta_T$, some extrapolated to the full $\cos\theta_T$ range. Some of the experiments removed the contributions from $g \to b\bar{b}$ splitting (which are part of the singlet contributions) 'by hand', that is, by making a Monte Carlo estimate and subtraction from the data. What is more cumbersome from a theorist's point of view is that the way how the QCD corrections were applied differs from experiment to experiment. The various experimental analyses made in the past have different sensitivity to QCD corrections. Therefore, a bias factor s_q was introduced, as suggested in [211], in order to scale the QCD corrections computed by theory with the experimental sensitivity. Instead of the QCD correction factor $(1 - C_{\rm QCD}^T)$ the factor $(1 - s_q C_{\rm QCD}^T)$ was used in Eq. (5.28), and different experiments used different values of s_q which were estimated by Monte Carlo simulation. Therefore, a proper re-analysis of b-quark $A_{\rm FB}$ data at the Z resonance using our new results on the second-order QCD corrections can be done only in collaboration with experimental physicists that have access to respective uncorrected and to Monte Carlo corrected data.

Chapter 6

Summary and outlook

In this thesis we have developed, within the antenna subtraction framework, a formalism for calculating the production of a massive quark-antiquark pair in electron-positron collisions at NNLO QCD. Our approach is fully differential and can be used to compute any infrared-safe observable for this process. We have applied this formalism to top-quark pair production in the continuum in the context of a future high-energy e^+e^- collider and also to bottom-quark pair production at the Z resonance.

In the top-quark case, we have calculated, besides the $t\bar{t}$ cross section $\sigma_{t\bar{t}}(s)$, also several distributions in order to demonstrate the usefulness of this approach, namely the $\cos\theta_t$ and transverse momentum distribution of the top quark, the transverse momentum of the $t\bar{t}$ system and the $t\bar{t}$ invariant mass distribution. The NNLO QCD corrections are sizable for center-of-mass energies $\sqrt{s}$ not too far away from the $t\bar{t}$ threshold. We have also computed the top-quark forward-backward asymmetry, which is an important precision observable for determining the neutral-current couplings of the top quark at a future e^+e^- collider, at NNLO QCD. In the center-mass energy region considered, $\sqrt{s} \lesssim 4m_t$, the NNLO QCD corrections increase the t-quark forward-backward asymmetry and the asymmetry is dominated by the contribution from the $t\bar{t}$ final state. This contribution is infrared finite, as is the sum of the contributions from the three- and four-parton final states. At a future e^+e^- collider, the top-quark forward-backward asymmetry is expected to be measurable with a precision $\delta A_{\rm FB}/A_{\rm FB}$ of about one percent, with data both from the full hadronic and lepton + jets channels [32]. We have found

that in order reach the same level of precision for this observable on the theoretical side, it is necessary to include the NNLO QCD corrections. In particular, we showed in section 5.2 that at a center-of-mass energy 500 GeV and with the chosen Standard Model input parameters the order α_s^2 QCD correction modifies the tree-level top-quark forward-backward asymmetry by 1.18%. Our results for the expanded and unexpanded asymmetry at order α_s^2 agree with previous calculations [80, 208] of this asymmetry.

Concerning the bottom-quark pair production at the Z peak, we have computed the production cross section, the p_T^b distribution, and the distributions of the b-quark direction of flight and of the oriented thrust axis, from which the forward-backward asymmetries with respect to these reference axes can be obtained. For $m_b = 4.89$ GeV, we have consistently included all the contributing diagrams listed in section 3.1. Our computation of the b-quark $A_{\rm FB}$ to order α_s^2, both for the b-quark axis and the oriented thrust axis definition of the asymmetry, is a new result. So far, the order α_s^2 corrections were known only for massless b quarks. In contrast to the top-quark forward-backward asymmetry as computed in section 5.2, the order α_s and α_s^2 QCD corrections to the b-quark asymmetry at the Z resonance are negative, and the sum of the three- and four-parton final-state contributions is much larger in magnitude than the contributions from the $b\bar{b}$ final state. This is a consequence of the fact that $m_b/m_Z \ll 1$ and that the universal $b\bar{b}$ final-state QCD corrections vanish for $m_b \to 0$ due to chiral invariance. Although the order α_s^2 QCD correction to the leading-order b-quark asymmetry is quite small in magnitude, it is nevertheless significant. The complete order α_s^2 correction, that is, the sum of the flavor non-singlet, flavor singlet, and triangle contributions, amounts to 37% of the order α_s correction. The NNLO correction changes (reduces, to be more specific) the tree-level asymmetry at the percent level, as shown in section 5.3. Thus the α_s^2 QCD correction must be taken into account in the SM prediction in order to match the precision with which this asymmetry was determined years ago from experimental data taken at LEP1. As a consistency check and also as an interesting exercise by itself, we computed the α_s^2 correction to the b-quark forward-backward asymmetry also for a sequence of decreasing values of m_b, in order to approach the massless results given in in [89, 90]. As shown in section 5.3.2, we are able to reproduce the values of [89, 90] within 1σ uncertainty.

Of experimental interest at the Z peak is the b-quark forward-backward asymmetry with respect to the oriented thrust direction. We have described in section 5.3.4 a procedure, proposed in [211, 212], how a pseudo-observable, the bare asymmetry $A_{\rm FB}^{0,b}$ was extracted by correcting the experimentally measured asymmetry $A_{\rm FB,exp}^{b,T}$ for QCD effects, and for photonic corrections and corrections due to an energy shift. Yet we also emphasized that the procedures how the various measurements made at LEP1 were corrected for QCD effects are not universal and more complicated than Eq. (5.28). Nevertheless, in these correction procedures for the thrust-axis $A_{\rm FB,exp}^{b,T}$ the order α_s^2 QCD correction obtained for $m_b = 0$ in [90] were used. This led to the well-known result [53–56] that among the set of precision observables measured at the Z peak, the value of the pseudo-observable $A_{\rm FB}^{0,b}$ shows the largest deviation, about 2.5σ, from the value obtained by a combined SM fit to all precision observables available. We have repeated the procedure to correct for QCD effects as described by the schematic formula Eq. (5.28), using our massive order α_s^2 result. Then we find that this increases slightly the value of the bare asymmetry $A_{\rm FB}^{0,b}$. As a consequence, the tension decreases from 2.5σ to 2.2σ. Furthermore we have computed the b-quark $A_{\rm FB}$ also for a cut on $\cos\theta_T$. Cuts on $\cos\theta_T$ were applied also by the experiments at LEP1. Using $|\cos\theta_T| \leq 0.8$ we find that the resulting QCD corrections increase the value of the bare asymmetry even further, which decreases the tension to about 2.0σ. This indicates that there is no real need to invoke new physics effects in order to account for the difference between the measured average value of the b-quark asymmetry and the SM prediction. However, we emphasized in section 5.3.4 that our schematic analysis of the phenomenological consequences of our new result on the b-quark asymmetry is no substitute for a detailed re-analysis of the experimental data. This is beyond the scope of this thesis. Such an analysis can only be done in collaboration with experimentalists that have access to LEP1 uncorrected and to Monte Carlo corrected data.

The research presented in this thesis can be applied and extended in a number of ways. An immediate application is to compute b-jet cross sections and distributions at NNLO QCD. An immediate extension would be to consider heavy quark pair production by longitudinally polarized electron and/or positron beams. This amounts to replacing the tree-level lepton tensors $L_{XY}^{\mu\nu}$ in Eq. (4.5) by the corresponding tensors where the polarization degrees of the

beams are incorporated. The order α_s and α_s^2 QCD corrections (more precisely, the universal ones) to the leading-order t-quark and b-quark forward-backward asymmetries computed in chapter 5 can be applied as multiplicative factors also to the respective LO asymmetries for polarized electron and/or positron beams. Of interest for future e^+e^- colliders would be to apply our set-up to the production of polarized $t\bar{t}$ pairs. The infrared singularity structure of the respective (squared) matrix elements does not change compared to the unpolarized case. Therefore, the (integrated) antenna functions can be used also for polarized $t\bar{t}$ production. If this extension to polarized $t\bar{t}$ is available, polarized t and $\bar{t}$ decay can be incorporated via the narrow width approximation. This would allow for a number of studies, including studies of top-spin effects, at the level of the $t\bar{t}$ decay products. Another follow-up of our work is to combine it with the known NLO electroweak corrections [66–69]. Finally, the antenna subtraction set-up developed in chapter 3 can be applied also to the computation of the NNLO QCD corrections to other reactions where a massive quark-antiquark pair is produced by an uncolored initial state, for example, to the decay of the 125 GeV Higgs boson to b-quark pairs.

Appendix A

Some formulas and conventions

In this appendix we list some formulas and conventions that are used in this thesis.

The n-particle phase-space measure $d\Phi_n$ in $D = 4 - 2\epsilon$ space-time dimensions is given by

$$d\Phi_n^D(k_j; q) = (\mu^{4-D})^{n-1} \prod_{i=1}^{n} \frac{d^{D-1}k_i}{(2\pi)^{D-1} 2k_i^0} (2\pi)^D \, \delta^{(D)}\left(q - \sum_{i=1}^{n} k_i\right) , \tag{A.1}$$

where $q = p_1 + p_2$ denotes the total 4-momentum of the initial state, k_i $(i = 1, \ldots, n)$ are the 4-momenta of the particles in the final state, and μ is the mass scale associated with dimensional regularization.

The quark and gluon fields transform under the fundamental and adjoint representation, respectively, of the color gauge group $\mathrm{SU}(N_c)$, where $N_c = 3$ is the number of colors. The generators of the fundamental representation are denoted by T_{ij}^a, $a = 1, \ldots, N_c^2 - 1$. Our normalization convention is

$$\mathrm{tr}(T^a T^b) = T_R \delta^{ab} , \quad T_R = \frac{1}{2} . \tag{A.2}$$

The Casimir invariants of the fundamental and adjoint representation are

$$C_F = \frac{N_c^2 - 1}{2N_C} , \quad C_A = N_c . \tag{A.3}$$

A.1 Electroweak coupling factors

In this section we list the electroweak coupling factors $k^{XY}_{F,X'Y'}$ defined in Eq. (4.5) that are taken out of the leptonic and hadronic tensors $L^{\mu\nu}_{XY}$ and $H^{(i,j),F,X',Y'}_{\mu\nu}$ which make up the differential cross sections $d\sigma^{(i,j)}$. We recall that the two superscripts X, Y (subscripts X', Y') in $k^{XY}_{F,X'Y'}$ refer to the type of electoweak current that couple to the electron (quark) in the lepton tensor (hadron tensor). The label F refers to the case where the two electroweak vertices in a hadron tensor are associated both with the heavy quark ($F = QQ$), both with a light quark ($F = qq$), and with a light and a heavy quark ($F = qQ$), respectively.

The electroweak couplings of f = electron, quark are

$$v_f^Z = \frac{1}{2s_W c_W}\left(I_{3f} - 2s_W^2 Q_f\right), \quad a_f^Z = -\frac{1}{2s_W c_W} I_{3f}, \quad v_f^\gamma = Q_f, \quad a_f^\gamma = 0, \tag{A.4}$$

where I_{3f} is the quantum number of f with respect to the third component of the weak isospin operator, Q_f is the electric charge of f in units of the positron charge $e > 0$, and s_W, c_W are the sine and cosine of the weak mixing angle θ_W. Moreover, we recall that $D_Z = s - m_Z^2 + \mathrm{i} m_Z \Gamma_Z$. Then we have for $F = QQ$:

$$\begin{aligned}
k^{\mathrm{VV}}_{Q,\mathrm{VV}} &= \left(v_e^Z\right)^2 \left(v_Q^Z\right)^2 + \frac{2\mathrm{Re}\left[D_Z\right] v_e^Z v_Q^Z v_e^\gamma v_Q^\gamma}{s} + \frac{\left|D_Z\right|^2 \left(v_e^\gamma\right)^2 \left(v_Q^\gamma\right)^2}{s^2}, \\
k^{\mathrm{AA}}_{Q,\mathrm{AA}} &= \left(a_e^Z\right)^2 \left(a_Q^Z\right)^2, \\
k^{\mathrm{VV}}_{Q,\mathrm{AA}} &= \left(a_Q^Z\right)^2 \left(v_e^Z\right)^2, \\
k^{\mathrm{AA}}_{Q,\mathrm{VV}} &= \left(a_e^Z\right)^2 \left(v_Q^Z\right)^2, \\
k^{\mathrm{VA}}_{Q,\mathrm{VA}} &= k^{\mathrm{AV}}_{Q,\mathrm{AV}} = a_e^Z a_Q^Z v_e^Z v_Q^Z + \frac{\mathrm{Re}\left[D_Z\right] a_e^Z a_Q^Z v_e^\gamma v_Q^\gamma}{s}, \\
k^{\mathrm{VA}}_{Q,\mathrm{AV}} &= k^{\mathrm{AV}}_{Q,\mathrm{VA}} = a_e^Z a_Q^Z v_e^Z v_Q^Z .
\end{aligned}$$

For $F = qq$ we have

$$\begin{aligned}
k^{\mathrm{VV}}_{q,\mathrm{VV}} &= \left(v_e^Z\right)^2 \left(v_q^Z\right)^2 + \frac{2\mathrm{Re}\left[D_Z\right] v_e^Z v_q^Z v_e^\gamma v_q^\gamma}{s} + \frac{\left|D_Z\right|^2 \left(v_e^\gamma\right)^2 \left(v_q^\gamma\right)^2}{s^2}, \\
k^{\mathrm{AA}}_{q,\mathrm{AA}} &= \left(a_e^Z\right)^2 \left(a_q^Z\right)^2,
\end{aligned}$$

$$
\begin{aligned}
k^{\mathrm{VV}}_{q,\mathrm{AA}} &= \left(a_q^Z\right)^2 \left(v_e^Z\right)^2 , \\
k^{\mathrm{AA}}_{q,\mathrm{VV}} &= \left(a_e^Z\right)^2 \left(v_q^Z\right)^2 , \\
k^{\mathrm{VA}}_{q,\mathrm{VA}} &= k^{\mathrm{AV}}_{q,\mathrm{AV}} = a_e^Z a_q^Z v_e^Z v_q^Z + \frac{\mathrm{Re}\left[D_Z\right] a_e^Z a_q^Z v_e^\gamma v_q^\gamma}{s}, \\
k^{\mathrm{VA}}_{q,\mathrm{AV}} &= k^{\mathrm{AV}}_{q,\mathrm{VA}} = a_e^Z a_q^Z v_e^Z v_q^Z .
\end{aligned}
$$

For $F = qQ$ the factors are

$$
\begin{aligned}
k^{\mathrm{VV}}_{\mathrm{qQ,VV}} &= \left(v_e^Z\right)^2 v_q^Z v_Q^Z + \frac{\mathrm{Re}\left[D_Z\right] v_e^Z v_Q^Z v_e^\gamma v_q^\gamma}{s} + \frac{\mathrm{Re}\left[D_Z\right] v_e^Z v_q^Z v_e^\gamma v_Q^\gamma}{s} + \frac{\left|D_Z\right|^2 \left(v_e^\gamma\right)^2 v_q^\gamma v_Q^\gamma}{s^2}, \\
k^{\mathrm{AA}}_{\mathrm{qQ,AA}} &= \left(a_e^Z\right)^2 a_q^Z a_Q^Z, \\
k^{\mathrm{VV}}_{\mathrm{qQ,AA}} &= a_q^Z a_Q^Z \left(v_e^Z\right)^2 , \\
k^{\mathrm{AA}}_{\mathrm{qQ,VV}} &= \left(a_e^Z\right)^2 v_q^Z v_Q^Z, \\
k^{\mathrm{VA}}_{\mathrm{qQ,VA}} &= a_e^Z a_Q^Z v_e^Z v_q^Z + \frac{\mathrm{Re}\left[D_Z\right] a_e^Z a_Q^Z v_e^\gamma v_q^\gamma}{s}, \\
k^{\mathrm{VA}}_{\mathrm{qQ,AV}} &= a_e^Z a_q^Z v_e^Z v_Q^Z, \\
k^{\mathrm{AV}}_{\mathrm{qQ,AV}} &= a_e^Z a_q^Z v_e^Z v_Q^Z + \frac{\mathrm{Re}\left[D_Z\right] a_e^Z a_q^Z v_e^\gamma v_Q^\gamma}{s}, \\
k^{\mathrm{AV}}_{\mathrm{qQ,VA}} &= a_e^Z a_Q^Z v_e^Z v_q^Z .
\end{aligned}
$$

A.2 Renormalization constants

We consider QCD with n_f massless and one massive quark flavor. As stated in chapter 3 we use a hybrid renormalization scheme. In the following we list the renormalization constants that are used to compute the 3-parton $Q\bar{Q}g$ amplitude at 1-loop and the 2-parton $Q\bar{Q}$ amplitude at 1- and 2-loop order. The 1-loop and 2-loop term in the perturbative expansion of a renormalization constant Z is defined in the following by

$$
Z = 1 + Z^{(1)} + Z^{(2)} + \mathcal{O}(\alpha_s^3) . \tag{A.5}
$$

The QCD coupling α_s is defined in the $\overline{\rm MS}$ renormalization scheme. In the following we denote $g_{\overline{\rm MS}} = \sqrt{4\pi\alpha_s}$. The relation between $g_{\overline{\rm MS}}$ and the bare QCD coupling $g_0 = \sqrt{4\pi\alpha_{s,0}}$ is

$$g_0 = Z_{g,\overline{\rm MS}}\, g_{\overline{\rm MS}}\, \mu^\epsilon\,, \tag{A.6}$$

where $\epsilon = (4-D)/2$. (We keep the renormalized coupling dimensionless also in $D \neq 4$ dimensions. For ease of notation we use the same symbol μ for the mass scale of dimensional regularization and the renormalization scale.) We need the relation (A.6), i.e., the renormalization constant $Z_{g,\overline{\rm MS}}$ to 1-loop. We have

$$Z^{(1)}_{g,\overline{\rm MS}} = -\frac{\alpha_s}{2\pi}(4\pi)^\epsilon\Gamma(1+\epsilon)\frac{1}{4\epsilon}\left(\frac{11}{3}C_A - \frac{4}{3}T_R(n_f+1)\right)\,. \tag{A.7}$$

We define the gluon and the quark fields and the mass of the heavy quark in the on-shell (OS) scheme:

$$G^{a,\mu}_0(x) = \sqrt{Z_{3,OS}}\; G^{a,\mu}_{OS}(x)\,, \quad Q_0(x) = \sqrt{Z_{2,OS}}\; Q_{OS}(x)\,, \quad m_{Q,0} = Z_{m,OS}\; m_Q\,, \tag{A.8}$$

where $m_Q \equiv m_{Q,OS}$. We need $Z_{3,OS}$ to 1-loop. For n_f massless and one massive quark with on-shell mass m_Q the 1-loop term is given in the Feynman gauge by

$$Z^{(1)}_{3,OS} = -\frac{\alpha_s}{2\pi}(4\pi)^\epsilon\Gamma(1+\epsilon)\left(\frac{\mu^2}{m_Q^2}\right)^\epsilon\frac{2}{3\epsilon}T_R\,. \tag{A.9}$$

The relation between the bare and renormalized heavy quark mass is required to 1-loop while the wave function renormalization constant $Z_{2,OS}$ is needed to 2-loop order (for computing the renormalized 2-loop $Q\bar{Q}$ amplitude). The 1-loop terms are

$$\begin{aligned} Z^{(1)}_{m,OS} &= -\frac{\alpha_s}{2\pi}(4\pi)^\epsilon\Gamma(1+\epsilon)\frac{1}{2\epsilon}\left(\frac{\mu^2}{m_Q^2}\right)^\epsilon C_F\frac{(3-2\epsilon)}{(1-2\epsilon)}\,,\\ Z^{(1)}_{2,OS} &= -\frac{\alpha_s}{2\pi}(4\pi)^\epsilon\Gamma(1+\epsilon)\frac{1}{2\epsilon}\left(\frac{\mu^2}{m_Q^2}\right)^\epsilon C_F\frac{(3-2\epsilon)}{(1-2\epsilon)}\,, \end{aligned} \tag{A.10}$$

The quark wave function renormalization constant in the on-shell scheme was computed at 2 loops in [214, 215] and given in terms of the $\overline{\text{MS}}$ coupling α_s for instance in [176]. For the sake of brevity we do not list $Z_{2,OS}^{(2)}$ here.

Finally, we need the renormalization constant $Z_{1,F}$ for the QQg vertex. It is obtained from the Slavnov-Taylor identity

$$Z_{1,F} = Z_{g,\overline{\text{MS}}}\ Z_{2,OS}\ \sqrt{Z_{3,OS}}\,. \tag{A.11}$$

We require this renormalization constant to 1-loop. Expanding (A.11) to first order in α_s and using the respective 1-loop terms listed above we get

$$\begin{aligned} Z_{1,F}^{(1)} = &-\frac{\alpha_s}{2\pi}(4\pi)^\epsilon\Gamma(1+\epsilon)\frac{1}{2\epsilon}\left(\frac{11}{6}C_A + \left(\frac{\mu^2}{m_Q^2}\right)^\epsilon C_F\frac{(3-2\epsilon)}{(1-2\epsilon)}\right. \\ &\left.-\frac{2}{3}T_R n_f + \frac{2}{3}T_R\left[\left(\frac{\mu^2}{m_Q^2}\right)^\epsilon - 1\right]\right)\,. \end{aligned} \tag{A.12}$$

A.3 Matching relation for α_s

As is well-known, the definition of of the QCD coupling in the (modified) minimal subtraction scheme provides a gauge- and vertex independent definition of this basic parameter. However, decoupling of heavy quarks is not manifest in this scheme. In the energy region $\mu^2 \ll m_Q^2$ the contribution of the heavy quark Q to an observable blows up with some power of $\ln(m_Q^2/\mu^2)$, depending on the order of perturbation theory. This behavior is related to the fact that there is also no decoupling of a heavy quark from the β function in this scheme that governs the scale dependence of α_s. In order to establish decoupling, one has to sum these logarithms. This is done by matching the full theory – i.e., without loss of generality, QCD with n_f light and one heavy quark – and the effective theory with n_f light quark flavors below the heavy quark threshold. The resulting matching relation to order α_s^3 for the $\overline{\text{MS}}$ QCD couplings in the full and effective light-flavor QCD is [190]

$$\alpha_s^{(n_f)}(\mu) = \alpha_s^{(n_f+1)}(\mu)\left[1 + \frac{x}{6}\frac{\alpha_s^{(n_f+1)}}{\pi} + \left(\frac{x^2}{36} + \frac{11x}{24} + \frac{11}{72}\right)\left(\frac{\alpha_s^{(n_f+1)}}{\pi}\right)^2\right]\,, \tag{A.13}$$

where

$$x \equiv \ln(\bar{m}_Q^2/\mu^2)\,, \tag{A.14}$$

and $\alpha_s^{(n_f+1)}$ and $\alpha_s^{(n_f)}$ are the QCD couplings in n_f+1 flavor and n_f flavor QCD, respectively. The matching relation (A.13) is given for $N_c = 3$. There are also matching relations for the running light quark masses in the (modified) minimal subtraction scheme [216], but we do not need them in this thesis. The mass $\bar{m}_Q$ in Eq. (A.14) is not the on-shell mass of Q but its mass defined in the (modified) minimal subtraction scheme.

We need the relation (A.13) for computing α_s in QCD with 6 quarks (i.e., above the top-quark threshold) from the value $\alpha_s^{(n_f=5)}(\mu = m_Z) = 0.118$ (see Eq. (4.2)) in 5-flavor QCD. With this starting values we perform a renormalization group (RG) evolution (using the first three coefficients of the β function with $n_f = 5$, given for instance in [186]) of $\alpha_s^{(n_f=5)}(\mu)$ up to some high scale μ^*. Then we use (A.13) to compute $\alpha_s^{(n_f=6)}(\mu^*)$ from $\alpha_s^{(n_f=5)}(\mu^*)$. It is convenient, but not necessary, to choose $\mu^* = \bar{m}_Q$. The value of $\alpha_s^{(n_f=6)}(\mu^*)$ is then used as a starting value for computing $\alpha_s^{(n_f=6)}(\mu)$ at other scales μ by RG evolution using the β function with $n_f = 6$ flavors.

Appendix B

Phase-space momentum mappings

In this appendix we describe the four-momentum mappings in the three- and four-particle phase-spaces that are used in the construction of the antenna subtraction terms of section 3.2 and 3.3. The momenta are associated with massless and massive quarks and with massless gluons. The momentum mappings required in our case are related either to a single or double unresolved parton configuration in the final state. These mappings must obey four-momentum conservation, must keep the mapped momenta on their respective mass shell, and the mapped momenta must converge to the correct momentum configurations in the the soft and collinear limits. We follow the mapping procedures of [170], which apply to the case where all partons are massless, respectively of [172] where the massless case was extended to configurations involving massive partons. However, the formulas published in [172] have the deficit that the mapped four-momenta do not obey the correct mass-shell conditions away from the soft and collinear limits. The correct analytic formulas of Abelof and Gehrmann-De Ridder that keep the mapped momenta on-shell in the massive case have not been published so far [184].

Therefore we have constructed an alternative numerical mapping method which is sufficient for computing the observables discussed in this thesis. This method is described in the following.

B.1 Three parton final states

We consider the final state $Q(k_1)\bar{Q}(k_2)g(k_3)$. The NLO subtraction term $d\sigma^S_{Q\bar{Q}g}$ of eq. (3.16) and the NNLO subtraction terms $d\sigma^{T,b,Q\bar{Q}g}_{\rm NNLO}$ and $d\sigma^{T,c,Q\bar{Q}g}_{\rm NNLO}$ of eq. (3.46) and (3.48) depend on mapped momenta obtained from a $3 \to 2$ mapping $k_1, k_3, k_2 \to \widetilde{k_{13}}, \widetilde{k_{32}}$. Let's consider the mapping $k_1, k_3, k_2 \to p_I \equiv \widetilde{p_{13}}, p_J \equiv \widetilde{p_{32}}$ defined in [170] and in appendix B1.1 of [172]:

$$\begin{aligned} p_I &= x k_1^\mu + r k_3^\mu + z k_2^\mu \,, \\ p_J &= (1-x) k_1^\mu + (1-r) k_3^\mu + (1-z) k_2^\mu \,, \end{aligned} \tag{B.1}$$

where the parameters x, r, z are given by

$$\begin{aligned} x &= \frac{1}{2(s_{ij}+s_{ik})} \left[(1+\rho) s_{ijk} - 2 r s_{jk}\right] \,, \\ z &= \frac{1}{2(s_{jk}+s_{ik})} \left[(1-\rho) s_{ijk} - 2 r s_{ij}\right] \,, \\ \rho^2 &= 1 + \frac{4 r (1-r) s_{ij} s_{jk}}{s_{ijk} s_{ik}} \,, \\ r &= \frac{s_{jk}}{s_{ij}+s_{jk}} \,, \end{aligned} \tag{B.2}$$

and $s_{ik} = 2 k_i \cdot k_k$, $s_{ijk} = s_{ij} + s_{ik} + s_{jk}$. The mapping (B.1) satisfies four-momentum conservation, $p_I + p_J = k_1 + k_3 + k_2$, and the mapped momenta behave correctly when the gluon becomes soft: $p_I \to k_1, p_J \to k_2$ if $k_3 \to 0$. If all three partons were massless, the mapped momenta remain massless, $p_I^2 = p_J^2 = 0$ [170]. However, if one or two massive (anti)quarks Q are involved, as in our case, the mapped momenta are no longer on their mass shell, except in the limit $k_3 \to 0$, as can be checked straightforwardly. Thus modified formulas must be used for the parameters x, r, z in order to get $p_I^2, p_J^2 = m_Q^2$ [184]. We emphasize that on-shellness of the mapped momenta is crucial for deriving the correct integrated antenna subtraction terms from the unintegrated ones.

Here we describe, as an alternative to the analytic formulas of Abelof and Gehrmann-De Ridder a numerical method to obtain on-shell mapped momenta $\widetilde{k_{13}}, \widetilde{k_{32}}$. We use the mapping (B.1) with the parameters x, r, z given in [172] for an intermediate step. Four-momentum

conservation in the e^-e^+ c.m. frame reads:

$$\sqrt{s} = p_{0I} + p_{0J}\,, \quad 0 = \mathbf{p}_I + \mathbf{p}_J\,. \tag{B.3}$$

The second equation is the crucial one. It allows to rescale the 3-momenta by a factor ξ such that the 4-momenta p_I^μ, p_J^μ are transformed into on-shell 4-momenta k_I, k_J with mass $m_I = m_J = m_Q$ without destroying 4-momentum conservation.

$$\mathbf{k}_i = \xi \mathbf{p}_i\,, \quad k_{0i} = \sqrt{m_i^2 + \xi^2(p_{0i}^2 - p_i^2)}\,, \qquad i = I, J\,, \tag{B.4}$$

where ξ is the solution of the equation

$$\sqrt{s} = \sqrt{m_I^2 + \xi^2(p_{0I}^2 - p_I^2)} + \sqrt{m_J^2 + \xi^2(p_{0J}^2 - p_J^2)}\,. \tag{B.5}$$

Eq. (B.5) can be solved numerically by iteration using the Newton-Raphson method. One can start the iterative solution of (B.5) with the value $\xi = \sqrt{(1 - (2m_Q/\sqrt{s})^2)}$. We found that a few iterations ($n \leq 6$) are enough to get an accuracy of $10^{-14}\sqrt{s}/[\mathrm{GeV}]$. Or method based on eq. (B.4) and (B.5) is analogous to the procedure used in the phase-space generator `RAMBO` [217] for constructing massive four-momenta from massless ones.

B.2 Four parton final states

We consider the final states $Q(k_1)\bar{Q}(k_2)a(k_3)b(k_4)$, where $ab = q\bar{q}, gg$. For the a- and b-type subtraction terms of section 3.3.1 we need $3 \to 2$ and $4 \to 2$ momentum mappings associated with single and double unresolved configurations.

$3 \to 2$ mappings for a-type antenna subtraction terms:
For evaluating the a-type subtraction term $d\sigma_{\mathrm{NNLO}}^{S,a,Q\bar{Q}q\bar{q}}$ of (3.27) one needs mapped momenta obtained by the two $3 \to 2$ mappings

$$k_1, k_3, k_4 \to \widetilde{k_{13}}, \widetilde{k_{34}}\,, \qquad k_3, k_4, k_2 \to \widetilde{k_{34}}, \widetilde{k_{42}}\,, \tag{B.6}$$

where the massless (anti)quark with momentum k_3, respectively k_4 becomes unresolved. For definiteness we describe for the mapping on the left side of (B.6) how one can obtain, with a procedure analogous to that of section B.1, mapped momenta that satisfy four-momentum conservation and the on-shell conditions $\widetilde{k_{13}^2} = m_Q^2$, $\widetilde{k_{34}^2} = 0$. We use again in an intermediate step the $3 \to 2$ mapping

$$\begin{aligned} p_I &= x k_1^\mu + r k_3^\mu + z k_4^\mu \,, \\ p_J &= (1-x) k_1^\mu + (1-r) k_3^\mu + (1-z) k_4^\mu \,, \end{aligned} \tag{B.7}$$

where the parameters x, r, z are given in (B.2). We have $p_I^2 \neq m_Q^2$ and $p_J^2 \neq 0$ for general configurations k_j. In the case of four-parton final states, momentum conservation in the e^-e^+ c.m. frame reads in terms of the mapped momenta p_I, p_J:

$$Q_2^\mu = p_I^\mu + p_J^\mu \,, \tag{B.8}$$

where $Q_2^\mu = (\sqrt{s} - k_{02}, -\mathbf{k}_2)$. Now we boost to the rest frame IS' of Q_2^μ with the boost vector $\boldsymbol{\beta}_2 = -\mathbf{k_2}/Q_{02}$. Four-momentum conservation in IS' reads

$$Q'_{02} = p'_{0I} + p'_{0J} \,, \qquad 0 = \mathbf{p'}_I + \mathbf{p'}_J \,. \tag{B.9}$$

As above, the second equation allows to rescale the 3-momenta by a factor ξ such that the 4-momenta $p_I'^\mu, p_J'^\mu$ are transformed into on-shell 4-momenta $k_I'^\mu, k_J'^\mu$ with mass $m_I = m_Q$ and $m_J = 0$, respectively, without destroying 4-momentum conservation.

$$\mathbf{k'}_i = \xi \mathbf{p'}_i \,, \quad k'_{0i} = \sqrt{m_i^2 + \xi^2 (p'^2_{0i} - p'^2_i)} \,, \qquad i = I, J \,, \tag{B.10}$$

where ξ is the solution of the equation

$$Q'_{02} = \sqrt{m_I^2 + \xi^2 (p'^2_{0I} - p'^2_I)} + \sqrt{m_J^2 + \xi^2 (p'^2_{0J} - p'^2_J)} \,. \tag{B.11}$$

Again, eq. (B.11) can be solved numerically by iteration using the Newton-Raphson method.

In this case it is advantageous to start the iteration with the value $\xi = \sqrt{(1-(m_Q/Q'_{02})^2)}$. A few iterations ($n \leq 6$) are enough to get an accuracy of $10^{-14}Q'_{02}/[\mathrm{GeV}]$.
Finally we boost k'^{μ}_I, k'^{μ}_J back to the e^-e^+ c.m. frame IS with the boost vector $-\boldsymbol{\beta}_2$ and we obtain $k_I \equiv \widetilde{k_{13}}, k_J \equiv \widetilde{k_{34}}$. The on-shell 4-momenta k^{μ}_I, k^{μ}_J satisfy 4-momentum conservation in IS and behave correctly in all singular limits.

For the second set of momenta in (B.6) mapped on-shell momenta are constructed in completely analogous fashion with the 'spectator' k_2 replaced by k_1. The above procedure applies also to the various $3 \to 2$ mappings that are required for the a-type subtraction term $d\sigma^{S,a,Q\bar{Q}gg}_{\mathrm{NNLO}}$ of (3.35).

Abelof and Gehrmann-De Ridder have derived analytic formulas for the mapped on-shell 4-momenta k^{μ}_I, k^{μ}_J, but have not published them so far [184].

$4 \to 2$ mappings for b-type antenna subtraction terms:
The b-type antenna subtraction term $d\sigma^{S,b,2,Q\bar{Q}q\bar{q}}_{\mathrm{NNLO}}$ of (3.25) is evaluated with mapped momenta that are obtained by a $4 \to 2$ mapping

$$k_1, k_3, k_4, k_2 \to k_I \equiv \widetilde{k_{134}},\ k_J \equiv \widetilde{k_{342}}\,. \tag{B.12}$$

As an intermediate step we use the $4 \to 2$ mapping $k_1, k_3, k_4, k_2 \to p_I, p_J$, where

$$\begin{aligned} p_I &= xk^{\mu}_1 + r_1 k^{\mu}_3 + r_2 k^{\mu}_4 + z k^{\mu}_2\,, \\ p_J &= (1-x)k^{\mu}_1 + (1-r_1)k^{\mu}_3 + (1-r_2)k^{\mu}_4 + (1-z)k^{\mu}_2\,, \end{aligned} \tag{B.13}$$

and the parameters x, r_1, r_2, z are given[1] in appendix B.2.1 of [172]. For general configurations k_j the mapped momenta are not on the m_Q mass shell, $p_I^2, p_J^2 \neq m_Q^2$. Four-momentum conservation in the e^-e^+ c.m. frame reads

$$\sqrt{s} = p_{0I} + p_{0J}\,, \quad 0 = \mathbf{p}_I + \mathbf{p}_J\,. \tag{B.14}$$

[1]There are a few typos in the $4 \to 2$ mapping formulas in Appendix B.1.1 of [172] as compared to the formulas of [170]. The parameter r_1 should read $r_1 = (s_{jk}+s_{jl})/(s_{ij}+s_{jk}+s_{jl})$. The term proportional to $(r_1 - r_2)$ in the definition of the parameter z should read $-(r_1-r_2)(s_{ij}s_{kl} - s_{ik}s_{jl})/s_{il}$.

Because of the second equation the mapped momenta can be transformed without boost into on-shell four-momenta k_I, k_J with mass $m_I = m_J = m_Q$. We have, analogous to the equations above,

$$\mathbf{k}_i = \xi \mathbf{p}_i\,, \quad k_{0i} = \sqrt{m_i^2 + \xi^2(p_{0i}^2 - p_i^2)}\,, \qquad i = I, J\,, \tag{B.15}$$

where ξ is the solution of the equation

$$\sqrt{s} = \sqrt{m_I^2 + \xi^2(p_{0I}^2 - p_I^2)} + \sqrt{m_J^2 + \xi^2(p_{0J}^2 - p_J^2)}\,. \tag{B.16}$$

As in the case of equation (B.5) the iterative solution of (B.16) can be started with the value $\xi = \sqrt{(1 - (2m_Q/\sqrt{s})^2)}$. A few iterations ($n \leq 6$) are enough to get an accuracy of $10^{-14}\sqrt{s}/[\mathrm{GeV}]$. The mapped momenta k_I, k_J converge to the correct momenta in the double unresolved limits. The mapped momenta required for $d\sigma_{\mathrm{NNLO}}^{S,b,2,Q\bar{Q}gg}$ of eq. (3.36) are obtained in the same fashion. Abelof and Gehrmann-De Ridder have derived analytic formulas for the on-shell massive 4-momenta k_I^μ, k_J^μ [184].

Finally, for the antenna subtraction term $d\sigma_{\mathrm{NNLO}}^{S,b,1,Q\bar{Q}q\bar{q}}$ of (3.28) two iterated $3 \to 2$ momentum mappings are needed:

$$1_Q, 3_q, 4_{\bar{q}} \text{ with spectator } 2_{\bar{Q}} \xrightarrow{\mathrm{I}} \widetilde{(13)}_Q, \widetilde{(34)}_g,\ 2_{\bar{Q}} \xrightarrow{\mathrm{II}} (\widetilde{\widetilde{(13)}\widetilde{(34)}})_Q, (\widetilde{\widetilde{(34)}2})_{\bar{Q}} \tag{B.17}$$

and

$$2_{\bar{Q}}, 4_{\bar{q}}, 3_q \text{ with spectator } 1_Q \xrightarrow{\mathrm{I}} 1_Q,\ \widetilde{(34)}_g, \widetilde{(42)}_{\bar{Q}} \xrightarrow{\mathrm{II}} (\widetilde{1\widetilde{(34)}})_Q, (\widetilde{\widetilde{(34)}\widetilde{(42)}})_{\bar{Q}}\,. \tag{B.18}$$

Let us consider (B.17). The $3 \to 2$ mapping I is done as described below eq. (B.6): boost to the rest frame of Q_2^μ, rescale, and then boost back to the e^-e^+ c.m. frame. The rescaling involved in the subsequent mapping II is done directly in the e^-e^+ c.m. frame. This yields the two mapped on-shell momenta with mass m_Q on the right-hand side of (B.17). The iterated $3 \to 2$ mappings (B.18) and those involved in constructing the antenna subtraction term $d\sigma_{\mathrm{NNLO}}^{S,b,1,Q\bar{Q}gg}$ of (3.37) are performed in analogous fashion.

Appendix C

Angular correlations and averaging

As discussed in sections 2.4 and 3.3.1, our antenna subtraction terms for the squared S-matrix elements associated with the $Q\bar{Q}q\bar{q}$ and $Q\bar{Q}gg$ final states are not completely local. The squared S-matrix elements contain spin correlations (or angular correlations) that arise from the 'sub-processes' where a virtual gluon splits into a pair of massless quarks or gluons, $g^* \to q\bar{q}, gg$. In the antenna subtraction terms discussed in section 3.3.1 these angular correlations are not present by construction. Thus the point-wise cancellation of IR singularities fails in the single unresolved limit when the pair of massless quarks or gluons from $g^* \to q\bar{q}, gg$ becomes collinear.

This issue is resolved, as outlined in section 3.3.1, by evaluating the unsubtracted squared matrix elements for each set of final-state momenta also for the momentum configuration where the momenta of the two massless partons ($q, \bar{q}$ or g, g) are rotated by an angle $\phi = \pi/2$ around the collinear axis with respect to the original configuration and then take the average. In this appendix we discuss how to construct these rotated 4-momenta for the massless partons.

C.1 Light-cone basis and decomposition of lightlike momenta

First, we introduce a set of 4-vectors $\{n_+^\mu, n_-^\mu, n_\perp^\mu\}$ in 4-dimensional Minkowski space which is called the light-cone basis. Here n_-^μ is a lightlike vector which is dual to n_+^μ, i.e., $n_-^\mu \equiv n_{+\mu}$.

The 4-vector $n_\perp^\mu$ is by definition transverse to $n_\pm^\mu$. The light-cone basis satisfies

$$\begin{aligned} n_+ \cdot n_+ &= 0\,, \\ n_- \cdot n_- &= 0 \\ n_+ \cdot n_- &= n_- \cdot n_+ = 1\,, \\ n_\perp \cdot n_\pm &= 0\,, \\ n_\perp \cdot n_\perp &= -1\,, \end{aligned} \tag{C.1}$$

where it is understood that the above normalization equation for $n_\perp^\mu$ involves only one degree of freedom of the two transverse components.

Now we decompose a given pair of lightlike 4-momenta, k_i^μ and k_j^μ, with respect to the light-cone basis, with the additional requirement that the transverse momentum components are defined to be orthogonal to the 4-vector $k_i^\mu + k_j^\mu$. We define

$$k_i^\mu + k_j^\mu \equiv K^\mu = (K_0, |\mathbf{K}|\mathbf{e}) \tag{C.2}$$

where $\mathbf{e} = \mathbf{K}/|\mathbf{K}|$. Eq. (C.2) suggests to construct the following two lightlike 4-vectors which are dual to each other:

$$\begin{aligned} n_+{}^\mu &= \frac{1}{\sqrt{2}}\,(1, \mathbf{e})\ , \\ n_-{}^\mu &= \frac{1}{\sqrt{2}}\,(1, -\mathbf{e})\ . \end{aligned} \tag{C.3}$$

Now we decompose K^μ and k_a^μ $(a = i, j)$ with respect to n_+^μ, n_-^μ, and $n_\perp^\mu$, where $n_\perp^\mu$ will be given below:

$$\begin{aligned} K^\mu &= \kappa^+ n_+^\mu + \kappa^- n_-^\mu\,, \\ k_a^\mu &= k_a^+ n_+^\mu + k_a^- n_-^\mu + k_a^\perp n_\perp^\mu\,, \quad a = i, j\,. \end{aligned} \tag{C.4}$$

From Eq. (C.4) it is clear that the parameter

$$k^{\perp} \equiv k_i^{\perp} = -k_j^{\perp}. \tag{C.5}$$

Using Eq. (C.1), it is straightforward to obtain the coefficients

$$\begin{aligned} \kappa^{+} &= n_{-} \cdot K = \frac{1}{\sqrt{2}} \left(K_0 + |\mathbf{K}|\right) , \\ \kappa^{-} &= n_{+} \cdot K = \frac{1}{\sqrt{2}} \left(K_0 - |\mathbf{K}|\right) , \end{aligned} \tag{C.6}$$

and similarly the coefficients

$$\begin{aligned} k_i^{+} &= n_{-} \cdot k_i \, , \\ k_i^{-} &= n_{+} \cdot k_i \, . \end{aligned} \tag{C.7}$$

We need to compute these only for one momentum i or j.

From the Lorentz-square $k_i^2 = 2k_i^{+}\mathbf{k_i^{-}} - |k^{\perp}|^2$, we see that the squared transverse momentum of a lightlike 4-momentum k_i^{μ} is given by

$$|k^{\perp}|^2 = 2k_i^{+}k_i^{-} \, , \tag{C.8}$$

where the seeming sign-ambiguity is related to the freedom of choosing the positive direction of the transverse coordinates.

What is left is to construct the 4-vector ${n_{\perp}}^{\mu}$ explicitly. It is obtained in straightforward fashion from the formulae above. By rewriting the second equation in Eq. (C.4), we get immediately

$${n_{\perp}}^{\mu} = \frac{1}{k^{\perp}} \left(k_a^{\mu} - k_a^{+}{n_{+}}^{\mu} + k_a^{-}{n_{-}}^{\mu}\right) , \quad a = i \text{ or } j \, . \tag{C.9}$$

For the definition of the azimuthal angle ϕ, i.e. the angle that describes a rotation around the spacial direction $\mathbf{e}$ of K^{μ} we choose a coordinate frame. In view of the fact that $|k^{\perp}|$ characterizes how close the divergent collinear region $k_i^{\mu}||k_j^{\mu}$ is approached, we simply choose the plane formed by these two quasi-collinear lightlike 4-momenta as $\phi = 0$ plane, and then

take the transverse part of one of them, say k_j^μ, to be the positive "x direction". (Of course, this choice is technically not possible if the Monte-Carlo code VEGAS that we use for numerical phase-space integration samples the point exactly at the collinear configuration. However, the probability for this to happen is practically zero.)

The unit 3-vector $\mathbf{N}$ which is normal to the plane determined by $\mathbf{e}$ (defined by Eq. (C.2)) and the spatial direction of $n_\perp^\mu$, denoted by $\mathbf{n}_\perp$, is

$$\mathbf{N} = \mathbf{e} \times \mathbf{n}_\perp \,. \tag{C.10}$$

We define $n_{\perp N}^\mu \equiv (0, \vec{\mathbf{N}})$. At this point, we have decomposed all relevant lightlike 4-momenta.

Implementation of the $\pi/2$ rotation:

If we choose the azimuthal $\phi = 0$ plane according to the above convention then we can focus on dealing with only one of the two massless momenta, say k_i. The $\pi/2$ rotation of k_i is achieved by the following "subtraction and addition":

$$\tilde{k}_i^\mu = \left(k_i^\mu - k^\perp n_\perp^{\ \mu}\right) + k^\perp n_{\perp N}^\mu \,, \tag{C.11}$$

where $\tilde{k}_i^\mu$ is the new 4-momentum obtained from a $\pi/2$ rotation of k_i^μ around the collinear axis. We get it via simply removing the transverse part $k^\perp n_\perp^{\ \mu}$ from k_i^μ and add the new $\pi/2$-rotated transverse part $k^\perp \vec{n}_{\perp N}$.

The $\pi/2$ rotated 4-momentum $\tilde{k}_j$ is given by

$$\tilde{k}_j^\mu = K^\mu - \tilde{k}_i^\mu \,. \tag{C.12}$$

A few additional remarks are in order:

- The unsubtracted squared matrix elements associated with the final states $Q\bar{Q}q\bar{q}$ and $Q\bar{Q}gg$ contain terms that are linear in $k^\perp$. (Obviously the 4-momenta of $q, \bar{q}$, respectively of g, g correspond to the above momenta k_i, k_j.) These terms will vanish if one of the following two conditions holds. The first one is obvious, if the azimuthal angle ϕ

as defined above is integrated over the full range $[0, 2\pi]$. The second condition is that the kinematics approaches the collinear limit between k_i and k_j. In this case the form of the spin-dependent gluon splitting function shows that there are only terms bilinear in $k^\perp$ in the unsubtracted squared 4-parton S-matrix elements. This indicates that summing/averaging over two phase-space points with azimuthal angles $\phi = 0$ and $\pi/2$ should be sufficient to remove, after adding the corresponding antenna subtraction terms, all the singular ϕ-dependent terms in the single unresolved collinear limit in the case of $g^* \to q\bar{q}, gg$. We have checked that this is indeed the case, see section 3.3.1.

- In the single collinear limit $g^* \to q\bar{q}, gg$ the associated spin correlation terms in the squared 4-parton matrix elements behave as

$$\sim \mathcal{A}_\mu k_\perp^\mu k_\perp^\nu \mathcal{A}_\nu \sim A + B\cos(2\phi + \alpha)\,, \tag{C.13}$$

where $k_\perp^\mu = (0, \mathbf{k}_\perp, 0)$ with $\mathbf{k}_\perp = (|(\mathbf{k}_\perp|\cos\phi, |\mathbf{k}_\perp|\sin\phi)$ is the transverse part of the k_i^μ (or alternatively of k_j^μ) with respect to the above coordinate frame. Eq. (C.13) can be understood without much computation as follows. Inserting $k_\perp^\mu$ into the left side of (C.13) we get a sum of terms bilinear in $\sin\phi, \cos\phi$ which can be decomposed with respect to the "basis" $\{1, (\cos^2\phi - \sin^2\phi), \sin\phi\cos\phi\}$. The ϕ-independent term is denoted by A in eq. (C.13). Using the trigonometric identity

$$\begin{aligned} \cos(2\phi + \alpha) &= \cos 2\phi \cos\alpha - \sin 2\phi \sin\alpha \\ &= \cos\alpha(\cos^2\phi - \sin^2\phi) - 2\sin\alpha\sin\phi\cos\phi \end{aligned} \tag{C.14}$$

one sees that, using the two parameters B and α, one can parametrize the coefficients of $(\cos^2\phi - \sin^2\phi)$ and $\sin\phi\cos\phi$ which appear on the left side of (C.13). Eq. (C.13) shows that performing a $\pi/2$ rotation and averaging does the job of getting rid of the spin correlation term.

Alternative numerical implementation:

Alternatively, we can obtain the $\pi/2$-rotated massless 4-vectors as follows. Using the

components of the unit 3-vector

$$\mathbf{e} = \big(e_1,\, e_2,\, e_3\big)^T$$

defined in Eq. (C.2) it is straightforward to construct two vectors spanning the plane orthogonal to $\mathbf{e}$:

$$\mathbf{e}_{\perp,1} = \frac{1}{\sqrt{e_2^2+e_3^2}}\big(0,\, -e_3,\, e_2\big)^T,\ \mathbf{e}_{\perp,2} = \frac{1}{\sqrt{e_2^2+e_3^2}}\big(1-e_1^2,\, -e_1e_2,\, -e_1e_3\big)^T,$$

or, if $e_1 = 1$ (which is highly unlikely):

$$\mathbf{e}_{\perp,1} = \big(0,\, 1,\, 0\big)^T,\ \mathbf{e}_{\perp,2} = \big(0,\, 0,\, 1\big)^T.$$

The set $\{\mathbf{e},\, \mathbf{e}_{\perp,1},\, \mathbf{e}_{\perp,2}\}$ forms an orthonormal basis and $\mathbf{k}_\perp \in \mathrm{span}\big(\mathbf{e}_{\perp,1},\, \mathbf{e}_{\perp,2}\big)$.
In terms of this basis, an arbitrary 3-vector $\mathbf{v}$ is written as

$$\mathbf{v} = v_e\mathbf{e} + v_{\perp,1}\mathbf{e}_{\perp,1} + v_{\perp,2}\mathbf{e}_{\perp,2}.$$

The vector $\tilde{\mathbf{v}}$, obtained by rotating $\mathbf{v}$ around $\mathbf{e}$ by an angle of $\pi/2$, is then

$$\tilde{\mathbf{v}} = v_e\mathbf{e} - v_{\perp,2}\mathbf{e}_{\perp,1} + v_{\perp,1}\mathbf{e}_{\perp,2}.$$

Hence

$$\tilde{\mathbf{v}} = \mathbf{v} - \big(v_{\perp,1} + v_{\perp,2}\big)\,\mathbf{e}_{\perp,1} - \big(v_{\perp,2} - v_{\perp,1}\big)\,\mathbf{e}_{\perp,2}. \tag{C.15}$$

Applying this to $\mathbf{k}_i$ and $\mathbf{k}_j$ gives the desired rotation.

Bibliography

[1] CDF Collaboration, F. Abe et al., *Observation of top quark production in $\bar{p}p$ collisions*, Phys. Rev. Lett. **74** (1995) 2626–2631, arXiv:hep-ex/9503002 [hep-ex].

[2] D0 Collaboration, S. Abachi et al., *Observation of the top quark*, Phys. Rev. Lett. **74** (1995) 2632–2637, arXiv:hep-ex/9503003 [hep-ex].

[3] M. Czakon, P. Fiedler, and A. Mitov, *Total Top-Quark Pair-Production Cross Section at Hadron Colliders Through $O(\alpha_s^4)$*, Phys. Rev. Lett. **110** (2013) 252004, arXiv:1303.6254 [hep-ph].

[4] N. Kidonakis, *Next-to-next-to-leading-order collinear and soft gluon corrections for t-channel single top quark production*, Phys. Rev. **D83** (2011) 091503, arXiv:1103.2792 [hep-ph].

[5] N. Kidonakis, *Differential and total cross sections for top pair and single top production*, in *Proceedings, 20th International Workshop on Deep-Inelastic Scattering and Related Subjects (DIS 2012): Bonn, Germany, March 26-30, 2012*, pp. 831–834. 2012. http://inspirehep.net/record/1114754/files/arXiv:1205.3453.pdf.

[6] M. Brucherseifer, F. Caola, and K. Melnikov, *On the NNLO QCD corrections to single-top production at the LHC*, Phys. Lett. **B736** (2014) 58–63, arXiv:1404.7116 [hep-ph].

[7] ATLAS, CDF, CMS, D0 Collaboration, *First combination of Tevatron and LHC measurements of the top-quark mass*, arXiv:1403.4427 [hep-ex].

[8] O. Brandt, *Measurements of the top quark mass from the LHC and the Tevatron*, in *9th International Workshop on the CKM Unitarity Triangle (CKM 2016) Mumbai, India, November 28-December 3, 2016*. 2017. arXiv:1701.05486 [hep-ex]. http://inspirehep.net/record/1509921/files/arXiv:1701.05486.pdf.

[9] A. H. Hoang, *The Top Mass: Interpretation and Theoretical Uncertainties*, in *Proceedings, 7th International Workshop on Top Quark Physics (TOP2014): Cannes, France, September 28-October 3, 2014*. 2014. arXiv:1412.3649 [hep-ph]. http://inspirehep.net/record/1333866/files/arXiv:1412.3649.pdf.

[10] C. E. Gerber and C. Vellidis, *Review of Physics Results from the Tevatron: Top Quark Physics*, Submitted to: Int. J. Mod. Phys. A (2014) , arXiv:1409.5038 [hep-ex].

[11] ATLAS, CDF, LHCb, CMS, D0 Collaboration, K. Kawade, *Review of top quark production at LHC and Tevatron*, PoS **HQL2016** (2017) 038.

[12] K. Kroeninger, A. B. Meyer, and P. Uwer, *Top-Quark Physics at the LHC*, in *The Large Hadron Collider: Harvest of Run 1*, T. Schorner-Sadenius, ed., pp. 259–300. 2015. arXiv:1506.02800 [hep-ex]. http://inspirehep.net/record/1375310/files/arXiv:1506.02800.pdf.

[13] D0 Collaboration, V. M. Abazov et al., *Measurement of the forward-backward asymmetry in top quark-antiquark production in ppbar collisions using the lepton+jets channel*, Phys. Rev. **D90** (2014) 072011, arXiv:1405.0421 [hep-ex].

[14] W. Hollik and D. Pagani, *The electroweak contribution to the top quark forward-backward asymmetry at the Tevatron*, Phys. Rev. **D84** (2011) 093003, arXiv:1107.2606 [hep-ph].

[15] J. H. Kuhn and G. Rodrigo, *Charge asymmetries of top quarks at hadron colliders revisited*, JHEP **01** (2012) 063, arXiv:1109.6830 [hep-ph].

[16] W. Bernreuther and Z.-G. Si, *Top quark and leptonic charge asymmetries for the Tevatron and LHC*, Phys. Rev. **D86** (2012) 034026, arXiv:1205.6580 [hep-ph].

[17] CDF Collaboration, T. Aaltonen et al., *Measurement of the top quark forward-backward production asymmetry and its dependence on event kinematic properties*, Phys. Rev. **D87** no. 9, (2013) 092002, arXiv:1211.1003 [hep-ex].

[18] J. A. Aguilar-Saavedra, D. Amidei, A. Juste, and M. Perez-Victoria, *Asymmetries in top quark pair production at hadron colliders*, Rev. Mod. Phys. **87** (2015) 421–455, arXiv:1406.1798 [hep-ph].

[19] M. Czakon, P. Fiedler, and A. Mitov, *Resolving the Tevatron Top Quark Forward-Backward Asymmetry Puzzle: Fully Differential Next-to-Next-to-Leading-Order Calculation*, Phys. Rev. Lett. **115** no. 5, (2015) 052001, arXiv:1411.3007 [hep-ph].

[20] ATLAS Collaboration, G. Aad et al., *Measurement of the charge asymmetry in top-quark pair production in the lepton-plus-jets final state in pp collision data at* $\sqrt{s} = 8\,\mathrm{T}eV$ *with the ATLAS detector*, Eur. Phys. J. **C76** no. 2, (2016) 87, arXiv:1509.02358 [hep-ex].

[21] CMS Collaboration, V. Khachatryan et al., *Inclusive and differential measurements of the* $t\bar{t}$ *charge asymmetry in pp collisions at* $\sqrt{s} = 8\ TeV$, Phys. Lett. **B757** (2016) 154–179, arXiv:1507.03119 [hep-ex].

[22] ECFA/DESY LC Physics Working Group Collaboration, J. A. Aguilar-Saavedra et al., *TESLA: The Superconducting electron positron linear collider with an integrated x-ray laser laboratory. Technical design report. Part 3. Physics at an* e^+e^- *linear collider*, arXiv:hep-ph/0106315 [hep-ph].

[23] H. Baer, T. Barklow, K. Fujii, Y. Gao, A. Hoang, S. Kanemura, J. List, H. E. Logan, A. Nomerotski, M. Perelstein, et al., *The International Linear Collider Technical Design Report - Volume 2: Physics*, arXiv:1306.6352 [hep-ph].

[24] L. Linssen, A. Miyamoto, M. Stanitzki, and H. Weerts, *Physics and Detectors at CLIC: CLIC Conceptual Design Report*, arXiv:1202.5940 [physics.ins-det].

[25] TLEP Design Study Working Group Collaboration, M. Bicer et al., *First Look at the Physics Case of TLEP*, JHEP **01** (2014) 164, arXiv:1308.6176 [hep-ex].

[26] A. Arbey et al., *Physics at the e^+e^- Linear Collider*, Eur. Phys. J. **C75** no. 8, (2015) 371, arXiv:1504.01726 [hep-ph].

[27] M. Vos et al., *Top physics at high-energy lepton colliders*, arXiv:1604.08122 [hep-ex].

[28] A. Czarnecki and K. Melnikov, *Two loop QCD corrections to top quark width*, Nucl. Phys. **B544** (1999) 520–531, arXiv:hep-ph/9806244 [hep-ph].

[29] K. G. Chetyrkin, R. Harlander, T. Seidensticker, and M. Steinhauser, *Second order QCD corrections to* $\Gamma(t \to Wb)$, Phys. Rev. **D60** (1999) 114015, arXiv:hep-ph/9906273 [hep-ph].

[30] H. S. Do, S. Groote, J. G. Korner, and M. C. Mauser, *Electroweak and finite width corrections to top quark decays into transverse and longitudinal W bosons*, Phys. Rev. **D67** (2003) 091501, arXiv:hep-ph/0209185 [hep-ph].

[31] K. Seidel, F. Simon, M. Tesar, and S. Poss, *Top quark mass measurements at and above threshold at CLIC*, Eur. Phys. J. **C73** no. 8, (2013) 2530, arXiv:1303.3758 [hep-ex].

[32] E. Devetak, A. Nomerotski, and M. Peskin, *Top quark anomalous couplings at the International Linear Collider*, Phys. Rev. **D84** (2011) 034029, arXiv:1005.1756 [hep-ex].

[33] R. Roentsch and M. Schulze, *Probing top-Z dipole moments at the LHC and ILC*, JHEP **08** (2015) 044, arXiv:1501.05939 [hep-ph].

[34] P. H. Khiem, E. Kou, Y. Kurihara, and F. Le Diberder, *Probing New Physics using top quark polarization in the $e^+e^- \to t\bar{t}$ process at future Linear Colliders*, 2015. arXiv:1503.04247 [hep-ph]. http://inspirehep.net/record/1352820/files/arXiv:1503.04247.pdf.

[35] P. Janot, *Top-quark electroweak couplings at the FCC-ee*, JHEP **04** (2015) 182, arXiv:1503.01325 [hep-ph].

[36] M. S. Amjad et al., *A precise characterisation of the top quark electro-weak vertices at the ILC*, Eur. Phys. J. **C75** no. 10, (2015) 512, arXiv:1505.06020 [hep-ex].

[37] M. Beneke, Y. Kiyo, P. Marquard, A. Penin, J. Piclum, and M. Steinhauser, *Next-to-Next-to-Next-to-Leading Order QCD Prediction for the Top Antitop S-Wave Pair Production Cross Section Near Threshold in e^+e^- Annihilation*, Phys. Rev. Lett. **115** no. 19, (2015) 192001, arXiv:1506.06864 [hep-ph].

[38] Belle, BaBar Collaboration, A. J. Bevan et al., *The Physics of the B Factories*, Eur. Phys. J. **C74** (2014) 3026, arXiv:1406.6311 [hep-ex].

[39] C. Bozzi, *Review of B and B_s decays*, Int. J. Mod. Phys. Conf. Ser. **31** (2014) 1460290.

[40] M. G. Gandara, *Review of direct CP violation in two and three body B decays at LHCb*, in *8th International Workshop on the CKM Unitarity Triangle (CKM 2014) Vienna, Austria, September 8-12, 2014*. 2014. arXiv:1411.1873 [hep-ex]. http://inspirehep.net/record/1326643/files/arXiv:1411.1873.pdf.

[41] J. Dingfelder and T. Mannel, *Leptonic and semileptonic decays of B mesons*, Rev. Mod. Phys. **88** no. 3, (2016) 035008.

[42] Y. Amhis et al., *Averages of b-hadron, c-hadron, and τ-lepton properties as of summer 2016*, arXiv:1612.07233 [hep-ex].

[43] LHCb Collaboration, R. Aaij et al., *Measurement of Form-Factor-Independent Observables in the Decay $B^0 \to K^{*0}\mu^+\mu^-$*, Phys. Rev. Lett. **111** (2013) 191801, arXiv:1308.1707 [hep-ex].

[44] LHCb Collaboration, R. Aaij et al., *Angular analysis of the $B^0 \to K^{*0}\mu^+\mu^-$ decay using 3 fb^{-1} of integrated luminosity*, JHEP **02** (2016) 104, arXiv:1512.04442 [hep-ex].

[45] Belle Collaboration, A. Abdesselam et al., *Angular analysis of $B^0 \to K^*(892)^0\ell^+\ell^-$*, in *Proceedings, LHCSki 2016 - A First Discussion of 13 TeV Results: Obergurgl, Austria, April 10-15, 2016*. 2016. arXiv:1604.04042 [hep-ex]. http://inspirehep.net/record/1446979/files/arXiv:1604.04042.pdf.

[46] LHCb Collaboration, R. Aaij et al., *Angular analysis and differential branching fraction of the decay $B_s^0 \to \phi\mu^+\mu^-$*, JHEP **09** (2015) 179, arXiv:1506.08777 [hep-ex].

[47] W. Altmannshofer and D. M. Straub, *Implications of $b \to s$ measurements*, in *Proceedings, 50th Rencontres de Moriond Electroweak Interactions and Unified Theories: La Thuile, Italy, March 14-21, 2015*, pp. 333–338. 2015. arXiv:1503.06199 [hep-ph]. http://inspirehep.net/record/1353682/files/arXiv:1503.06199.pdf.

[48] S. Descotes-Genon, L. Hofer, J. Matias, and J. Virto, *Global analysis of $b \to s\ell\ell$ anomalies*, JHEP **06** (2016) 092, arXiv:1510.04239 [hep-ph].

[49] T. Hurth, F. Mahmoudi, and S. Neshatpour, *On the anomalies in the latest LHCb data*, Nucl. Phys. **B909** (2016) 737–777, arXiv:1603.00865 [hep-ph].

[50] T. Blake, M. Gersabeck, L. Hofer, S. Jaeger, Z. Liu, and R. Zwicky, *Round table: Flavour anomalies in $b \to s\ell^+\ell^-$ processes*, EPJ Web Conf. **137** (2017) 01001, arXiv:1703.10005 [hep-ph].

[51] ATLAS Collaboration, M. Aaboud et al., *Measurement of the $b\bar{b}$ dijet cross section in pp collisions at $\sqrt{s} = 7$ TeV with the ATLAS detector*, Eur. Phys. J. **C76** no. 12, (2016) 670, arXiv:1607.08430 [hep-ex].

[52] CMS Collaboration, V. Khachatryan et al., *Measurements of the associated production of a Z boson and b jets in pp collisions at $\sqrt{s} = 8$ TeV*, Submitted to: Eur. Phys. J. C (2016) , arXiv:1611.06507 [hep-ex].

[53] SLD Electroweak Group, DELPHI, ALEPH, SLD, SLD Heavy Flavour Group, OPAL, LEP Electroweak Working Group, L3 Collaboration, S. Schael et al., *Precision electroweak measurements on the Z resonance*, Phys. Rept. **427** (2006) 257–454, arXiv:hep-ex/0509008 [hep-ex].

[54] Tevatron Electroweak Working Group, CDF, SLD Heavy Flavor Group, DELPHI, ALEPH, SLD Electroweak Working Group, LEP Electroweak Working Group, SLD, OPAL, D0, L3 Collaboration, J. Alcaraz et al., *Precision Electroweak Measurements and Constraints on the Standard Model*, arXiv:0911.2604 [hep-ex].

[55] Tevatron Electroweak Working Group, CDF, DELPHI, SLD Electroweak and Heavy Flavour Groups, ALEPH, LEP Electroweak Working Group, SLD, OPAL, D0, L3

Collaboration, L. E. W. Group, *Precision Electroweak Measurements and Constraints on the Standard Model*, arXiv:1012.2367 [hep-ex].

[56] Gfitter Group Collaboration, M. Baak, J. Cuth, J. Haller, A. Hoecker, R. Kogler, K. Moenig, M. Schott, and J. Stelzer, *The global electroweak fit at NNLO and prospects for the LHC and ILC*, Eur. Phys. J. **C74** (2014) 3046, arXiv:1407.3792 [hep-ph].

[57] R. Hawkings and K. Monig, *Electroweak and CP violation physics at a linear collider Z factory*, Eur. Phys. J.direct **C1** (1999) 8, arXiv:hep-ex/9910022 [hep-ex].

[58] J. Erler, S. Heinemeyer, W. Hollik, G. Weiglein, and P. M. Zerwas, *Physics impact of GigaZ*, Phys. Lett. **B486** (2000) 125–133.

[59] J. Jersak, E. Laermann, and P. M. Zerwas, *Electroweak Production of Heavy Quarks in e^+e^- Annihilation*, Phys. Rev. **D25** (1982) 1218. [Erratum: Phys. Rev.D36,310(1987)].

[60] W. Bernreuther, A. Brandenburg, and P. Uwer, *Next-to-leading order QCD corrections to three jet cross-sections with massive quarks*, Phys. Rev. Lett. **79** (1997) 189–192, arXiv:hep-ph/9703305 [hep-ph].

[61] A. Brandenburg and P. Uwer, *Next-to-leading order QCD corrections and massive quarks in $e^+e^- \to$ three jets*, Nucl. Phys. **B515** (1998) 279–320, arXiv:hep-ph/9708350 [hep-ph].

[62] G. Rodrigo, A. Santamaria, and M. S. Bilenky, *Do the quark masses run? Extracting $\overline{m}_b(m_Z)$ from LEP data*, Phys. Rev. Lett. **79** (1997) 193–196, arXiv:hep-ph/9703358 [hep-ph].

[63] G. Rodrigo, M. S. Bilenky, and A. Santamaria, *Quark mass effects for jet production in e^+e^- collisions at the next-to-leading order: Results and applications*, Nucl. Phys. **B554** (1999) 257–297, arXiv:hep-ph/9905276 [hep-ph].

[64] P. Nason and C. Oleari, *Next-to-leading order corrections to momentum correlations in $Z^0 \to b\bar{b}$*, Phys. Lett. **B407** (1997) 57–60, arXiv:hep-ph/9705295 [hep-ph].

[65] P. Nason and C. Oleari, *Next-to-leading order corrections to the production of heavy flavor jets in e^+e^- collisions*, Nucl. Phys. **B521** (1998) 237–273, arXiv:hep-ph/9709360 [hep-ph].

[66] W. Beenakker, S. C. van der Marck, and W. Hollik, *e^+e^- annihilation into heavy fermion pairs at high-energy colliders*, Nucl. Phys. **B365** (1991) 24–78.

[67] J. Fleischer, A. Leike, T. Riemann, and A. Werthenbach, *Electroweak one loop corrections for e^+e^- annihilation into t anti-top including hard bremsstrahlung*, Eur. Phys. J. **C31** (2003) 37–56, arXiv:hep-ph/0302259 [hep-ph].

[68] T. Hahn, W. Hollik, A. Lorca, T. Riemann, and A. Werthenbach, *$O(\alpha)$ electroweak corrections to the processes $e^+e^- \to \tau^-\tau^+, c\bar{c}, b\bar{b}, t\bar{t}$: A Comparison*, in *Proceedings, 4th ECFA / DESY Workshop on Physics and Detectors for a 90-GeV to 800-GeV Linear e^+e^- Collider: Amsterdam, Netherlands, April 1-4, 2003*. 2003. arXiv:hep-ph/0307132 [hep-ph]. http://inspirehep.net/record/623116/files/arXiv:hep-ph_0307132.pdf.

[69] P. H. Khiem, J. Fujimoto, T. Ishikawa, T. Kaneko, K. Kato, Y. Kurihara, Y. Shimizu, T. Ueda, J. A. M. Vermaseren, and Y. Yasui, *Full $\mathcal{O}(\alpha)$ electroweak radiative corrections to $e^+e^- \to t\bar{t}\gamma$ with GRACE-Loop*, Eur. Phys. J. **C73** no. 4, (2013) 2400, arXiv:1211.1112 [hep-ph].

[70] C. R. Schmidt, *Top quark production and decay at next-to-leading order in e^+e^- annihilation*, Phys. Rev. **D54** (1996) 3250–3265, arXiv:hep-ph/9504434 [hep-ph].

[71] A. Brandenburg, M. Flesch, and P. Uwer, *The spin density matrix of top quark pairs produced in electron - positron annihilation including QCD radiative corrections*, Phys. Rev. **D59** (1999) 014001, arXiv:hep-ph/9806306 [hep-ph].

[72] B. Chokoufe Nejad, W. Kilian, J. M. Lindert, S. Pozzorini, J. Reuter, and C. Weiss, *NLO QCD predictions for off-shell $t\bar{t}$ and $t\bar{t}H$ production and decay at a linear collider*, JHEP **12** (2016) 075, arXiv:1609.03390 [hep-ph].

[73] S. G. Gorishnii, A. L. Kataev, and S. A. Larin, *Three Loop Corrections of Order $O(M^2)$ to the Correlator of Electromagnetic Quark Currents*, Nuovo Cim. **A92** (1986) 119–131.

[74] K. G. Chetyrkin, J. H. Kuhn, and M. Steinhauser, *Three loop polarization function and $O(\alpha_s^2)$ corrections to the production of heavy quarks*, Nucl. Phys. **B482** (1996) 213–240, arXiv:hep-ph/9606230 [hep-ph].

[75] K. G. Chetyrkin, R. Harlander, J. H. Kuhn, and M. Steinhauser, *Mass corrections to the vector current correlator*, Nucl. Phys. **B503** (1997) 339–353, arXiv:hep-ph/9704222 [hep-ph].

[76] K. G. Chetyrkin, A. H. Hoang, J. H. Kuhn, M. Steinhauser, and T. Teubner, *Massive quark production in electron positron annihilation to order α_s^2*, Eur. Phys. J. **C2** (1998) 137–150, arXiv:hep-ph/9711327 [hep-ph].

[77] Y. Kiyo, A. Maier, P. Maierhofer, and P. Marquard, *Reconstruction of heavy quark current correlators at $O(\alpha_s^3)$*, Nucl. Phys. **B823** (2009) 269–287, arXiv:0907.2120 [hep-ph].

[78] O. Dekkers and W. Bernreuther, *The real-virtual antenna functions for $S \to Q\bar{Q}X$ at NNLO QCD*, Phys. Lett. **B738** (2014) 325–333, arXiv:1409.3124 [hep-ph].

[79] J. Gao and H. X. Zhu, *Electroweak prodution of top-quark pairs in e^+e^- annihilation at NNLO in QCD: the vector contributions*, Phys. Rev. **D90** no. 11, (2014) 114022, arXiv:1408.5150 [hep-ph].

[80] J. Gao and H. X. Zhu, *Top Quark Forward-Backward Asymmetry in e^+e^- Annihilation at Next-to-Next-to-Leading Order in QCD*, Phys. Rev. Lett. **113** no. 26, (2014) 262001, arXiv:1410.3165 [hep-ph].

[81] J. Gao, C. S. Li, and H. X. Zhu, *Top Quark Decay at Next-to-Next-to Leading Order in QCD*, Phys. Rev. Lett. **110** no. 4, (2013) 042001, arXiv:1210.2808 [hep-ph].

[82] A. von Manteuffel, R. M. Schabinger, and H. X. Zhu, *The two-loop soft function for heavy quark pair production at future linear colliders*, Phys. Rev. **D92** no. 4, (2015) 045034, arXiv:1408.5134 [hep-ph].

[83] G. Altarelli, R. Kleiss, and C. Verzegnassi, eds., *Z PHYSICS AT LEP-1. PROCEEDINGS, WORKSHOP, GENEVA, SWITZERLAND, SEPTEMBER 4-5, 1989. VOL. 1: STANDARD PHYSICS*. 1989. http://inspirehep.net/record/288139/files/CERN-89-08-V-1.pdf.

[84] D. Yu. Bardin, P. Christova, M. Jack, L. Kalinovskaya, A. Olchevski, S. Riemann, and T. Riemann, *ZFITTER v.6.21: A Semianalytical program for fermion pair production in e^+e^- annihilation*, Comput. Phys. Commun. **133** (2001) 229–395, arXiv:hep-ph/9908433 [hep-ph].

[85] A. Freitas and K. Monig, *Corrections to quark asymmetries at LEP*, Eur. Phys. J. **C40** (2005) 493, arXiv:hep-ph/0411304 [hep-ph].

[86] A. B. Arbuzov, D. Yu. Bardin, and A. Leike, *Analytic final state corrections with cut for $e^+e^- \to$ massive fermions*, Mod. Phys. Lett. **A7** (1992) 2029–2038. [Erratum: Mod. Phys. Lett.A9,1515(1994)].

[87] A. Djouadi, B. Lampe, and P. M. Zerwas, *A Note on the QCD corrections to forward - backward asymmetries of heavy quark jets in Z decays*, Z. Phys. **C67** (1995) 123–128, arXiv:hep-ph/9411386 [hep-ph].

[88] G. Altarelli and B. Lampe, *Second order QCD corrections to heavy quark forward - backward asymmetries*, Nucl. Phys. **B391** (1993) 3–22.

[89] V. Ravindran and W. L. van Neerven, *Second order QCD corrections to the forward - backward asymmetry in e^+e^- collisions*, Phys. Lett. **B445** (1998) 214–222, arXiv:hep-ph/9809411 [hep-ph].

[90] S. Catani and M. H. Seymour, *Corrections of $O(\alpha_s^2)$ to the forward backward asymmetry*, JHEP **07** (1999) 023, arXiv:hep-ph/9905424 [hep-ph].

[91] S. Weinzierl, *The Forward-backward asymmetry at NNLO revisited*, Phys. Lett. **B644** (2007) 331–335, arXiv:hep-ph/0609021 [hep-ph].

[92] M. E. Peskin and D. V. Schroeder, *An Introduction to quantum field theory*. Addison-Wesley, Reading (USA), 1995.

[93] M. D. Schwartz, *Quantum Field Theory and the Standard Model*. Cambridge University Press, 2014.

[94] D. R. Yennie, S. C. Frautschi, and H. Suura, *The infrared divergence phenomena and high-energy processes*, Annals Phys. **13** (1961) 379–452.

[95] S. Weinberg, *Infrared photons and gravitons*, Phys. Rev. **140** (1965) B516–B524.

[96] G. Grammer, Jr. and D. R. Yennie, *Improved treatment for the infrared divergence problem in quantum electrodynamics*, Phys. Rev. **D8** (1973) 4332–4344.

[97] S. Catani and M. Grazzini, *Infrared factorization of tree level QCD amplitudes at the next-to-next-to-leading order and beyond*, Nucl. Phys. **B570** (2000) 287–325, arXiv:hep-ph/9908523 [hep-ph].

[98] Z. Bern and G. Chalmers, *Factorization in one loop gauge theory*, Nucl. Phys. **B447** (1995) 465–518, arXiv:hep-ph/9503236 [hep-ph].

[99] Z. Bern, V. Del Duca, and C. R. Schmidt, *The Infrared behavior of one loop gluon amplitudes at next-to-next-to-leading order*, Phys. Lett. **B445** (1998) 168–177, arXiv:hep-ph/9810409 [hep-ph].

[100] Z. Bern, V. Del Duca, W. B. Kilgore, and C. R. Schmidt, *The infrared behavior of one loop QCD amplitudes at next-to-next-to leading order*, Phys. Rev. **D60** (1999) 116001, arXiv:hep-ph/9903516 [hep-ph].

[101] S. Catani and M. Grazzini, *The soft gluon current at one loop order*, Nucl. Phys. **B591** (2000) 435–454, arXiv:hep-ph/0007142 [hep-ph].

[102] I. Bierenbaum, M. Czakon, and A. Mitov, *The singular behavior of one-loop massive QCD amplitudes with one external soft gluon*, Nucl. Phys. **B856** (2012) 228–246, arXiv:1107.4384 [hep-ph].

[103] Y. Li and H. X. Zhu, *Single soft gluon emission at two loops*, JHEP **11** (2013) 080, arXiv:1309.4391 [hep-ph].

[104] C. Duhr and T. Gehrmann, *The two-loop soft current in dimensional regularization*, Phys. Lett. **B727** (2013) 452–455, arXiv:1309.4393 [hep-ph].

[105] G. Altarelli and G. Parisi, *Asymptotic Freedom in Parton Language*, Nucl. Phys. **B126** (1977) 298–318.

[106] M. L. Mangano and S. J. Parke, *Multiparton amplitudes in gauge theories*, Phys. Rept. **200** (1991) 301–367, arXiv:hep-th/0509223 [hep-th].

[107] Z. Bern, L. J. Dixon, D. C. Dunbar, and D. A. Kosower, *One loop n point gauge theory amplitudes, unitarity and collinear limits*, Nucl. Phys. **B425** (1994) 217–260, arXiv:hep-ph/9403226 [hep-ph].

[108] Z. Bern, L. J. Dixon, and D. A. Kosower, *One loop corrections to two quark three gluon amplitudes*, Nucl. Phys. **B437** (1995) 259–304, arXiv:hep-ph/9409393 [hep-ph].

[109] Z. Bern, L. J. Dixon, and D. A. Kosower, *Unitarity based techniques for one loop calculations in QCD*, Nucl. Phys. Proc. Suppl. **51C** (1996) 243–249, arXiv:hep-ph/9606378 [hep-ph].

[110] S. J. Parke and T. R. Taylor, *An Amplitude for n Gluon Scattering*, Phys. Rev. Lett. **56** (1986) 2459.

[111] F. A. Berends and W. T. Giele, *Multiple Soft Gluon Radiation in Parton Processes*, Nucl. Phys. **B313** (1989) 595–633.

[112] D. A. Kosower, *All order collinear behavior in gauge theories*, Nucl. Phys. **B552** (1999) 319–336, arXiv:hep-ph/9901201 [hep-ph].

[113] I. Feige and M. D. Schwartz, *Hard-Soft-Collinear Factorization to All Orders*, Phys. Rev. **D90** no. 10, (2014) 105020, arXiv:1403.6472 [hep-ph].

[114] F. Bloch and A. Nordsieck, *Note on the radiation field of the electron*, Phys. Rev. **52** (1937) 54–59.

[115] G. F. Sterman and S. Weinberg, *Jets from Quantum Chromodynamics*, Phys. Rev. Lett. **39** (1977) 1436.

[116] T. Kinoshita, *Mass singularities of Feynman amplitudes*, J. Math. Phys. **3** (1962) 650–677.

[117] T. D. Lee and M. Nauenberg, *Degenerate Systems and Mass Singularities*, Phys. Rev. **133** (1964) B1549–B1562.

[118] G. F. Sterman, *An Introduction to quantum field theory*. Cambridge University Press, 1993.

[119] D. Amati, R. Petronzio, and G. Veneziano, *Relating Hard QCD Processes Through Universality of Mass Singularities*, Nucl. Phys. **B140** (1978) 54–72.

[120] R. K. Ellis, H. Georgi, M. Machacek, H. D. Politzer, and G. G. Ross, *Perturbation Theory and the Parton Model in QCD*, Nucl. Phys. **B152** (1979) 285–329.

[121] S. B. Libby and G. F. Sterman, *Jet and Lepton Pair Production in High-Energy Lepton-Hadron and Hadron-Hadron Scattering*, Phys. Rev. **D18** (1978) 3252.

[122] J. C. Collins, D. E. Soper, and G. F. Sterman, *Factorization for Short Distance Hadron - Hadron Scattering*, Nucl. Phys. **B261** (1985) 104–142.

[123] J. C. Collins and D. E. Soper, *The Theorems of Perturbative QCD*, Ann. Rev. Nucl. Part. Sci. **37** (1987) 383–409.

[124] R. Doria, J. Frenkel, and J. C. Taylor, *Counter Example to Nonabelian Bloch-Nordsieck Theorem*, Nucl. Phys. **B168** (1980) 93–110.

[125] C. Di'Lieto, S. Gendron, I. G. Halliday, and C. T. Sachrajda, *A Counter Example to the Bloch-Nordsieck Theorem in Nonabelian Gauge Theories*, Nucl. Phys. **B183** (1981) 223–250.

[126] G. P. Salam, *Towards Jetography*, Eur. Phys. J. **C67** (2010) 637–686, arXiv:0906.1833 [hep-ph].

[127] R. K. Ellis, D. A. Ross, and A. E. Terrano, *The Perturbative Calculation of Jet Structure in e^+e^- Annihilation*, Nucl. Phys. **B178** (1981) 421–456.

[128] S. Catani and M. H. Seymour, *A General algorithm for calculating jet cross-sections in NLO QCD*, Nucl. Phys. **B485** (1997) 291–419, arXiv:hep-ph/9605323 [hep-ph]. [Erratum: Nucl. Phys.B510,503(1998)].

[129] L. Phaf and S. Weinzierl, *Dipole formalism with heavy fermions*, JHEP **04** (2001) 006, arXiv:hep-ph/0102207 [hep-ph].

[130] S. Catani, S. Dittmaier, M. H. Seymour, and Z. Trocsanyi, *The Dipole formalism for next-to-leading order QCD calculations with massive partons*, Nucl. Phys. **B627** (2002) 189–265, arXiv:hep-ph/0201036 [hep-ph].

[131] Z. Nagy and Z. Trocsanyi, *Next-to-leading order calculation of four jet observables in electron positron annihilation*, Phys. Rev. **D59** (1999) 014020, arXiv:hep-ph/9806317 [hep-ph]. [Erratum: Phys. Rev.D62,099902(2000)].

[132] M. Czakon, C. G. Papadopoulos, and M. Worek, *Polarizing the Dipoles*, JHEP **08** (2009) 085, arXiv:0905.0883 [hep-ph].

[133] G. Bevilacqua, M. Czakon, C. G. Papadopoulos, R. Pittau, and M. Worek, *Assault on the NLO Wishlist: $pp \to t\bar{t}b\bar{b}$*, JHEP **09** (2009) 109, arXiv:0907.4723 [hep-ph].

[134] R. Frederix, T. Gehrmann, and N. Greiner, *Integrated dipoles with MadDipole in the MadGraph framework*, JHEP **06** (2010) 086, arXiv:1004.2905 [hep-ph].

[135] D. Goetz, C. Schwan, and S. Weinzierl, *Random Polarisations of the Dipoles*, Phys. Rev. **D85** (2012) 116011, arXiv:1205.4109 [hep-ph].

[136] J. M. Campbell, R. K. Ellis, and F. Tramontano, *Single top production and decay at next-to-leading order*, Phys. Rev. **D70** (2004) 094012, arXiv:hep-ph/0408158 [hep-ph].

[137] W. Bernreuther, P. Gonzalez, and C. Mellein, *Decays of polarized top quarks to lepton, neutrino and jets at NLO QCD*, Eur. Phys. J. **C74** no. 3, (2014) 2815, arXiv:1401.5930 [hep-ph].

[138] S. Frixione, Z. Kunszt, and A. Signer, *Three jet cross-sections to next-to-leading order*, Nucl. Phys. **B467** (1996) 399–442, arXiv:hep-ph/9512328 [hep-ph].

[139] Z. Nagy and Z. Trocsanyi, *Calculation of QCD jet cross-sections at next-to-leading order*, Nucl. Phys. **B486** (1997) 189–226, arXiv:hep-ph/9610498 [hep-ph].

[140] S. Frixione, *A General approach to jet cross-sections in QCD*, Nucl. Phys. **B507** (1997) 295–314, arXiv:hep-ph/9706545 [hep-ph].

[141] Z. Nagy and D. E. Soper, *General subtraction method for numerical calculation of one loop QCD matrix elements*, JHEP **09** (2003) 055, arXiv:hep-ph/0308127 [hep-ph].

[142] G. Bevilacqua, M. Czakon, M. Kubocz, and M. Worek, *Complete Nagy-Soper subtraction for next-to-leading order calculations in QCD*, JHEP **10** (2013) 204, arXiv:1308.5605 [hep-ph].

[143] D. A. Kosower, *Antenna factorization of gauge theory amplitudes*, Phys. Rev. **D57** (1998) 5410–5416, arXiv:hep-ph/9710213 [hep-ph].

[144] D. A. Kosower, *Antenna factorization in strongly ordered limits*, Phys. Rev. **D71** (2005) 045016, arXiv:hep-ph/0311272 [hep-ph].

[145] A. Gehrmann-De Ridder, T. Gehrmann, and E. W. N. Glover, *Antenna subtraction at NNLO*, JHEP **09** (2005) 056, arXiv:hep-ph/0505111 [hep-ph].

[146] K. Fabricius, I. Schmitt, G. Kramer, and G. Schierholz, *Higher Order Perturbative QCD Calculation of Jet Cross-Sections in e^+e^- Annihilation*, Z. Phys. **C11** (1981) 315.

[147] W. T. Giele and E. W. N. Glover, *Higher order corrections to jet cross-sections in e^+e^- annihilation*, Phys. Rev. **D46** (1992) 1980–2010.

[148] W. Bernreuther, A. Brandenburg, Z. G. Si, and P. Uwer, *Top quark pair production and decay at hadron colliders*, Nucl. Phys. **B690** (2004) 81–137, arXiv:hep-ph/0403035 [hep-ph].

[149] M. Czakon, *A novel subtraction scheme for double-real radiation at NNLO*, Phys. Lett. **B693** (2010) 259–268, arXiv:1005.0274 [hep-ph].

[150] M. Czakon, *Double-real radiation in hadronic top quark pair production as a proof of a certain concept*, Nucl. Phys. **B849** (2011) 250–295, arXiv:1101.0642 [hep-ph].

[151] T. Binoth and G. Heinrich, *An automatized algorithm to compute infrared divergent multiloop integrals*, Nucl. Phys. **B585** (2000) 741–759, arXiv:hep-ph/0004013 [hep-ph].

[152] T. Binoth and G. Heinrich, *Numerical evaluation of multiloop integrals by sector decomposition*, Nucl. Phys. **B680** (2004) 375–388, arXiv:hep-ph/0305234 [hep-ph].

[153] P. Baernreuther, M. Czakon, and A. Mitov, *Percent Level Precision Physics at the Tevatron: First Genuine NNLO QCD Corrections to $q\bar{q} \to t\bar{t} + X$*, Phys. Rev. Lett. **109** (2012) 132001, arXiv:1204.5201 [hep-ph].

[154] M. Czakon and A. Mitov, *NNLO corrections to top pair production at hadron colliders: the quark-gluon reaction*, JHEP **01** (2013) 080, arXiv:1210.6832 [hep-ph].

[155] M. Czakon and A. Mitov, *NNLO corrections to top-pair production at hadron colliders: the all-fermionic scattering channels*, JHEP **12** (2012) 054, arXiv:1207.0236 [hep-ph].

[156] M. Czakon, D. Heymes, and A. Mitov, *High-precision differential predictions for top-quark pairs at the LHC*, Phys. Rev. Lett. **116** no. 8, (2016) 082003, arXiv:1511.00549 [hep-ph].

[157] M. Czakon, P. Fiedler, D. Heymes, and A. Mitov, *NNLO QCD predictions for fully-differential top-quark pair production at the Tevatron*, JHEP **05** (2016) 034, arXiv:1601.05375 [hep-ph].

[158] C. Anastasiou, K. Melnikov, and F. Petriello, *A new method for real radiation at NNLO*, Phys. Rev. **D69** (2004) 076010, arXiv:hep-ph/0311311 [hep-ph].

[159] S. Catani and M. Grazzini, *An NNLO subtraction formalism in hadron collisions and its application to Higgs boson production at the LHC*, Phys. Rev. Lett. **98** (2007) 222002, arXiv:hep-ph/0703012 [hep-ph].

[160] G. Somogyi and Z. Trocsanyi, *A New subtraction scheme for computing QCD jet cross sections at next-to-leading order accuracy*, arXiv:hep-ph/0609041 [hep-ph].

[161] G. Somogyi, Z. Trocsanyi, and V. Del Duca, *A Subtraction scheme for computing QCD jet cross sections at NNLO: Regularization of doubly-real emissions*, JHEP **01** (2007) 070, arXiv:hep-ph/0609042 [hep-ph].

[162] G. Somogyi and Z. Trocsanyi, *A Subtraction scheme for computing QCD jet cross sections at NNLO: Regularization of real-virtual emission*, JHEP **01** (2007) 052, arXiv:hep-ph/0609043 [hep-ph].

[163] C. Anastasiou, K. Melnikov, and F. Petriello, *Higgs boson production at hadron colliders: Differential cross sections through next-to-next-to-leading order*, Phys. Rev. Lett. **93** (2004) 262002, arXiv:hep-ph/0409088 [hep-ph].

[164] J. Gaunt, M. Stahlhofen, F. J. Tackmann, and J. R. Walsh, *N-jettiness Subtractions for NNLO QCD Calculations*, JHEP **09** (2015) 058, arXiv:1505.04794 [hep-ph].

[165] I. W. Stewart, F. J. Tackmann, and W. J. Waalewijn, *N-Jettiness: An Inclusive Event Shape to Veto Jets*, Phys. Rev. Lett. **105** (2010) 092002, arXiv:1004.2489 [hep-ph].

[166] M. L. Mangano, S. J. Parke, and Z. Xu, *Duality and Multi - Gluon Scattering*, Nucl. Phys. **B298** (1988) 653–672.

[167] F. A. Berends and W. Giele, *The Six Gluon Process as an Example of Weyl-Van Der Waerden Spinor Calculus*, Nucl. Phys. **B294** (1987) 700–732.

[168] J. M. Campbell and E. W. N. Glover, *Double unresolved approximations to multiparton scattering amplitudes*, Nucl. Phys. **B527** (1998) 264–288, arXiv:hep-ph/9710255 [hep-ph].

[169] A. Gehrmann-De Ridder, T. Gehrmann, and G. Heinrich, *Four particle phase space integrals in massless QCD*, Nucl. Phys. **B682** (2004) 265–288, arXiv:hep-ph/0311276 [hep-ph].

[170] A. Gehrmann-De Ridder, T. Gehrmann, E. W. N. Glover, and G. Heinrich, *Infrared structure of $e^+e^- \to 3$ jets at NNLO*, JHEP **11** (2007) 058, arXiv:0710.0346 [hep-ph].

[171] S. Weinzierl, *NNLO corrections to 2-jet observables in electron-positron annihilation*, Phys. Rev. **D74** (2006) 014020, arXiv:hep-ph/0606008 [hep-ph].

[172] G. Abelof and A. Gehrmann-De Ridder, *Double real radiation corrections to $t\bar{t}$ production at the LHC: the all-fermion processes*, JHEP **04** (2012) 076, arXiv:1112.4736 [hep-ph].

[173] J. Currie, A. Gehrmann-De Ridder, E. W. N. Glover, and J. Pires, *NNLO QCD corrections to jet production at hadron colliders from gluon scattering*, JHEP **01** (2014) 110, arXiv:1310.3993 [hep-ph].

[174] W. Bernreuther, C. Bogner, and O. Dekkers, *The real radiation antenna functions for $S \to Q\bar{Q}gg$ at NNLO QCD*, JHEP **10** (2013) 161, arXiv:1309.6887 [hep-ph].

[175] W. Bernreuther, R. Bonciani, T. Gehrmann, R. Heinesch, T. Leineweber, P. Mastrolia, and E. Remiddi, *Two-loop QCD corrections to the heavy quark form-factors: The Vector contributions*, Nucl. Phys. **B706** (2005) 245–324, arXiv:hep-ph/0406046 [hep-ph].

[176] W. Bernreuther, R. Bonciani, T. Gehrmann, R. Heinesch, T. Leineweber, P. Mastrolia, and E. Remiddi, *Two-loop QCD corrections to the heavy quark form-factors: Axial*

vector contributions, Nucl. Phys. **B712** (2005) 229–286, arXiv:hep-ph/0412259 [hep-ph].

[177] W. Bernreuther, R. Bonciani, T. Gehrmann, R. Heinesch, T. Leineweber, and E. Remiddi, *Two-loop QCD corrections to the heavy quark form-factors: Anomaly contributions*, Nucl. Phys. **B723** (2005) 91–116, arXiv:hep-ph/0504190 [hep-ph].

[178] A. Gehrmann-De Ridder and M. Ritzmann, *NLO Antenna Subtraction with Massive Fermions*, JHEP **07** (2009) 041, arXiv:0904.3297 [hep-ph].

[179] G. Abelof and A. Gehrmann-De Ridder, *Antenna subtraction for the production of heavy particles at hadron colliders*, JHEP **04** (2011) 063, arXiv:1102.2443 [hep-ph].

[180] E. Remiddi and J. A. M. Vermaseren, *Harmonic polylogarithms*, Int. J. Mod. Phys. **A15** (2000) 725–754, arXiv:hep-ph/9905237 [hep-ph].

[181] T. Gehrmann and E. Remiddi, *Numerical evaluation of harmonic polylogarithms*, Comput. Phys. Commun. **141** (2001) 296–312, arXiv:hep-ph/0107173 [hep-ph].

[182] D. Maitre, *HPL, a mathematica implementation of the harmonic polylogarithms*, Comput. Phys. Commun. **174** (2006) 222–240, arXiv:hep-ph/0507152 [hep-ph].

[183] W. Bernreuther, C. Bogner, and O. Dekkers, *The real radiation antenna function for $S \to Q\bar{Q}q\bar{q}$ at NNLO QCD*, JHEP **06** (2011) 032, arXiv:1105.0530 [hep-ph].

[184] A. Gehrmann-De Ridder, *private communication*,.

[185] Particle Data Group Collaboration, K. A. Olive et al., *Review of Particle Physics*, Chin. Phys. **C38** (2014) 090001.

[186] Particle Data Group Collaboration, C. Patrignani et al., *Review of Particle Physics*, Chin. Phys. **C40** no. 10, (2016) 100001.

[187] N. Gray, D. J. Broadhurst, W. Grafe, and K. Schilcher, *Three Loop Relation of Quark (Modified) MS and Pole Masses*, Z. Phys. **C48** (1990) 673–680.

[188] K. G. Chetyrkin and M. Steinhauser, *Short distance mass of a heavy quark at order α_s^3*, Phys. Rev. Lett. **83** (1999) 4001–4004, arXiv:hep-ph/9907509 [hep-ph].

[189] K. Melnikov and T. v. Ritbergen, *The three loop relation between the MS-bar and the pole quark masses*, Phys. Lett. **B482** (2000) 99–108, arXiv:hep-ph/9912391 [hep-ph].

[190] W. Bernreuther and W. Wetzel, *Decoupling of Heavy Quarks in the Minimal Subtraction Scheme*, Nucl. Phys. **B197** (1982) 228–236. [Erratum: Nucl. Phys.B513,758(1998)].

[191] J. Blumlein, *Structural Relations of Harmonic Sums and Mellin Transforms up to Weight $w = 5$*, Comput. Phys. Commun. **180** (2009) 2218–2249, arXiv:0901.3106 [hep-ph].

[192] J. Ablinger, J. Blumlein, and C. Schneider, *Harmonic Sums and Polylogarithms Generated by Cyclotomic Polynomials*, J. Math. Phys. **52** (2011) 102301, arXiv:1105.6063 [math-ph].

[193] J. Ablinger, J. Blümlein, and C. Schneider, *Analytic and Algorithmic Aspects of Generalized Harmonic Sums and Polylogarithms*, J. Math. Phys. **54** (2013) 082301, arXiv:1302.0378 [math-ph].

[194] B. A. Thacker and G. P. Lepage, *Heavy quark bound states in lattice QCD*, Phys. Rev. **D43** (1991) 196–208.

[195] G. P. Lepage, L. Magnea, C. Nakhleh, U. Magnea, and K. Hornbostel, *Improved nonrelativistic QCD for heavy quark physics*, Phys. Rev. **D46** (1992) 4052–4067, arXiv:hep-lat/9205007 [hep-lat].

[196] A. Pineda and J. Soto, *Effective field theory for ultrasoft momenta in NRQCD and NRQED*, Nucl. Phys. Proc. Suppl. **64** (1998) 428–432, arXiv:hep-ph/9707481 [hep-ph].

[197] N. Brambilla, A. Pineda, J. Soto, and A. Vairo, *Effective field theories for heavy quarkonium*, Rev. Mod. Phys. **77** (2005) 1423, arXiv:hep-ph/0410047 [hep-ph].

[198] A. Czarnecki and K. Melnikov, *Two loop QCD corrections to the heavy quark pair production cross-section in e^+e^- annihilation near the threshold*, Phys. Rev. Lett. **80** (1998) 2531–2534, arXiv:hep-ph/9712222 [hep-ph].

[199] M. Beneke, A. Signer, and V. A. Smirnov, *Two loop correction to the leptonic decay of quarkonium*, Phys. Rev. Lett. **80** (1998) 2535–2538, arXiv:hep-ph/9712302 [hep-ph].

[200] A. H. Hoang, *Two loop corrections to the electromagnetic vertex for energies close to threshold*, Phys. Rev. **D56** (1997) 7276–7283, arXiv:hep-ph/9703404 [hep-ph].

[201] W. Bernreuther, R. Bonciani, T. Gehrmann, R. Heinesch, T. Leineweber, P. Mastrolia, and E. Remiddi, *Two-Parton Contribution to the Heavy-Quark Forward-Backward Asymmetry in NNLO QCD*, Nucl. Phys. **B750** (2006) 83–107, arXiv:hep-ph/0604031 [hep-ph].

[202] B. H. Smith and M. B. Voloshin, *$e^+e^- \to \tau^+\tau^-$ at the threshold and beyond*, Phys. Lett. **B324** (1994) 117–120, arXiv:hep-ph/9312358 [hep-ph]. [Erratum: Phys. Lett.B333,564(1994)].

[203] S. Brandt, C. Peyrou, R. Sosnowski, and A. Wroblewski, *The Principal axis of jets. An Attempt to analyze high-energy collisions as two-body processes*, Phys. Lett. **12** (1964) 57–61.

[204] E. Farhi, *A QCD Test for Jets*, Phys. Rev. Lett. **39** (1977) 1587–1588.

[205] S. Brandt and H. D. Dahmen, *Axes and Scalar Measures of Two-Jet and Three-Jet Events*, Z. Phys. **C1** (1979) 61.

[206] A. Banfi, G. P. Salam, and G. Zanderighi, *Infrared safe definition of jet flavor*, Eur. Phys. J. **C47** (2006) 113–124, arXiv:hep-ph/0601139 [hep-ph].

[207] F. A. Berends, K. J. F. Gaemers, and R. Gastmans, *α^3 contribution to the angular asymmetry in $e^+e^- \to \mu^+\mu^-$*, Nucl. Phys. **B63** (1973) 381–397.

[208] K. Waninger, *Die Vorwärts-Rückwärts-Asymmetrie für schwere Quarks zur Ordnung NNLO*. PhD thesis, RWTH Aachen University.

[209] M. Bohm, A. Denner, and H. Joos, *Gauge theories of the strong and electroweak interaction, Stuttgart, Germany: Teubner*. 2001.

[210] M. Awramik, M. Czakon, A. Freitas, and B. A. Kniehl, *Two-loop electroweak fermionic corrections to* $\sin^2\theta^{b\bar{b}}_{eff}$, Nucl. Phys. **B813** (2009) 174–187, arXiv:0811.1364 [hep-ph].

[211] LEP Heavy Flavor Working Group Collaboration, D. Abbaneo, P. Antilogus, T. Behnke, S. C. Blyth, M. Elsing, R. Faccini, R. W. L. Jones, K. Monig, S. Petzold, and R. Tenchini, *QCD corrections to the forward - backward asymmetries of c and b quarks at the Z pole*, Eur. Phys. J. **C4** (1998) 185–191.

[212] D. Abbaneo et al., *LEP/SLD heavy flavour working group: Final Input Parameters for the LEP/SLD Heavy Flavour Analyses*, http://lepewwg.web.cern.ch/LEPEWWG/heavy/ (2001) .

[213] A. B. Arbuzov, M. Awramik, M. Czakon, A. Freitas, M. W. Grunewald, K. Monig, S. Riemann, and T. Riemann, *ZFITTER: A Semi-analytical program for fermion pair production in* e^+e^- *annihilation, from version 6.21 to version 6.42*, Comput. Phys. Commun. **174** (2006) 728–758, arXiv:hep-ph/0507146 [hep-ph].

[214] D. J. Broadhurst, N. Gray, and K. Schilcher, *Gauge invariant on-shell Z(2) in QED, QCD and the effective field theory of a static quark*, Z. Phys. **C52** (1991) 111–122.

[215] K. Melnikov and T. van Ritbergen, *The Three loop on-shell renormalization of QCD and QED*, Nucl. Phys. **B591** (2000) 515–546, arXiv:hep-ph/0005131 [hep-ph].

[216] W. Bernreuther, *Decoupling of Heavy Quarks in Quantum Chromodynamics*, Annals Phys. **151** (1983) 127.

[217] R. Kleiss, W. J. Stirling, and S. D. Ellis, *A New Monte Carlo Treatment of Multiparticle Phase Space at High-energies*, Comput. Phys. Commun. **40** (1986) 359.

Acknowledgements

I would first like to express my sincere gratitude to my advisor Prof. Werner Bernreuther at RWTH Aachen University, for his continuous support of my Ph.D. study and related research, and also for his kind all-around help covering almost every aspect of my life ever since I came to Germany. Precisely owing to this guidance and assistance my first experience of learning and living abroad has turned out to be a quite pleasant journey rather than a complete disaster. I am very grateful for his careful and patient explanation of all my questions regarding physics, with a strong emphasis on physical transparency and intuition, from which I have benefited a lot. I am also grateful for his patience with me when my progress was slow in the early stage of my Ph.D. study, especially concerning my struggle of getting along with computers which I personally regarded as an alien even after my bachelor study.

Prof. Michal Czakon is an important person in my scientific education at RWTH Aachen University. His insightful and comprehensive course and immense knowledge about Quantum Field Theory (QFT) certainly impressed me and motivated me to spend more time to reconsolidate and deepen my understanding of elementary particle physics, which I am still continuing. His lecture on QFT is very valuable for those who can understand it right on the spot, but is quite entertaining also for those who do not. His lecture notes are among my most frequently visited resources whenever I feel unsure about certain concepts. In addition, I would like to thank him for offering me the opportunity to learn state-of-the-art techniques, in his productive research group, for performing involved computations in higher-order perturbation theory, which is certainly of great value for my future career.

I am also thankful to Prof. Zong-Guo Si for introducing me to the research group at RWTH Aachen University, which made the above things possible.

Special thanks goes to my former office mate Dennis Heisler, who helped me learning stuff related to computer and programming, and provided various tips that made my daily life at Aachen much easier. I wish him a happy and successful business life in Berlin.

I thank Oliver Dekkers, Arnd Behring, Rene Poncelet, Lennart Oymanns, Mario Prausa, and Torsten Weber for teaching me tricks concerning manipulating computers, the accumulation of which really turned a computer into a great tool for me.

Thanks also to all the former and current Ph.D. students of the Institute for Theoretical Particle Physics and Cosmology of the RWTH Aachen University for their kind and welcoming

attitude towards me. It is really a productive community with love and care for each other which I have enjoyed a lot in the course of my Ph.D. study.

I would also like to express my thanks to my old Chinese friends, (quite a few of them might have no clue what is written in this language :-)), especially Yaqing Song. Through the communication with her I am still aware of what is going on around me other than physics.

I am gratefully indebted to my parents throughout my years of study. Even though they do not understand what I am doing, they still trust me, respect my choice of profession, and give me full and unfailing support, as always.

Last but not least, I would like to thank the China Scholarship Council (CSC) for its financial support through my Ph.D. study. Without this support nothing in the past 4 years mentioned above could have happened to me.